

**Additive Manufacturing of Free Standing Structure from Thermally Cured Resins**

Shervin Foroughi

A Thesis  
in  
The Department  
of  
Mechanical and Industrial Engineering

Presented in Partial Fulfillment of the Requirements  
for the Degree of Masters of Applied Science (Mechanical Engineering) at  
Concordia University  
Montreal, Quebec, Canada

July 2018

**CONCORDIA UNIVERSITY**  
**School of graduate Studies**

This is to certify that thesis prepared,

By: **SHERVIN FOROUGH**

Entitled: **Additive Manufacturing of Free Standing Structure from Thermally Cured Resins**

and submitted in the partial fulfilment of the requirements for the degree of

**Master of Applied Science (Mechanical and Industrial Engineering)**

Compiles with the regulation of the university and meets the accepted standards with respect to originality and quality.

Signed by final examining committee:

Dr. Subhash Rakheja Chair

Dr. Rama Bhat Examiner

Dr. Wei-Ping Zhu External to the department

\_\_\_\_\_ Co-supervisor

Dr. Muthukumaran Packirisamy Co-supervisor

Approved by

\_\_\_\_\_  
Graduate Program Director

\_\_\_\_\_  
Dean of Faculty

Date

\_\_\_\_\_

## **Abstract**

### **Additive Manufacturing of Free Standing Structure from Thermally Cured Resins**

3D printing or Additive Manufacturing is a class of manufacturing processes for creating three-dimensional objects. In an additive manufacturing process, an object is fabricated by printing multilayers of material successively until the final desired size of an object is obtained. The 3D printing technology can be used for both rapid and functional prototyping as well as small batch production. Stereolithography, Selective Laser Sintering and Fused Deposition Modeling are three common technologies for 3D printing of plastics which employ photosensitive resins or thermoplastic materials as a printing material. Laser and heat are the energy sources in these technologies.

In this research, a novel additive manufacturing technology using high intensity ultrasound as the energy source is introduced. Commercial thermally cured resin will be employed as a printing material. For a better understanding of developing a method for 3D printing of this kind of resin, the numerical analysis of the process is performed. In order to get familiar with the 3D printing process, a simple CAD model of an object is printed using one of the commercial 3D printers which work based on the stereolithography technology. Using the simulation results and finding the quality of 3D printed parts produced by a mentioned standard 3D printer, the employed setup for performing experiments will be introduced. Then, the obtained results from experiments are presented. Experiment results are utilized to find the optimum condition for performing the 3D printing with this new technology. Therefore, by applying the optimum conditions and using selected resin, a simple 3D object will be printed. The printing process takes about 10 minutes which is the fastest time for 3D printing. Measured dimensions of a product show that the resolution of printed part is affected by a size of a focal region, accuracy in determination of its location during the process, and streaming inside the cavity.

*To my beloved wife*  
*Nastaran*

## **Acknowledgment**

I would like to express my gratitude, first and foremost, to my advisor Professor Muthukumaran Packirisamy for letting me to be a part of his Optical-Bio Microsystems group. I am honored working under his supervision as a member of the 3D printing team, which has been working on a novel and cutting-edge technology. Dr. Packirisamy has mentored and directed me throughout the obscure and foggy path of the research. His positive attitude towards the burden of the scientific problem solving has inspired me to be creative and accomplish meaningful research.

Another person to whom I am immensely debtor is Dr. Mohsen Habibi, the research associate in the Optical-Bio Microsystems Lab, who has been involved completely in project and never hesitated to help me for accomplishing the project. I must also express my appreciation for assistance of my colleagues in this project including Vahid Karamzadeh and Mahdi Derayatifar.

At the end, I would like to thank my wife and kids for their unconditional supports and patience throughout my graduate study.

## CONTENTS

List of Figures	ix
List of Tables	xiii
Nomenclature	xiv
CHAPTER 1 INTRODUCTION AND LITERATURE REVIEW.....	1
1.1. Emergence and evolution of 3D printing.....	1
1.2. Additive manufacturing processes.....	2
1.3. 3D Microfabrication.....	3
1.4. Advantages and disadvantages of different AM technologies.....	4
1.5. 3D printing materials.....	5
1.6. Energy sources in 3D printing processes.....	6
1.7. High intensity focused ultrasound.....	6
1.8. Objective of research.....	7
1.9. Contributions.....	8
CHAPTER 2 EXISTING ADDITIVE MANUFACTURING TECHNOLOGIES.....	10
2.1. Direct Metal Deposition.....	11
2.2. Selective Laser Sintering.....	12
2.3. Selective Laser Melting.....	13
2.4. 3D Printing.....	13
2.5. Laminated Object Manufacturing.....	14
2.6. Stereolithography.....	15
2.7. Fused Deposition Modelling.....	16
2.8. Dispensing 3D printing.....	16
2.9. Conclusions.....	17

CHAPTER 3	HIFU NUMERICAL ANALYSIS, THEORY AND SIMULATION .....	18
3.1.	Acoustics.....	18
3.2.	Governing equations.....	21
3.3.	Numerical analysis.....	23
3.4.	Results.....	27
3.5.	Conclusions.....	39
CHAPTER 4	COMMERCIAL 3D PRINTERS .....	40
4.1.	3D printers working with plastics as printing materials .....	40
4.2.	3D printing of a free standing structure and setup .....	42
4.3.	Results.....	45
4.4.	Conclusions.....	49
CHAPTER 5	DESIGN AND INSTALLATION OF HIFU 3D MANUFACTURING ....	50
5.1.	HIFU transducer and pulse generator .....	51
5.2.	CNC machine.....	51
5.3.	Temperature measurement system.....	52
5.4.	Resins.....	54
5.5.	Tank and liquid cavity .....	58
CHAPTER 6	EXPERIMENTAL RESULTS AND DISCUSSION.....	59
6.1.	Experimental conditions .....	59
6.2.	Determination of focal region's location and size .....	59
6.3.	Temperature measurement inside water .....	65
6.4.	Curing of PDMS inside liquid cavity.....	67
6.5.	Temperature measurement at focal region inside PDMS .....	68
6.6.	Final printed product.....	70

6.7.	Elastic behavior of 3D printed cantilever beam.....	72
6.8.	Conclusions.....	79
CHAPTER 7	CONCLUSIONS AND FUTURE WORKS .....	81
REFERENCES	.....	83

## List of Figures

**Figure 1-1** Configuration of HIFU transducer

**Figure 2-1** Additive Manufacturing Processes Categories

**Figure 2-2** Schematic of Direct Metal Deposition Process

**Figure 2-3** Schematic of SLS process

**Figure 2-4** Schematic of Selective Laser Melting Process

**Figure 2-5** Schematic of 3D printing process for metals

**Figure 2-6** Schematic of LOM process

**Figure 2-7** Schematic of Stereolithography (SLA) Process

**Figure 2-8** Schematic of FDM process

**Figure 2-9** Schematic of dispensing 3D printing process

**Figure 3-1** Wave incident at two liquid interface and generated reflected and transmitted waves

**Figure 3-2** 2D Axisymmetric Model Implemented in Simulation

**Figure 3-3** Generated acoustic pressure fields by applying different input powers at frequency of 2.15 MHz

**Figure 3-4** Change in Maximum Pressure Wave at Focal Point with respect to Input Power

**Figure 3-5** Generated acoustic intensity fields by applying different input powers at frequency of 2.15 MHz

**Figure 3-6** Acoustic intensity profile along the symmetrical line for different input powers

**Figure 3-7** Acoustic pressure amplitude profiles for different input powers along the symmetrical line at frequency of 2.15 MHz

**Figure 3-8** Acoustic pressure amplitude profiles for multiple input powers along the radial line which passes through the focal point at frequency of 2.15 MHz

**Figure 3-9** The temperature distributions at time equal to 1(s) inside the water for different input powers and with insonation at frequency of 2.15 MHz

**Figure 3-10** The heat transfer over a period of 10 seconds inside the water

**Figure 3-11** Pressure field in the water at frequency of 2.15 MHz and input power of 218 W

**Figure 3-12** Intensity field in the water at frequency of 2.15 MHz and Input power of 218 W

**Figure 3-13** Heat transfer in a period of 10 seconds inside the water in presence of 2 different dividers at frequency of 2.15 MHz and input power 218 W

**Figure 3-14** Pressure field in the liquid cavity at frequency of 2.15 MHz and input power of 218 W in presence of Polystyrene divider

**Figure 3-15** Intensity field in the liquid cavity at frequency of 2.15 MHz and input power of 218 W in presence of Polystyrene divider

**Figure 3-16** Temperature field in the liquid cavity at frequency of 2.15 MHz and input power of 218 W in presence of polystyrene divider

**Figure 4-1** “LulzBot TAZ” FDM 3D printer and a “Flange” prototype printed with this machine

**Figure 4-2** “ProX SLS 6100” SLS 3D printer and a “Engine Body” printed with this technology

**Figure 4-3** “Form 2” SLA 3D printer and three different small prototypes of “Gears” built by this printer

**Figure 4-4** CAD models of designed cantilevers (all dimensions are in mm)

**Figure 4-5** Postcured parts – Printed in different directions with respect to the platform

**Figure 4-6** The direction of roughness measurement, and measured roughness over the length of printed cantilevers

**Figure 4-7** Schematic for layer-by-layer printing of a 3D object

**Figure 5-1** Schematic of experimental setup

**Figure 5-2** CNC machine used in this research and its axes of movements

**Figure 5-3** Viscosity vs Time for a thermoset resin material

**Figure 6-1** Schematic of the setup used for determination of focal location and effect of power on its size

**Figure 6-2** Rising up the surface of the water while running the transducer with

**Figure 6-3** Change in the size of the spindle's girth due to decreasing the applied input power

**Figure 6-4** Schematic of setup for using thermochromic sheet

**Figure 6-5** Focal region appearance on the thermochromic sheet that has been positioned along the vertical symmetrical plane of transducer

**Figure 6-6** Schematic of setup (Top View) in presence of Acrylic sheet in order to define the focal region's size

**Figure 6-7** Focal region sections appeared by burning the acrylic sheet

**Figure 6-8** Setup for positioning the thermocouple inside water tank

**Figure 6-9** Temperature profile at focal point inside water for 1 (s) sonication with input power of 218 W

**Figure 6-10** Schematic configuration of setup for printing the PDMS

**Figure 6-11** Sequence of building the layers

**Figure 6-12** Embedded thermocouple inside PDMS cavity to measure the temperature during sonication

**Figure 6-13** The heat transfer over a period of 10 seconds inside the PDMS resulted from experiment

**Figure 6-14** Directly 3D printed cantilever beams

**Figure 6-15** Selected cantilever with its average dimensions

**Figure 6-16** Preparation of box for fabrication of PDMS mold

**Figure 6-17** Fabricated PDMS mold

**Figure 6-18** Two side views of fabricated PDMS cantilever with an appendage to help for pulling out the part from the mold

**Figure 6-19** Schematic of employed balance method to obtain the stiffness of cantilevers

**Figure 6-20** Balance method setup for measuring the force on the tip of the cantilevers

**Figure 6-21** Force-Deflection graph for directly 3D printed cantilever and indirectly molded PDMS cantilever

**Figure 6-22** Linear graphs of force-deflection for 3D printed cantilever and PDMS cantilever

## List of Tables

**Table 1-1** Advantages and disadvantages of different AM technologies

**Table 3-1** Characteristics of HIFU transducer

**Table 3-2** Material Properties of Dividers

**Table 3-3** Liquid's Properties

**Table 3-4** Length of focal region through different frequencies

**Table 4-1** Characteristics of “Form 2” Flexible Resin

**Table 4-2** Dimensional comparison between the designed and printed samples

**Table 5-1** HIFU transducer's characteristics

**Table 5-2** Characteristics of the CNC machine

**Table 5-3** Specification of DAQ NI 9212

**Table 5-4** Thermocouples' specification

**Table 5-5** Liquid Crystal Specification

**Table 5-6** Selected resins' characteristics

**Table 5-7** Resin accelerator component

**Table 5-8** Sylgard resin component

**Table 5-9** Curing agent component

**Table 6-1** Material Properties of Acrylic Plastic

**Table 6-2** Optimized operation conditions of the printing

**Table 6-3** Dimensions of cantilevers (CAD designed and 3D printed)

## Nomenclature

AM	Additive Manufacturing
ABS	Acrylonitrile Butadiene Styrene
ASTM	American Society of Testing and Materials
CNC	Computer Numerical Control
DAQ	Data Acquisition System
EBDM	Electron Beam Direct Manufacturing
EFAB	Electrochemical Fabrication
FDM	Fused Deposition Modelling
FIB	Focused Ion Beam
HIFU	High Intensity Focused Ultrasound
LCVD	Laser Chemical Vapor Deposition
LIFT	Laser Induced Forward Transfer
LOM	laminated object manufacturing
MLS	Microlaser Sintering
MSL	Micro Stereolithography
PDMS	Polydimethylsiloxane
PML	Perfectly Matched Layer
PZT	Lead Zirconate Titanate
SDM	Shape Deposition Modeling
SLA	Stereolithography
SLM	Selective Laser Melting
SLS	Selective Laser Sintering
STL	Stereolithography

# CHAPTER 1

## INTRODUCTION AND LITERATURE REVIEW

3D printing or additive manufacturing (AM) is a class of manufacturing processes for creating three-dimensional objects. In an additive manufacturing process, an object is fabricated by printing multilayers of material successively until reaching the final desired shape of object. These layers form the final shape of the part, therefore, the resolution of printed object depends upon the layer thickness and type of energy or material projection on each layer. In AM processes material usage is more efficient than the traditional manufacturing methods which are based on subtractive process, cutting or drilling [1].

The 3D printing technology can be used for both rapid and functional prototyping as well as small batch production. The recent developments in 3D printing have increased their applications in a wide range of products in different industries such as automotive, aerospace, pharma & healthcare, fashion, and sports.

The 3D printed object's quality depends upon the type of technologies used for making solid object, the manufacturing process, and the material composition. In the following sections, additive manufacturing technologies and their characteristics are discussed in detail.

### 1.1. EMERGENCE AND EVOLUTION OF 3D PRINTING

In 1986 Chuck Hull conceptualized the idea of printing 3D objects and patented it as a stereolithography fabrication system [1]. In this method, an ultraviolet light laser is used for curing and adding layers of photopolymers. Sachs et al. [2] used mentioned patent for fabrication of a 3D part. They deposited a layer of base material such as powder on a substrate at first, then by selective deposition of binder at specific locations they made a layer of final part. This process is continued until formation of the object. At the end of the process, the unbounded materials are removed [2]. Later, Dr. Deckard developed a Selective Laser Sintering (SLS) technology, in which laser is used as a power source to sinter powdered material at points which have been defined by a 3D model [3]. Fused Deposition Modelling (FDM) technology was developed by S. Scott Crump in 1988. In this method, a range of materials including elastomers, ABS (acrylonitrile butadiene styrene), and investment casting wax are used to fabricate objects [4].

Seven years later, in 1995, Fraunhofer Institute developed another additive manufacturing process which is called Selective Laser Melting (SLM). In this process, like as SLS, thermal energy is provided by a laser or an electron beam which fuses selective regions of a powder bed according to the designed 3D model [5].

## **1.2. ADDITIVE MANUFACTURING PROCESSES**

Considering the mentioned technologies, American Society for Testing and Materials (ASTM) has categorized the additive manufacturing technologies based on 7 processes that are mentioned in the following [6]:

- 1- Material Jetting
- 2- Powder Bed Fusion
- 3- Binder Jetting
- 4- Direct Energy Deposition
- 5- Material Extrusion
- 6- Sheet Lamination
- 7- Vat Photopolymerization

Polyjet Process, SLS, Powder 3D Printing, Electron Beam Direct Manufacturing (EBDM), FDM, Laminated Object Manufacturing, and SLA are some examples of technologies based on mentioned processes respectively.

As a matter of fact, in all additive manufacturing technologies, the final part can be fabricated directly within a process or indirectly in combination with other traditional manufacturing techniques [1]. Selection of methods is performed upon the characteristics of parts.

In a direct process, the final part is produced directly with additive manufacturing machine. In this method, post processing will be applied in order to improve the surface finish of the component.

In some processes after fabrication of middle staged product which is called green part, further processes should be applied on it, then the final part will be produced. Sintering is an example of this kind of complementary processes. These processes are addressed as a Multi-stage process.

Indirect processes are the method in which additive manufacturing is combined with traditional manufacturing. For instance, the mold can be fabricated by using 3d printing technology which can be used for the casting process to produce the final part.

### **1.3. 3D MICROFABRICATION**

So far, the types of additive manufacturing technologies that have been widely utilized to produce complicated macro 3D components in the past decade were introduced. By applying some essential modifications and improvements proper to microfabrication characteristics to these technologies, fabrication of 3D microparts is also possible. There are 3 groups of additive manufacturing technologies that can be employed for fabrication of 3D micro-components [7].

The first group is scalable additive manufacturing that includes: micro stereolithography (MSL), microlaser sintering (MLS), inkjet printing processes, fused deposition modeling (FDM), and laminated object manufacturing (LOM). Since these technologies have been developed for fabrication of normal sized components, there are still some limitations on adaption of this category for micromanufacturing. But despite that, MSL can be identified as a promising approach for true 3D micromanufacturing in comparison with others.

The second group is 3D direct writing technologies. Although this category of technologies has been developed for 2D fabrication, some of them can be utilized for high resolution 3D microcomponents such as laser chemical vapor deposition (LCVD), focused ion beam (FIB), laser induced forward transfer (LIFT), and nozzle dispensing processes which includes a pump and syringe-based deposition. LCVD and FIB are more efficient technologies in order to be employed for 3D fabrication. Generally, bio 3D printers function based on a basic syringe/pump extrusion.

The third category of 3D micromanufacturing technology is the hybrid process. The shape deposition modeling (SDM) and electrochemical fabrication (EFAB) are additive manufacturing technologies that belong to this group. Additive and subtractive processes are used in SDM to produce microparts. EFAB employs electrochemical deposition and subtractive planarization to fabricate 3D microcomponent. EFAB is based on layer-by-layer process. This process is more applicable for 3D micromanufacturing among the third category.

#### 1.4. ADVANTAGES AND DISADVANTAGES OF DIFFERENT AM TECHNOLOGIES

Table 1-1 shows advantages and disadvantages of some different AM technologies which have been introduced so far [5-8].

**Table 1-1** Advantages and disadvantages of different AM technologies

No.	Technologies	Advantages	Disadvantages
1	Stereolithography (SLA)	<ul style="list-style-type: none"> <li>• Suitable for production of concept prototypes</li> <li>• Fast processing times</li> <li>• Good surface finish</li> <li>• Geometrical accuracy</li> </ul>	<ul style="list-style-type: none"> <li>• Just for non-metal materials such as resins or plastics</li> <li>• Requires support structures during printing</li> </ul>
2	Selective laser sintering (SLS)	<ul style="list-style-type: none"> <li>• Variety of materials that can be employed</li> <li>• suitable for functional prototypes and testing</li> <li>• No support structures are required</li> </ul>	<ul style="list-style-type: none"> <li>• Variety of metallic materials is narrow</li> <li>• An enclosed chamber is required</li> <li>• Metal sintering leads to porous and mechanically weak components</li> </ul>
3	Fused Deposition Modelling (FDM)	<ul style="list-style-type: none"> <li>• Inexpensive machines and materials</li> </ul>	<ul style="list-style-type: none"> <li>• Rough surface finish</li> <li>• High temperature process</li> </ul>
4	Laminated Object Manufacturing (LOM)	<ul style="list-style-type: none"> <li>• Suitable for processing of medium and large sized components</li> <li>• Wide choice of readily available materials in sheet form</li> </ul>	<ul style="list-style-type: none"> <li>• Possibility of poor layer bonding</li> <li>• Variable strength of the produced components in different directions</li> <li>• Various post processing is required</li> </ul>
5	3D Printing	<ul style="list-style-type: none"> <li>• High productivity</li> <li>• Good geometrical accuracy</li> <li>• No support structures are required</li> </ul>	<ul style="list-style-type: none"> <li>• Time-consuming post-processing operations are required</li> <li>• Furnace heating is required to eliminate the binder</li> <li>• Sintered part is porous</li> <li>• The low mechanical strength of produced parts</li> <li>• Limited choice of materials</li> </ul>
6	Electron Beam Direct Manufacturing (EBDM)	<ul style="list-style-type: none"> <li>• The layer can be fabricated in any orientation</li> <li>• Using variety of materials in powder form</li> <li>• Possibility for manufacturing large components and</li> <li>• Possibility for higher deposition rates</li> </ul>	<ul style="list-style-type: none"> <li>• Low geometrical accuracy</li> <li>• Requiring post-processing operations</li> </ul>
7	Polyjet	<ul style="list-style-type: none"> <li>• Fast process</li> <li>• The Possibility of using multiple materials</li> </ul>	<ul style="list-style-type: none"> <li>• Limited to materials with specific property such as low viscosity inks</li> </ul>

## 1.5. 3D PRINTING MATERIALS

Final mechanical properties of 3D printed parts, flexibility in design and fabrication are defined by properties of raw material [9]. Powder, filament, pellets, granules, resin etc., are different material types or states that are used in 3D printing. In addition, specific material types and material properties have been developed more precisely to suit the application. In following some of the popular types of AM materials are introduced.

- **Metals**

Metals are used in the form of powder. The most common types of metals are titanium, aluminum and cobalt derivatives. Stainless steel powder is one of the strongest metals for 3D printing.

- **Plastics**

In Fusion Deposition Modeling (FDM) process or sintering process nylon is used as a strong, flexible and durable plastic material. It can be in a filament or powder form. Nylon is naturally white but the color can be added to it also. It can be used as a bonding powder combined with aluminum powder to form Alumide which is used in SLS 3D printing.

ABS is another strong plastic which is available in filament form. Polylactic acid (PLA) is a biodegradable plastic material in forms of resin and filament that is employed in stereolithography and FDM processes respectively. Same as nylon it can be prepared in a variety of colors but it is not as flexible as ABS.

- **Ceramics**

The new group of material is ceramics. They can be used in stereolithography combined with the photosensitive liquid resin. The produced green part is needed to undergo sintering post-processing in order to obtain a final object.

- **Bio Compatible Materials**

A huge amount of researches are conducted in order to find and develop bio compatible materials for 3D printing of the parts. Even living tissue can be addressed as one of the 3D printing productions. Compositions of collagen, chitosan, hyaluronic acid, and alginate are widely being used in bio 3D printing [10]. Polydimethylsiloxane (PDMS) is another bio compatible material

that has been extensively used in medical applications such as tissue/organ on-a-chip devices and two-dimensional (2D) or three-dimensional (3D) cell culture. PDMS naturally is liquid resin and by adding a curing agent and exposing to heat becomes cured. It is transparent, gas permeable, and economical. PDMS is mostly used in dispensing 3D printing [11]. In this method, pure PDMS is not used individually, but its composition should be modified in order to utilize as 3D printing material [11].

## **1.6. ENERGY SOURCES IN 3D PRINTING PROCESSES**

3D printing process defines the type of material which can be used in AM technology and source of energy in each process could be different. Generally, in 3D printing processes light, laser or external heat are used to transform a raw material to the final part. The UV-light is used to activate a chemical reaction of photosensitive liquid material and starting the curing process. High energy laser, electron beam, or simple external heat source are employed to melt powder materials or plastic filaments.

Also in novel innovation which have been patented by Habibi and Packirisamy, high intensity focused ultrasound (HIFU) energy has been employed to polymerize the thermoset resins inside the chamber selectively. Polymerization of resin happens when the focused field interacts with liquid and causes to produce heat due to absorption of wave by material. The fabricated final part in this process has a layerless structure in contrast of 3D printed parts manufactured by so far mentioned conventional layer-by-layer processes. In addition, fast processing time is one of the main competitive factors of this technology. In this technology, focused ultrasound is produced by HIFU transducer. This is the first time that ultrasound energy is utilized in additive manufacturing. In following the HIFU and its common usages will be explained more.

## **1.7. HIGH INTENSITY FOCUSED ULTRASOUND**

High intensity ultrasound energy has been frequently employed as an operating energy in various devices for different applications. This energy can be used for plastic welding in automotive, electronic appliance, and medical equipment industries [12]. It also is being utilized in acoustic compressors, refrigerators, and other industrial processes [13].

In therapeutic methods for non-invasive ablation of tumors, high intensity focused ultrasound (HIFU) is used [14]. The possibility of performing treatment operation from outside of body on

a tissue is the main advantages of this method over other thermal ablation techniques [15]. Since ultrasound wave transfers through the materials such as liquids, targeting a specific point inside the medium by using HIFU is completely possible.

HIFU transducers are often formed as spherical or parabolic surfaces with a geometric focal point at a center of curvature. **Figure 1-1** illustrates the configuration of this kind of transducer.

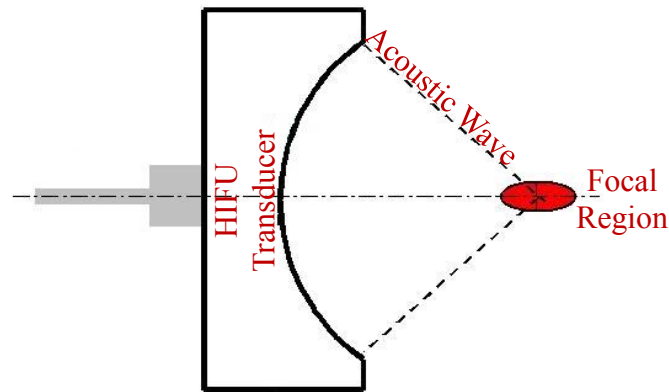


**Figure 1-1** Configuration of HIFU transducer

Mostly, transducers are made from PZT (Lead Zirconate Titanate) which is a piezoelectric ceramic material. The advantages of using a ceramic compared to other materials include ceramic's ability to be manufactured in different shapes and sizes and its capability of operating efficiently at low voltage. Piezoelectric transducers convert the electrical charges produced by their structural materials into energy. A piezoelectric ultrasonic transducer produces sound waves above the frequencies that can be heard by the human ear. It functions by rapidly expanding and contracting when appropriate electrical frequency and voltage is applied.

## 1.8. OBJECTIVE OF RESEARCH

The current research introduces an additive manufacturing technology using high intensity focused ultrasound as the energy source. As a result of investigations a thermally cured resin has been selected and printed directly without any additives. In fact, using pure thermally cured resin as a printing material can pave the way for new inventions in additive manufacturing using high intensity ultrasound.

In this work, after presenting more details about existing additive manufacturing technologies in Chapter 2, numerical analysis of HIFU wave propagation inside two Newtonian liquids water,

and a type of thermally cured resin, in presence of changes in physical properties of them as well as ultrasound source power will be performed in Chapter 3. It is believed that this physic brings a better understanding of developing a method for 3D printing of thermoset resins.

The applied acoustic pressure is generated by a HIFU transducer. This aperture concentrates pressure wave at a focal point and the following studies are performed in this region. As a matter of fact, analysis is done by implementation of basic governing equations for sound propagation and heat transfer. The result of acoustic study is heat energy due to absorbance of acoustic by the bulk of liquid during transmission of ultrasound. Therefore, heat transfer study can be performed in the time domain in presence of the computed heat source. Next, investigation of results is proceeded by implementing characteristics of multiple liquids in the simulation and altering acoustic source input parameters.

In Chapter 4, one of the standard 3D printers which has been fabricated based on Stereolithography technology will be introduced. Then, a simple designed sample will be printed by using this device. Dimensional precision and finishing quality are investigated after all.

By using the simulation results and finding the quality of 3D printed parts produced by one of the existing standard 3D printers, the employed setup for performing experiments in this work will be introduced in Chapter 5.

In Chapter 6, the obtained results from experiments will be presented. Discussion on experiment and simulation results will be done as well. By understanding the optimum condition for performing the 3D printing, a simple object will be printed by using selected resin. Finally, in order to find out the quality of the printing process, dimensional and finishing check will be performed.

The last chapter of this thesis is dedicated to concluding the findings and suggestions for future works.

## **1.9. CONTRIBUTIONS**

1. Sh.Foroughi, V.Karamzadeh, M.Packirisamy, “Design and Analysis of an Electro Thermally Symmetrical Actuated Microgripper”, ICME 2018:20th International Conference on Mechanical Engineering, Montreal, Canada, May 2018.

2. Sh.Foroughi, V.Karamzadeh, M.Habibi, M.Packirisamy, “Numerical Analysis of Acoustic Propagation inside Multiple Liquids”, 5th International Conference of Fluid Flow, Heat and Mass Transfer, Toronto, Canada, May 2018.
3. V.Karamzadeh, Sh.Foroughi, A.Sohrabi, M.Packirisamy, “Characterization of a 3D Printed Mold for a Cell Culturing Microfluidic Device”, 5th International Conference of Fluid Flow, Heat and Mass Transfer, Toronto, Canada, May 2018.
4. Sh.Foroughi, V.Karamzadeh, M.Habibi, M.Packirisamy, “Study the effect of lamilar orientation in layer-by-layer 3D printing for fabrication of free standing structure”, (Journal paper to be submitted).
5. V.Karamzadeh, Sh.Foroughi, and M.Packirisamy, “Characterization of a 3D Printed Mold for a Droplet Generation Microfluidic Device”, (Journal paper to be submitted).

# CHAPTER 2

## EXISTING ADDITIVE MANUFACTURING TECHNOLOGIES

In the previous chapter, a brief discussion on AM technology has been performed. In following detail characteristics of each technology will be introduced.

Additive Manufacturing (AM) is one of the best solutions for the fabrication of an object layer-by-layer. As it was mentioned due to the simplicity of working with plastic AM started with producing plastic parts in order to make a simple prototype. Today most of the materials are included in AM processes for instance even ceramic powders are utilized in SLA by Formlabs Company. In fact, based on material which is used in 3D printing operation the Additive Manufacturing processes can be divided into metal and non-metal categories. These categories are shown in **Figure 2-1**.

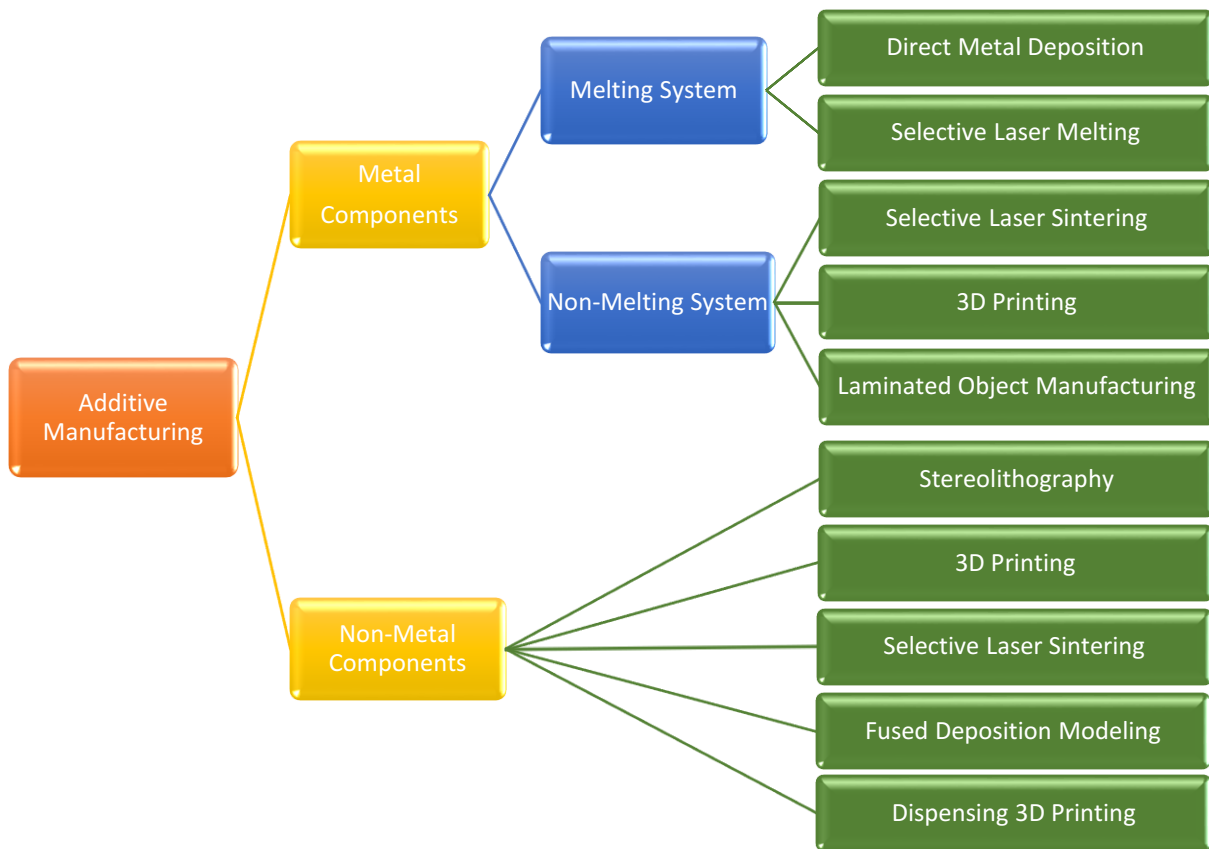


**Figure 2-1** Additive Manufacturing Processes Categories [16]

All AM techniques are based on the layer-by-layer fabrication approach. The first step in this fabrication includes the preparation of CAD model of the desired object. The CAD design is then transformed into a file format which is acceptable by the 3D printer. Normally files are generated in Stereolithography (STL) format. In this file format, the surfaces of a solid body are tessellated into triangles and geometrical properties of triangle nodes are kept in a database. Next, this database is mathematically cross-sectioned into small layers including a contour and a raster surface. Layer slicing separation depends on the characteristics of a specified 3D printing process. Finally, the 3D object will be printed layer by layer [17]. By considering mentioned steps to reach the final part, in following each 3D printing technologies is introduced in detail.

## 2.1. DIRECT METAL DEPOSITION

This technology is based on direct energy deposition process [18]. The basic working principle of Direct Metal Deposition is displayed in **Figure 2-2**. A high power laser beam is traveled over the metal substrate. In this process laser beam generates a small melt pool over the base then the powder is injected through a nozzle to a melting point which will be fused to the melt pool and be bonded with the last melted part. By continuing the process, a deposited layer over the substrate will be formed. The process is performed according to the pre-defined pattern which has been loaded to CNC system or robotic arm by using the proper software program. In this technology, the overlapping of melting tracks is used to create a layer and by stacking layers the three-dimensional shape will be formed [8].

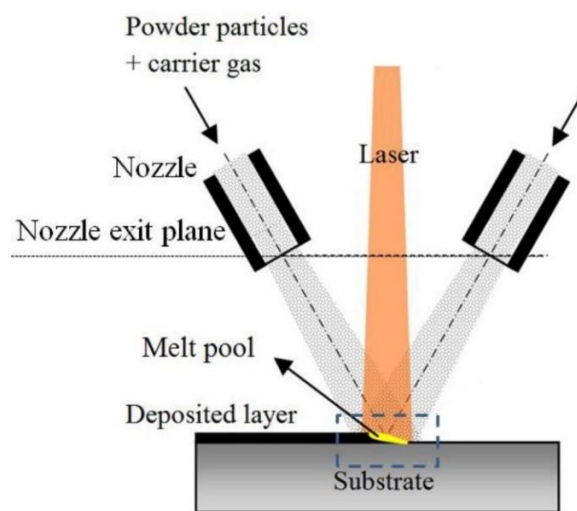


**Figure 2-2** Schematic of Direct Metal Deposition Process [19]

This process is also called as Laser Powder Fusion or Laser Direct Casting. In this technology fabrication of large components are possible but geometrical accuracy is low.

## 2.2. SELECTIVE LASER SINTERING

SLS is the most common additive manufacturing technology for industrial usages. In this technology, small particles of powder are fused by using a high-powered laser. Either metal powder or plastic powder can be used as a process material. Flatbed of powder is distributed over a movable substrate inside a small powder chamber. A predefined pattern will be scanned on the bed by moving a laser beam over the layer of power. Absorption of the laser energy by particles causes to a temperature rise of powder until reaching the sintering temperature. In this phase particles fuses to each other. **Figure 2-3** illustrates this process.

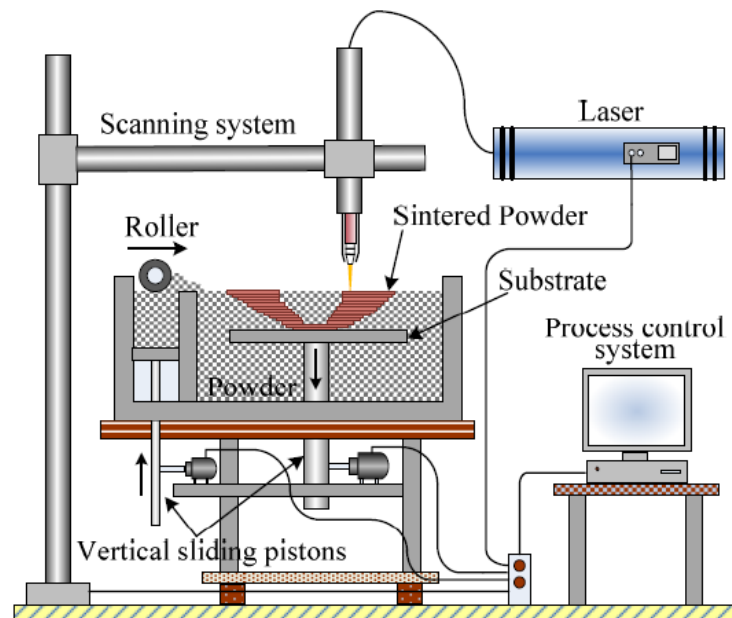


**Figure 2-3** Schematic of SLS process [20]

In SLS technology unfused powder supports the part, therefore, the need for support structures is eliminated. This makes SLS ideal for complex geometries with interior features, undercuts, thin walls, and negative features. SLS printed parts have excellent mechanical characteristics. These 3D printers are ideal for functional prototyping due to the low cost per part and high productivity characteristics of SLS [19].

### 2.3. SELECTIVE LASER MELTING (SLM)

This process is similar to SLS. The same as SLS, a laser beam scans over a bed of powder material which is mounted on a piston. After forming each layer, the piston is moved down equal to the desired thickness of the layer and a wiper tool deposits a new layer of powder material. This process is continued until forming the final part. **Figure 2-4** shows a schematic of this process.

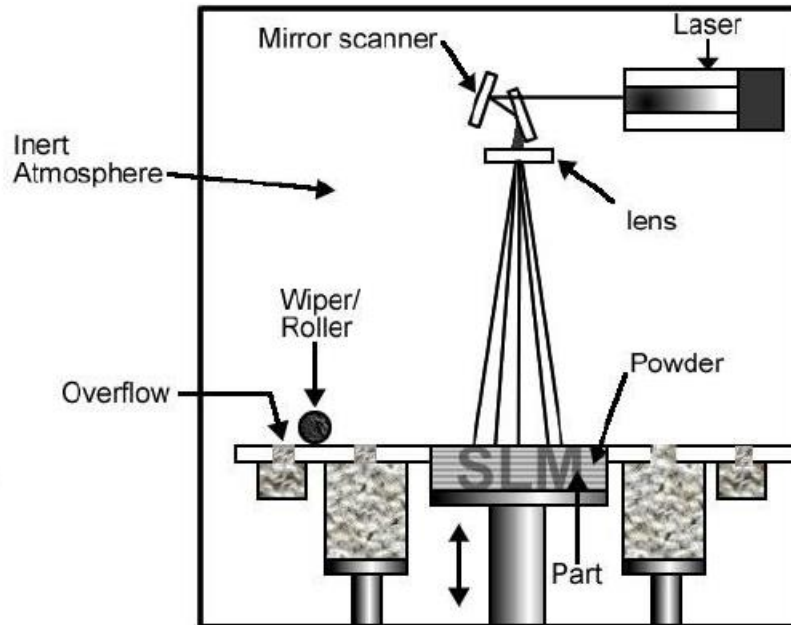


**Figure 2-4** Schematic of Selective Laser Melting Process [21]

### 2.4. 3D PRINTING

**Figure 2-5** presents the schematic of 3D printing process for metals. In this process after dispensing the powder by a roller over a movable platform, an inkjet printing head will print a binder over the powder bed based on the predefined pattern in order to build a layer. The same as previous processes the platform is moved down equal to the desired thickness of the layer. This process is continued until forming the final shape. In order to sinter the bounded metal particles and removing the binder, the produced part is put in a furnace. As a final post-process, the sintered part is infiltrated in a furnace using with a low-viscosity and low melting point material, such as copper [8].

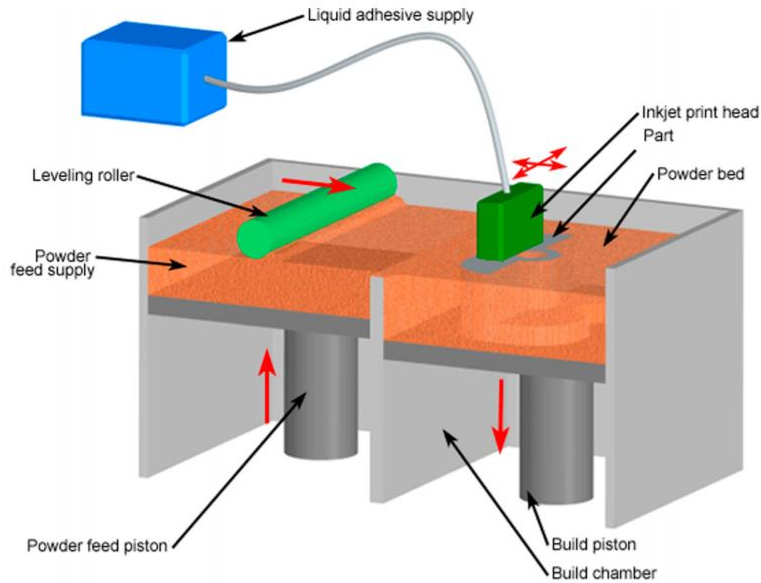


**Figure 2-5** Schematic of 3D printing process for metals [22]

## 2.5. LAMINATED OBJECT MANUFACTURING

The Laminated Object Manufacturing (LOM) process is based on stacking thin sheets of material in a suitable binding method. Each sheet is cut with a laser or cutter according to the predefined layer raster pattern. Paper, metals, plastics, fabrics, synthetic materials, and composites all are kind of materials that can be used in this process [23]. After cutting, all sheet layers are bonded together to form a three dimensional object. In fact, any material in sheet form can be utilized in this process but as it has been mentioned the suitable binding method should be considered. Making a 3D model by using paper layers and glue is the simplest example of this process [24]. **Figure 2-6** shows schematic of LOM.

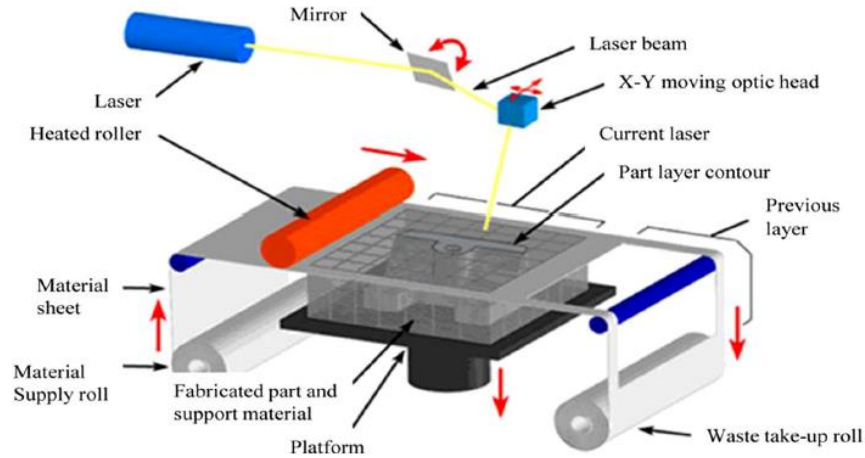


**Figure 2-6** Schematic of LOM process [24]

## 2.6. STEREOLITHOGRAPHY (SLA)

Stereolithography (SLA) is the first invented AM technology. In this process, a movable platform is submerged in tank which is filled with photo-curing resin. The height of resin over the surface of platform determines the layers' thickness. A layer will be built when the laser beam scans over the resin based on the CAD model STL file. The Laser beam is guided by galvo scanning mirrors. After finishing the curing of the layer, platform is lowered deep into the resin tank equal to the predefined height of each layer and the process is repeated and continues layer by layer until achieving the final shape of desired object. **Figure 2-7** shows the schematic of this process.

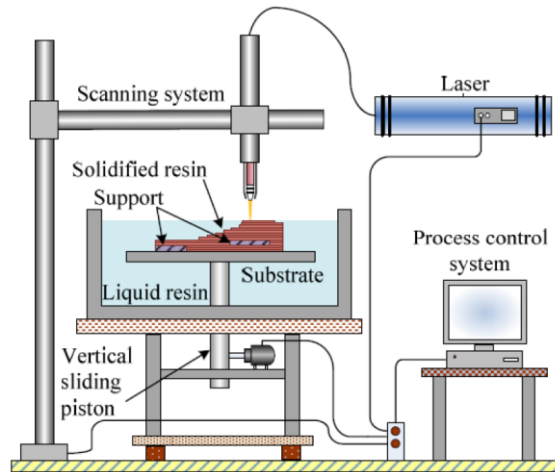


**Figure 2-7** Schematic of Stereolithography (SLA) Process [19]

Multiple laser cure resins have been manufactured for SLA 3D printers which have developed the application of SLA into different fields such as medicine. These materials cover a wide range of optical, mechanical, and thermal properties and are competitive with the standard and industrial thermoplastics.

## 2.7. FUSED DEPOSITION MODELLING (FDM)

Fused Deposition Modeling is the common form of 3D printing for rapid prototyping. In FDM 3D printers, printing starts by melting and extruding the thermoplastic filament. Then melted plastic is deposited layer by layer over the printing platform until building the part.

ABS and PLA are the common thermoplastics that are generally used in FDM printers. This technique is well-suited for printing a basic model as well as low-cost simple parts. **Figure 2-8** illustrates this process.

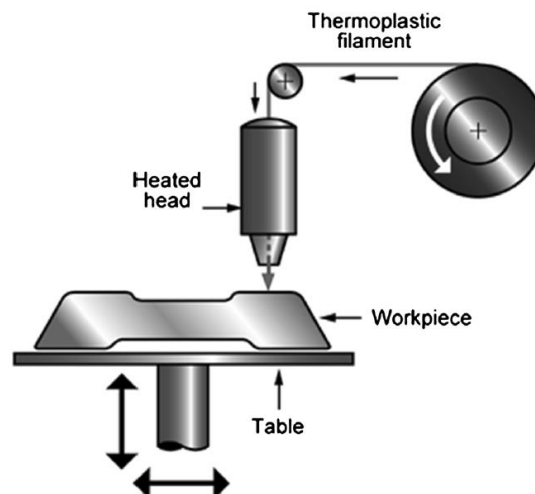


**Figure 2-8** Schematic of FDM process [25]

## 2.8. DISPENSING 3D PRINTING

Dispensing 3D printing originated from FDM technology and is classified under the category of extrusion process. This technology has been used in various fields but the main application of this technology is in biotechnology and organ-printing technology [26]. Unlike the SLA technology in dispensing additive manufacturing, the 3D part is fabricated directly with extruded material which dispenses from the nozzle.

This technology is based on layer-by-layer process. The 3D object is designed in a CAD software and is subdivided to 2D patterns with a specific thickness which is identified based on the specification of 3D printer machine. After loading the material into a syringe or dispensing equipment, plane patterns are stacked up in a layer-by-layer process, to build a final 3D object. The dispensing system includes a heater and/or cooler parts as well as dispenser which control the flow rate of material by applying the pressure. Although the application of this method is limited to the viscosity of the printing material, simplicity in use, the absence of post-processing and simple drive-mechanism parts are advantages of this technology in comparison with others [26]. **Figure 2-9** displays the schematic of this process.

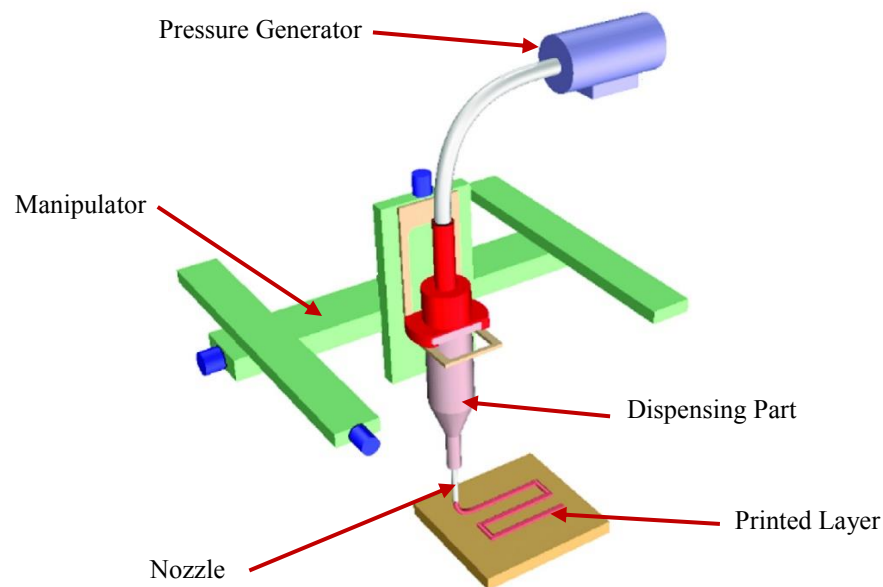


**Figure 2-9** Schematic of dispensing 3D printing process [27]

## 2.9. CONCLUSIONS

In this chapter existing additive manufacturing methods have been introduced. As it has been mentioned, powders made of either plastic or metal, plastic fibers, and photosensitive resins are the most common materials that are used in these technologies. They work based on layer-by-layer process and either high energy laser, simple external heat source or UV-light is employed to perform the process of fabrication. In this research the photosensitive resin and mentioned energy sources will be substituted by thermally cured resins and HIFU energy respectively. Therefore, in order to get familiar with the process of this new method numerical analysis of the problem will be performed in next chapter.

# CHAPTER 3

## HIFU NUMERICAL ANALYSIS, THEORY AND SIMULATION

In order to achieve the inclusive overview of the expected experimental results, numerical simulation of the problem, at first step, is a promising method to validate the accuracy of approaches. Therefore, in this research before carrying out the experiments on sound propagation inside the liquid media, numerical simulation and analysis of the problem will be performed in advance. In the following context, after introducing the acoustics and its characteristics, the governing equations will be explained. Next, the methodology of numerical analysis for problem's simulation will be described. Finally, investigation of results will be proceeded by implementing characteristics of multiple materials in the simulation.

### 3.1. ACOUSTICS

The sound is generated by oscillation of an object as a source inside the physical medium. Sound waves are either longitudinal or transverse. Longitudinal acoustic waves are waves which are produced by changing the pressure from equilibrium state. In other definition, when the wave motion is in direction or opposite direction of energy moving, the wave is called longitudinal while transverse waves are generated due to altering the sheer stress perpendicular to the wave transmission direction. Inside fluids and solids, sound propagates as a longitudinal or compression wave. Also, the transverse or shear waves transmit in solids. For instance, in the air sound is a longitudinal wave where the wave motion is in direction of the movement of energy. When the air is influenced by an oscillating object, speaker as an example, starts to follow the motion behavior of the speaker's cone. As the cone moves forward, the air is compressed that causes increasing the air pressure. In reverse, when the cone moves back and passes its static position the air pressure will reduce. In fact, along with the harmonic sinusoidal shape of the longitudinal acoustic wave, crests and troughs represent the maximum and minimum pressure respectively. In a solid medium, sound propagation happens by a small-amplitude elastic vibration of solid's shape [28, 29].

### 3.1.1. ACOUSTIC WAVE CHARACTERISTICS

Acoustic waves are often characterized by the following properties:

1. Frequency and Period
2. Wavelength and Amplitude
3. Speed of sound
4. Intensity

These parameters are the fundamentals that distinguish waves from each other. One of the forms of the sound is Ultrasound. Ultrasound is no different from the normal sound in physical properties except its frequency is higher than the audible limit of human hearing and is approximately 20 kilohertz (KHz).

As a matter of fact, the acoustic wave transports its energy during traveling through the medium. The energy of a sound wave per unit volume is called the energy density. The energy flow due to sound wave movement is characterized by the sound intensity and also called energy flux density [29]. Sound intensity describes the rate of energy flow through a unit area.

Acoustic waves can pass through one or multiple mediums. Different physical properties of mediums cause to alter the speed and intensity characteristics. For instance, during traveling the sound wave between two different liquids, reflection, and refraction of pressure waves at the interface will happen. In this process, the amplitudes of the transmitted and reflected waves are only the function of Acoustic Impedance. The meaning of the term impedance is resistance. Acoustic impedance is defined as a ratio of a sound pressure (in complex form) to an oscillation velocity which almost is used to describe the acoustic wave propagation. In the propagation of a plane harmonic wave in liquids, acoustic impedance is calculated by the following formula:

$$z = \frac{p}{V} = \rho c \quad (3-1)$$

where  $z$  is acoustic impedance,  $p$  complex form of sound pressure,  $V$  is the vibration velocity,  $\rho$  is the density of the liquid medium and  $c$  is the velocity of sound in liquid. Acoustic impedance characterizes a medium of wave propagation [30].

When an acoustic wave strikes an interface between two liquid media part of the wave will transmit and refract through the second media and the rest will reflect. **Figure 3-1** shows the geometry of the process.

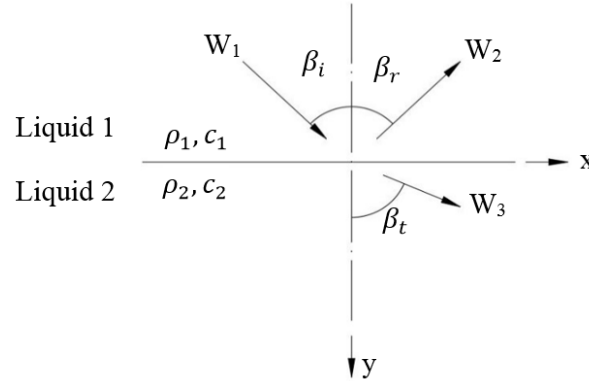


**Figure 3-1** Wave incident at two liquid interface and generated reflected and transmitted waves

$\beta_i$ ,  $\beta_r$  and  $\beta_t$  are the angle of incident, reflection and transmission, respectively. In this figure,  $\rho$  is the density of the liquid medium and  $c$  is the velocity of sound in liquid. The magnitude of the transmitted wave angle with the normal vector of interface plane is dependent on the wave speeds in each media and the angle of incident [31]:

$$\frac{\sin \beta_i}{c_1} = \frac{\sin \beta_t}{c_2} \tag{3-2}$$

Equation “3-2” is called Snell’s Law for acoustic waves.

In reality, acoustic wave’s energy is dissipated during propagating through the medium. This process is defined as attenuation [30]. Generally, the source of attenuation in materials are:

- Attenuation due to grain scattering
- Attenuation due to absorption

Energy loss due to grain scattering comes from the scattering of incident wave in different directions that results in increasing the net loss of amplitude with distance in propagation’s direction. In contrast, the absorption attenuation is the energy loss due to the conversion of wave energy to heat during wave movement in medium. This type of material’s attenuation typically

varies with the frequency of the wave passing through the material. For example, in water at room temperature the attenuation can be determined by the following relation [31]:

$$\alpha_w(f) = 25.3 \times 10^{-15} f^2 \left( \frac{Np}{m} \right) \quad (3-3)$$

where  $f$  is the frequency in  $Hz$  and the unit of  $\alpha_w$  is Nepers (Np) per meter.

As it has been mentioned in Chapter 1, in HIFU transducers the intensity of ultrasound wave is focused at a certain location which is called focal point. Focal region is one of the characteristics that determines the application of transducer. Normally the size of focal region is altered by changing the magnitude of wave's frequency and can be calculated by using the following equation [32]:

$$F_r = \frac{8 \times F_t^2 \times c}{D_t^2 \times f + 2F_t \times c} \quad (m) \quad (3-4)$$

where  $F_r$  is the focal region size,  $F_t$  is focal length of transducer in (m),  $D_t$  is the transducer's diameter in (m),  $c$  is velocity of the sound in medium in  $\left(\frac{m}{s}\right)$  and  $f$  is the frequency of the acoustic wave generated by transducer in (Hz).

## 3.2. GOVERNING EQUATIONS

### 3.2.1. ACOUSTICS EQUATION

In an ideal fluid, the equation of wave can be obtained by using conservation of mass equation, Euler's equation and the adiabatic equation of state. By retaining the only first-order terms in these equations the linear wave equation is achieved [33]:

$$\nabla^2 \mathbf{p} - \frac{1}{c^2} \frac{\partial^2 \mathbf{p}}{\partial t^2} = 0 \quad (3-5)$$

where  $\mathbf{p}$  is the pressure and  $c$  is the sound speed. This equation is represented in time domain since by using frequency–time Fourier transform the equation in the frequency domain will be obtained [28,33]:

$$\frac{1}{\rho \omega^2} \left[ \nabla^2 + \left( \frac{\omega}{c} \right)^2 \right] \mathbf{p}(r, z) = 0 \quad (3-6)$$

which is presented in the cylindrical coordinate. In this relation  $\omega$  is angular velocity,  $\mathbf{p}$  is an acoustic pressure and  $\rho$  is the fluid's density. Equation "3-6" represents homogeneous form of linear Helmholtz equation. In axisymmetric cylindrical coordinate  $\nabla^2$  is defined as:

$$\nabla^2 = \frac{1}{r} \frac{\partial}{\partial r} r \frac{\partial}{\partial r} + \frac{\partial^2}{\partial z^2} \quad (3-7)$$

As it has been mentioned so far, the major effect of acoustic propagation inside liquid is the thermal energy produced due to absorption of ultrasound wave by liquid that yields to rising medium temperature. The temperature distribution depends on a convection and conduction properties of the liquid. The amount of generated ultrasound power per unit volume  $\mathbf{Q}_A$  is obtained by applying the following expression [34]:

$$\mathbf{Q}_A = 2\alpha_{Ab}I \quad (3-8)$$

where,  $\alpha_{Ab}$  is the local absorption coefficient or attenuation of the liquid,  $I$  is the local acoustic intensity.

Considering having a time-harmonic wave the  $I$  can be given by:

$$I = \frac{1}{\omega^2 \rho c} \left\langle \left( \frac{\partial P_1}{\partial t} \right)^2 \right\rangle \quad (3-9)$$

where  $\omega$  is angular velocity,  $P_1$  is the first-order approximation of acoustic pressure,  $\rho$  is the fluid's density,  $c$  is the sound speed, and the brackets defines a time average over one acoustic cycle.

### 3.2.2. HEAT TRANSFER EQUATION

In Section 3.1.1 it was indicated that the absorption attenuation of a fluid causes the energy loss due to the conversion of wave energy to heat during wave movement in medium. Therefore, to investigate the effect of generated heat energy in an incompressible liquid media of wave propagation without considering the effect of viscosity, the following equation is used to model the heat transfer [35]:

$$\rho C_p \frac{DT}{Dt} = -(\nabla \cdot \mathbf{q}) + \mathbf{Q}_A \quad (3-10)$$

where  $\rho$  is the density of liquid,  $C_p$  is the specific heat capacity at constant pressure,  $T$  is the absolute temperature,  $q$  is the heat flux from conduction, and  $Q_A$  is an additional heat source due to acoustic pressure. The term  $(\nabla \cdot q)$  governs the thermal diffusion through the fluid and can be expanded as  $k\nabla^2 T$ . In which  $k$  is the thermal conductivity of the fluid.

Therefore, the final form of Equation “3-10” for incompressible fluid will be:

$$\rho C_p \frac{DT}{Dt} = -k\nabla^2 T + Q_A \quad (3-11)$$

By solving this equation temperature distribution through the liquid media can be determined.

### 3.3. NUMERICAL ANALYSIS

So far governing equations of acoustic wave propagation inside a liquid media have been introduced. Therefore, to solve the equations and for determination of the acoustic effects, pressure and temperature distributions as well as intensity, in liquid media, a finite difference analysis will be performed by using COMSOL Multiphysics 5.2 in a two-step process:

1. Solving acoustic Equation “3-6” in frequency domain in absence of nonlinear acoustic wave propagation effects to find acoustic pressure distribution as well as heat energy due to absorption of sound wave by liquid.
2. Obtaining temperature distribution by solving heat transfer Equation “3-11” incorporated with computed heat source from acoustic stage, in time domain. This heat energy will apply during 1 second in simulation. Multiple time steps are considered in order to assure the accuracy of computation. The final results are presented for 0.1 second time step in total process duration of 10 seconds to illustrate the temperature propagation inside the liquids.

In COMSOL, pressure acoustics physics in a frequency domain study, as well as Heat Transfer physics in a time domain study, will be used to perform the simulation.

#### 3.3.1. MODEL

The model includes two parts: Acoustic apparatus and Fluid container. In this study, as it has been indicated so far, a high intensity focused ultrasound (HIFU) transducer has been selected as a sound source. The fluid container is divided into two compartments, one is liquid cavity which contains the liquid of experiment that the focal point will be placed at there and another part is

filled by pure water which provides medium for operation of transducer. In experiments, liquid cavity will be a closed plastic container which is filled by the liquid of experiment. Since, only the front face of this container has an interaction with the transmitted acoustic waves and acts as a barrier, from now on this face will be called a divider.

It is assumed that the geometry of model elements is symmetrical and water medium has uniform acoustic properties. Therefore, 2D axisymmetric assumption for acoustic field model will be an acceptable approximation that leads to reduce computation time. The COMSOL model of a system under investigation and its components are shown in **Figure 3-2**. The 5mm perfectly matched layers (PML) region are considered in model to absorb the outgoing acoustic waves.

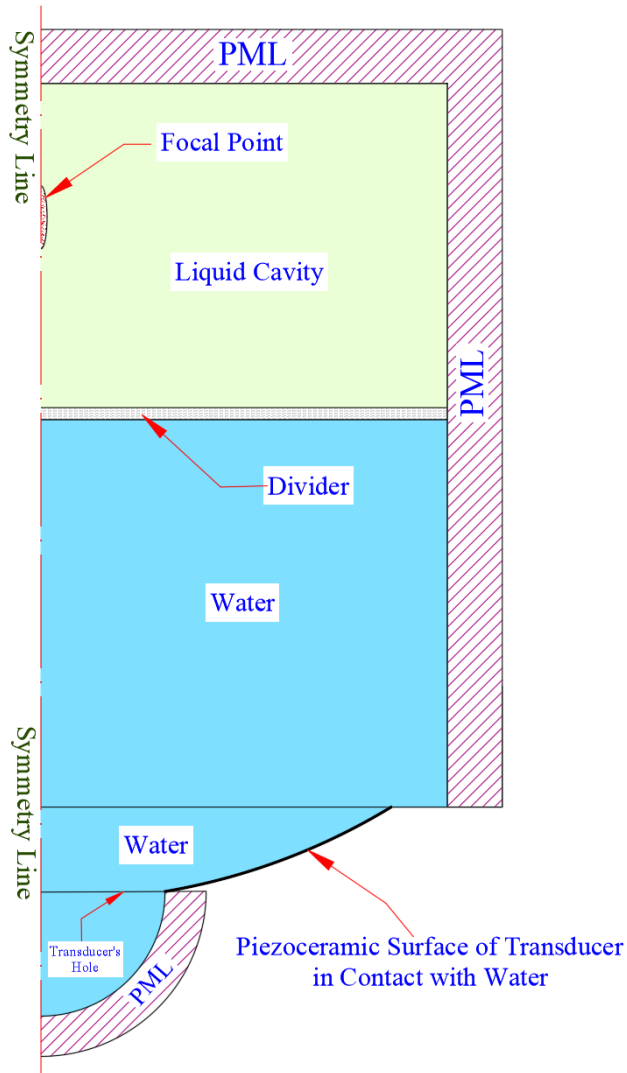


**Figure 3-2** 2D Axisymmetric Model Implemented in Simulation

In this figure, the liquid cavity and divider sheet has a rectangle shape in a size of 42mm x 35mm (width x height) and 42mm x 1.1mm (width x height) respectively. Forty-one-millimeter height rectangle in a width of 42 mm has been considered as a space between sound source and divider sheet. This part and the rest of the remained spaces will be filled by the pure water.

The sound source specification has been displayed in **Table 3-1**. This device is a spherically focused piezoceramic transducer and the focal region has an oval shape. This type of HIFU transducer is used in biomedical applications and need to be immersed in water during operation for transmitting the wave to the target medium. This transducer has a hole at the center.

**Table 3-1** Characteristics of HIFU transducer

Frequency (MHz)	Focal Length (mm)	Aperture Diameter (mm)	Hole Diameter (mm)	Input Powers (Watts)	Power Efficiency (%)
2.15	63.2	64	22.6	218, 131, 67	85

The simulation of pressure acoustics is implemented in all domains. But because of the small size of the focal region compare to the size of the liquid cavity the heat transfer simulation is performed only in the liquid cavity domain.

### 3.3.2. MESH CONFIGURATION

To obtain accurate results from numerical analysis of acoustics pressure, the fine triangular meshes with size  $\lambda/6$  ( $\lambda$  is the wavelength of the acoustic wave) and coarser triangular meshes with size  $\lambda/4$  are chosen for the focal region and the rest of domain respectively [28]. For heat transfer simulation, the entire liquid cavity is meshed with the triangular elements with a size of  $\lambda/8$ .

### 3.3.3. CALCULATIONS AND CASE STUDIES

Acoustics pressure and heat transfer studies of the model is performed by using COMSOL Multiphysics 5.2. Three case studies have been considered to investigate the effect of altering input parameters such as power and material properties on wave pressure and temperature. Each case is described as follow:

### Case Study No.1:

In this case study, the size of focal region will be calculated. Then, in the absence of a divider, multiple powers are applied in the simulation. Therefore, the effect of altering power on pressure wave and temperature field will be reported.

### Case Study No.2:

Case study no.2 includes applying multiple dividers' material in the simulation. As a result, the effect of changing material property on pressure wave and temperature field will be illustrated in figures.

### Case Study No.3:

In this case, multiple liquids in presence of divider will be implemented in simulation. Therefore, the effect of altering liquid's property on pressure wave and temperature field will be reported.

### 3.3.4. INPUT DATA

In addition to the transducer's characteristics, material properties of dividers and liquids should be gathered for accomplishment of input data. In this work, PDMS (Polydimethylsiloxane) resin as well as water have been selected as a liquid of experiments by which the liquid cavity will be filled. The reason for selection of PDMS will be discussed in detail in section 5.4. Divider's material is chosen as either Polystyrene or ABS. In **Table 3-2** and **Table 3-3** material properties of dividers and liquids have been identified respectively.

**Table 3-2** Material Properties of Dividers [36]

Material	Density (kg/m <sup>3</sup> )	Sound Speed (m/s)	Acoustic Impedance (kg/m <sup>2</sup> .s)	Attenuation (Np/m) @ 2.15 (MHz)	Thickness (mm)
ABS, grey	1070	2170	$2.32 \times 10^6$	24.060	1.1
Polystyrene, GP	1050	2400	$2.52 \times 10^6$	3.991	1.1

**Table 3-3** Liquid's Properties [37-40]

Liquid	Density (kg/m <sup>3</sup> )	Specific Heat (J/kg.°C)	Heat Conductivity (W/m.°C)	Sound Speed (m/s)	Attenuation (Np/m) @ 2.15 MHz
Fresh Water @ 21°C	997	4180	0.6076	1483.6	0.115
PDMS 10:1 @ 25°C	1030	1464	0.27	1055	27.55

Attenuation of water for different wave frequencies is measured using Equation “3-3”. Attenuation of PDMS resin with the ratio of 10:1 has not been reported in the literatures. Since the PDMS is a silicon base material, the attenuation of similar silicon material “DC 710 Silicon Oil” which is determined according to the following equation has been implemented in the simulation.

$$\alpha_s(f) = 7.3 f^{1.79} \left( \frac{Np}{m} \right) \quad (3-12)$$

where  $f$  is the frequency in *MHz* and  $\alpha_s$  is in Nepers (Np) per meter [41].

### 3.4. RESULTS

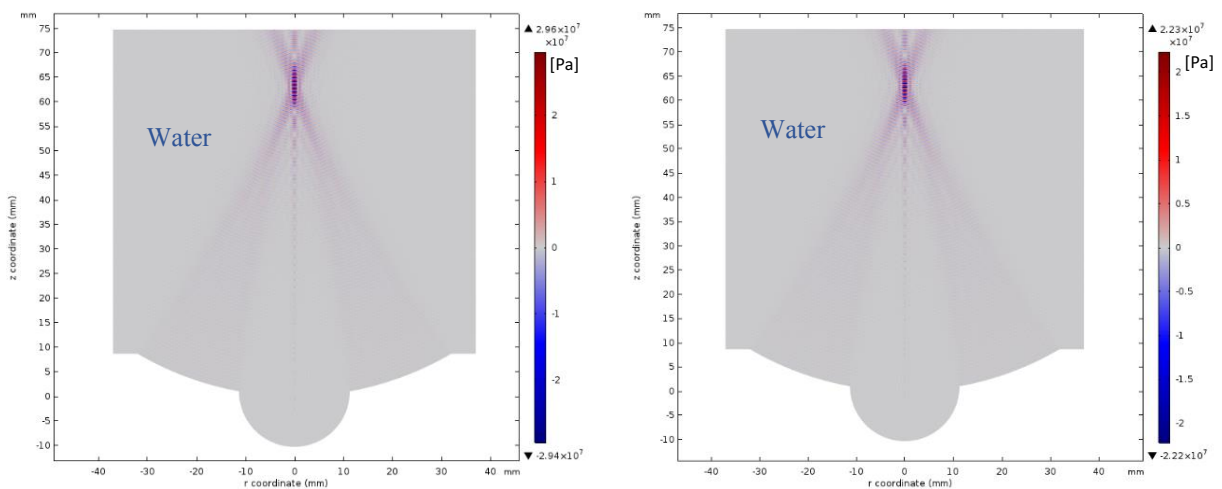
Using Equation “3-4” the size of focal point in the water with frequency of 2.15 MHz is calculated as 5.27 mm that is in agreement with the transducer's datasheet. Input data were chosen from **Table 3-1** and **Table 3-3**. Further calculations for various frequencies show that by increasing the magnitude of frequency the length of the focal region will decrease. The results are shown in **Table 3-4**.

**Table 3-4** Length of focal region through different frequencies

Frequency (MHz)	Medium of Focal Region	Length of Focal Region (mm)
2.15	Water	5.27
3		3.8
6		1.91
20		0.58

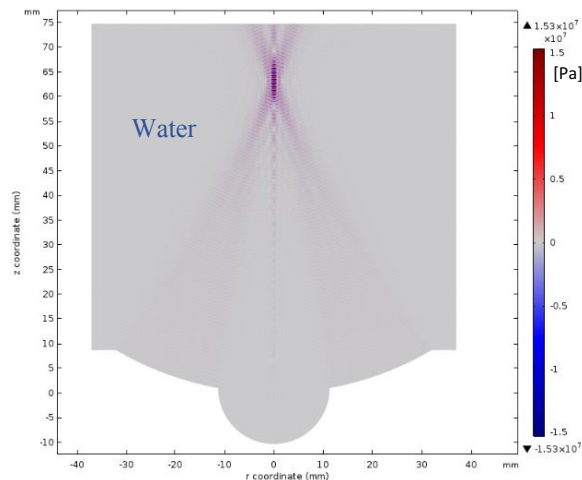
The effect of applying multiple powers on pressure and temperature fields are shown as follow. **Figure 3-3** shows the generated acoustic pressure fields by applying different input powers. Magnitude of input powers is selected from **Table 3-1**. It should be mentioned that since the efficiency of the transducer is 85% the amount of power that is converted to pressure wave would be 15% less than the input power which is shown in the **Table 3-1**.

Results show that by decreasing the power the magnitude of pressure wave decreases. As it was expected the higher pressure occurs at the focal region. Also, the convergence of beams into the focal point after traveling inside water is clearly presented.



a) Input power = 218 W

b) Input power = 131 W



c) Input power = 67 W

**Figure 3-3** Generated acoustic pressure fields by applying different input powers at frequency of 2.15 MHz

Using achieved data from **Figure 3-3**, the rate of change in maximum pressure wave at the focal point with respect to input power can be found. These results are shown in **Figure 3-4**. The graph shows by applying 10 watts deduction in input power the pressure wave will decrease 3% approximately.

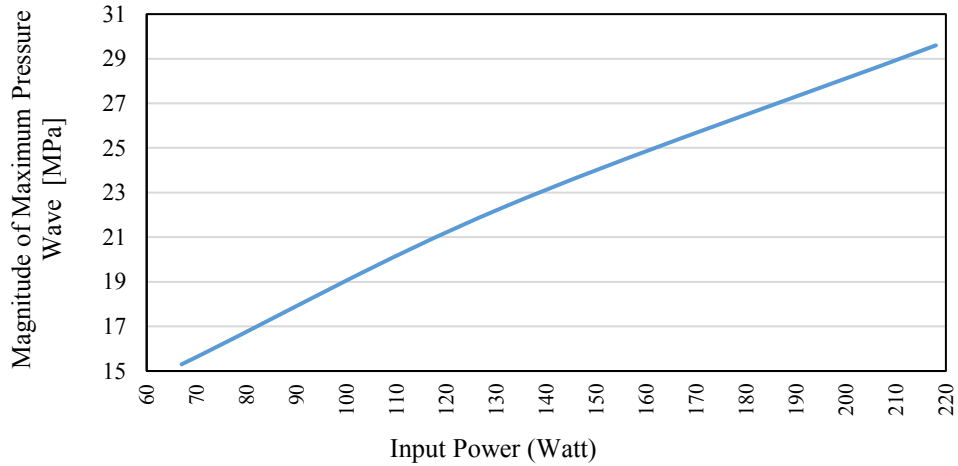
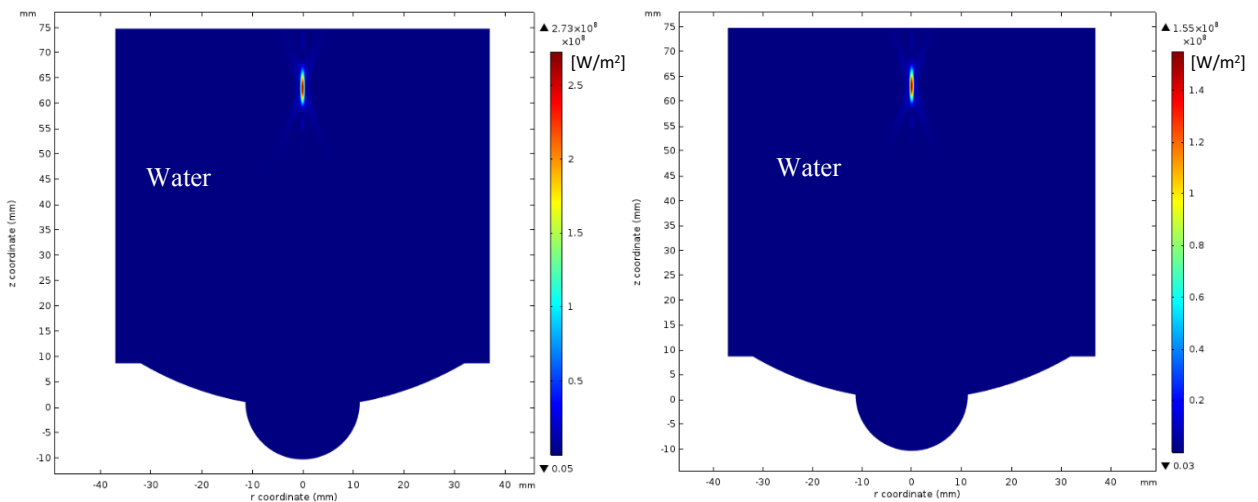


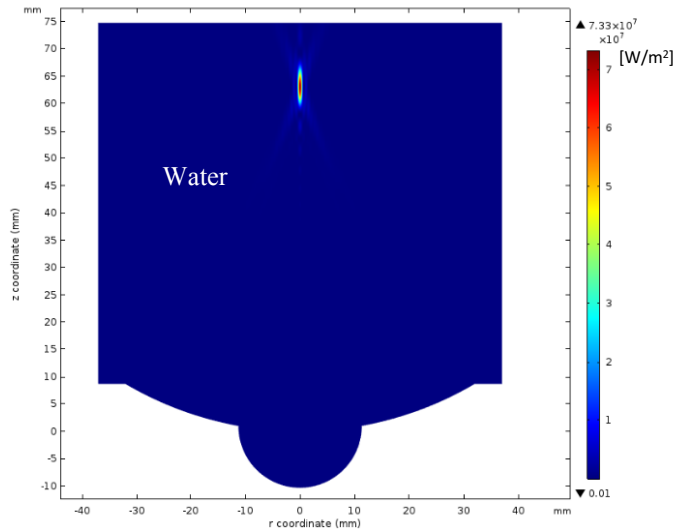
**Figure 3-4** Change in Maximum Pressure Wave at Focal Point with respect to Input Power

The intensity fields of different input powers are presented in **Figure 3-5**. Results clearly show the distribution of acoustic energy inside the fluid. It can be seen that the most of the acoustic energy is focused at the focal region with the oval shape. Focal region's length is determined about 5.21 mm which agrees with the calculated data in **Table 3-4** for frequency 2.15 MHz.



a) Input power = 218 W

b) Input power = 131 W



c) Input power = 67 W

**Figure 3-5** Generated acoustic intensity fields by applying different input powers at frequency of 2.15 MHz

The acoustic intensity profile along the symmetrical axis of the model is represented in **Figure 3-6**. The highest magnitude of intensity occurs at the focal point. As it has been mentioned so far, the diversity in intensities' amplitudes is due to different input powers. Peak points on graphs happened at focal point and they reveal its location. The location of focal is about 63 mm far from the center point of the transducer which agrees with the presented focal length in **Table 3-1**.

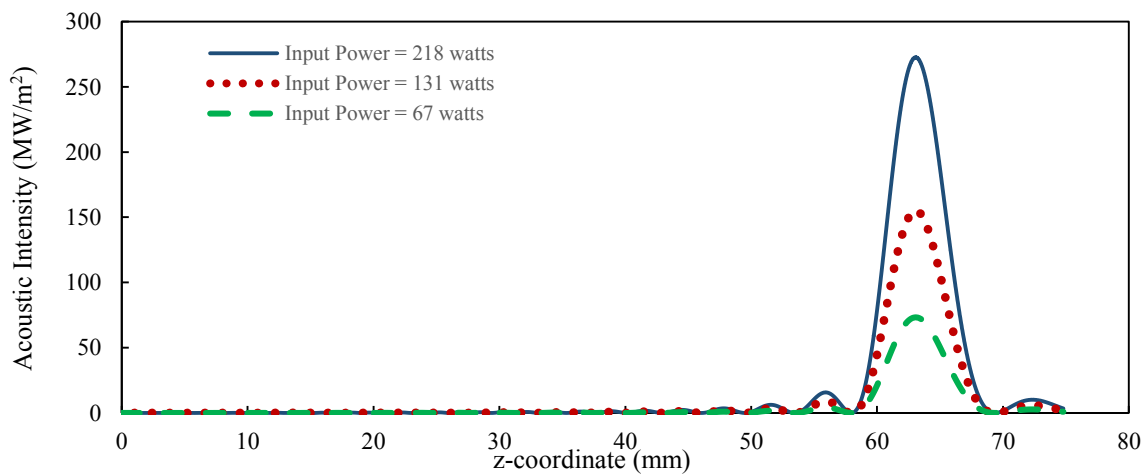
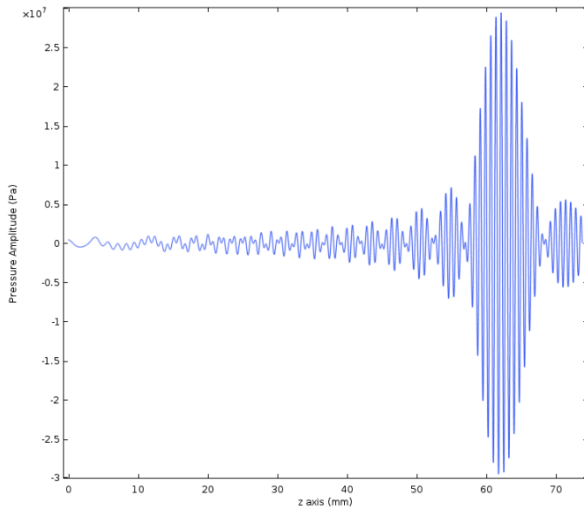
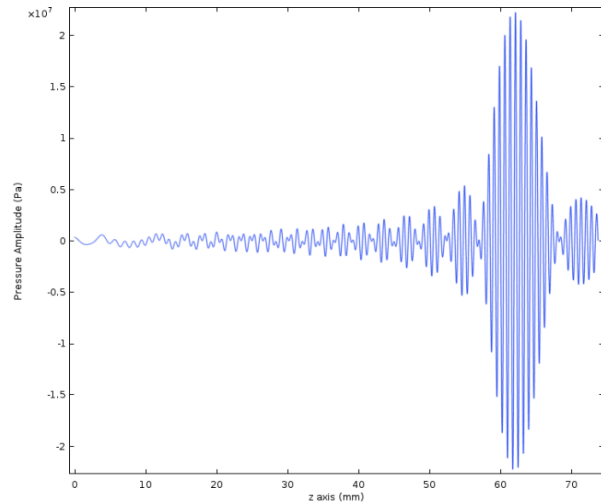


**Figure 3-6** Acoustic intensity profile along the symmetrical line for different input powers

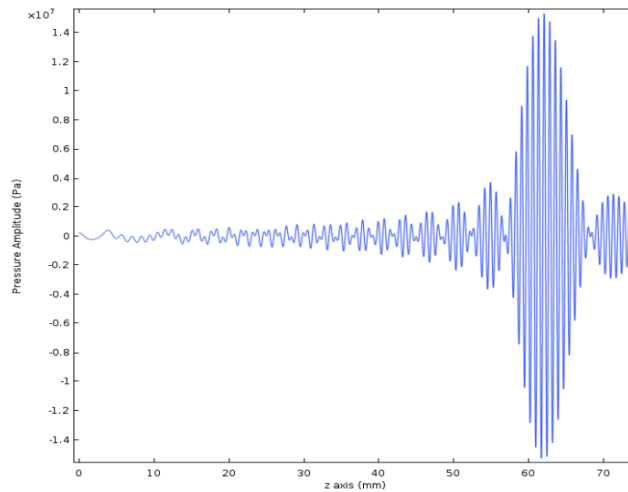
The acoustic pressure amplitude profiles for multiple input powers along the symmetrical line and the radial line which passes through the focal point are presented in **Figure 3-7** and **Figure 3-8** respectively. The existence of higher and lower magnitude of pressure field around the focal region are illustrated in these figures.



a) Input power = 218 W

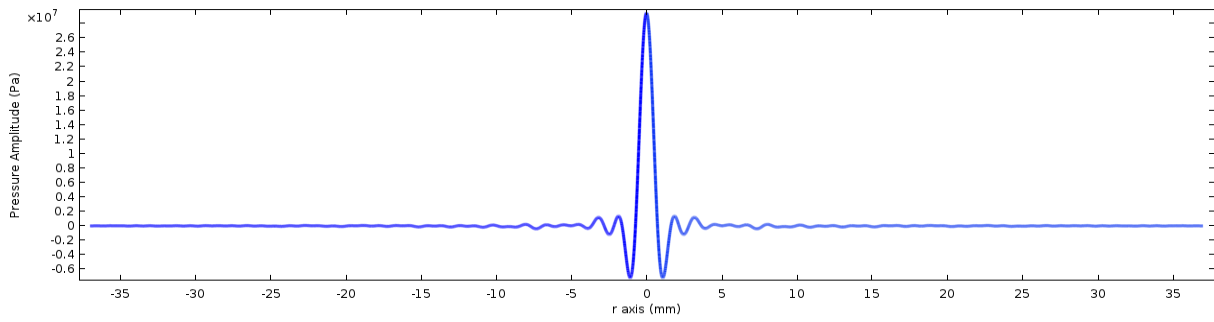


b) Input power = 131 W

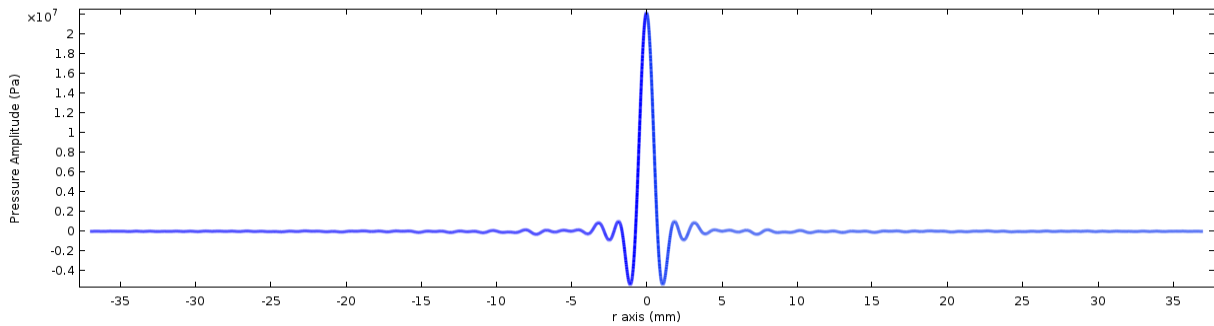


c) Input power = 67 W

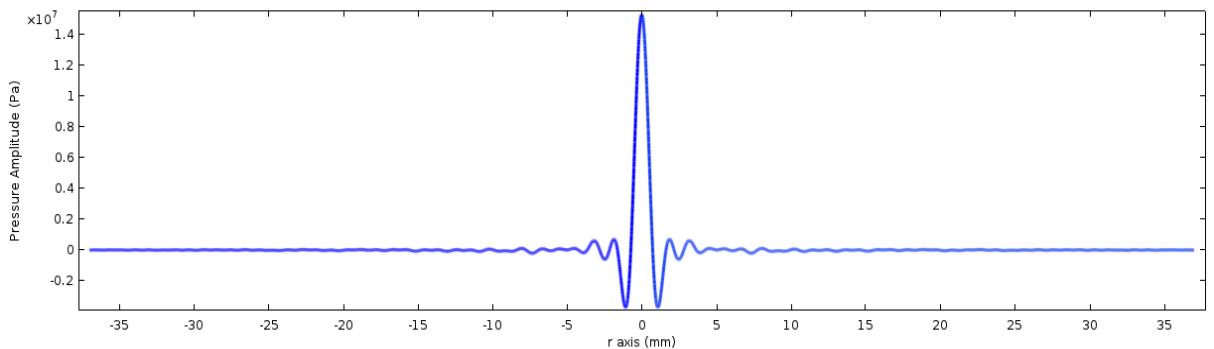
**Figure 3-7** Acoustic pressure amplitude profiles for different input powers along the symmetrical line at frequency of 2.15 MHz



a) Input power = 218 W



b) Input power = 131 W



c) Input power = 67 W

**Figure 3-8** Acoustic pressure amplitude profiles for multiple input powers along the radial line which passes through the focal point at frequency of 2.15 MHz

The profiles in **Figure 3-8** show that by going a bit far (about 1.5 mm) from the focal point that locates at  $r=0$  the acoustic pressure drastically reduces which is completely in agreement with the definition of compressed waves inside liquids. The narrow band around the focal point in these graphs is in agreement with the oval geometry of the focal region.

As it has been mentioned, the heat source energy is determined from acoustics study. Therefore, for different input power different heat energies have been calculated and employed in heat transfer simulation. These energies have been implemented for 1 second. In other word, the temperature distribution has been determined for 1 second insonation. The temperature distributions inside the water at  $t=1s$  are illustrated in **Figure 3-9**. It is clearly illustrated that the most of the heat energy is concentrated at the focal region.

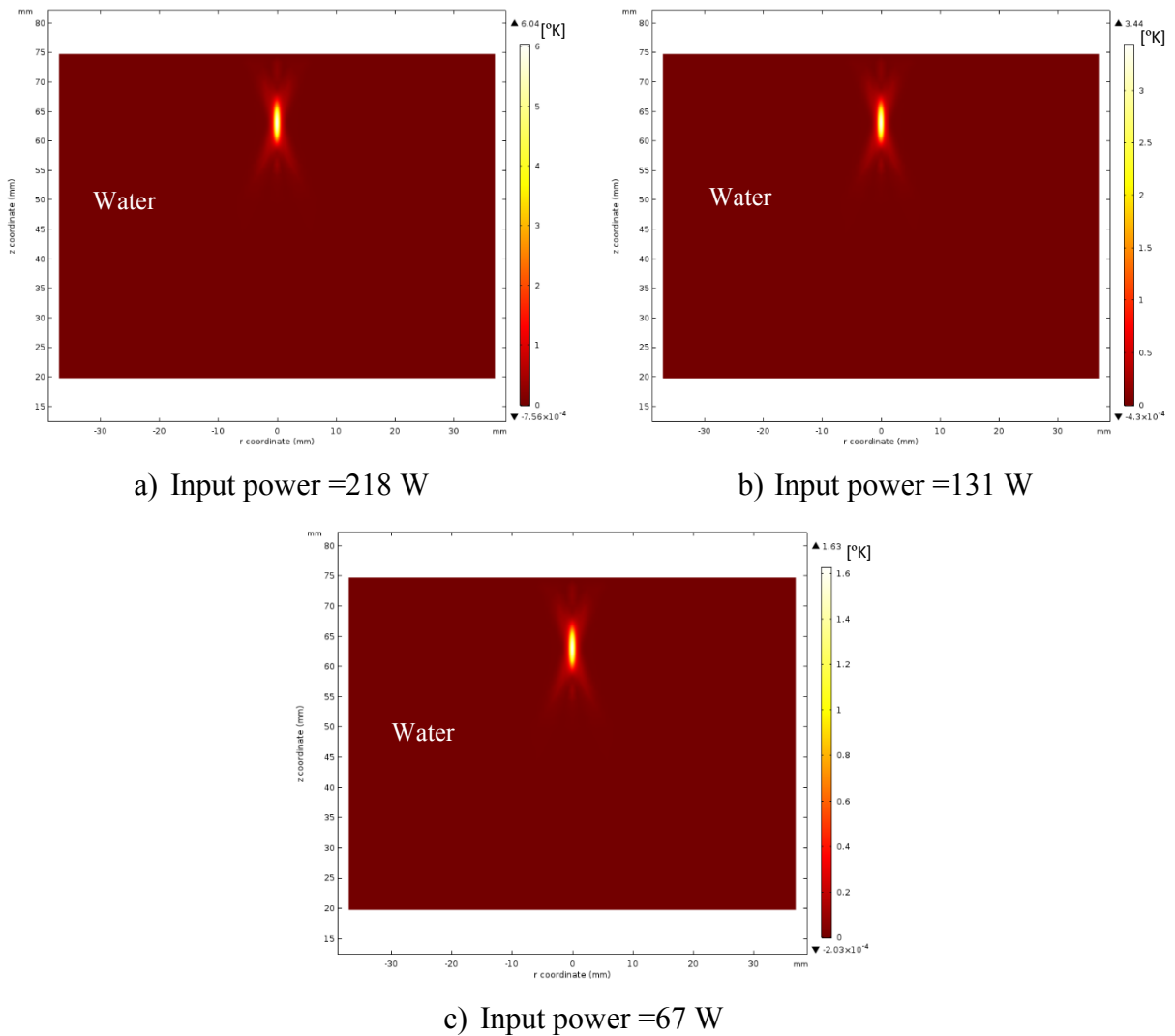


**Figure 3-9** The temperature distributions at time equal to 1(s) inside the water for different input powers and with insonation at frequency of 2.15 MHz

**Figure 3-10** displays the heating up and heat dissipation process at focal region for a period of 10 seconds for different pressure wave generated from applying different input powers. In this situation when the liquid is insonated for a second it heats up and after that it starts to cool down

because of the natural conduction. By increasing the duration of insonation higher temperature rise will be obtained.

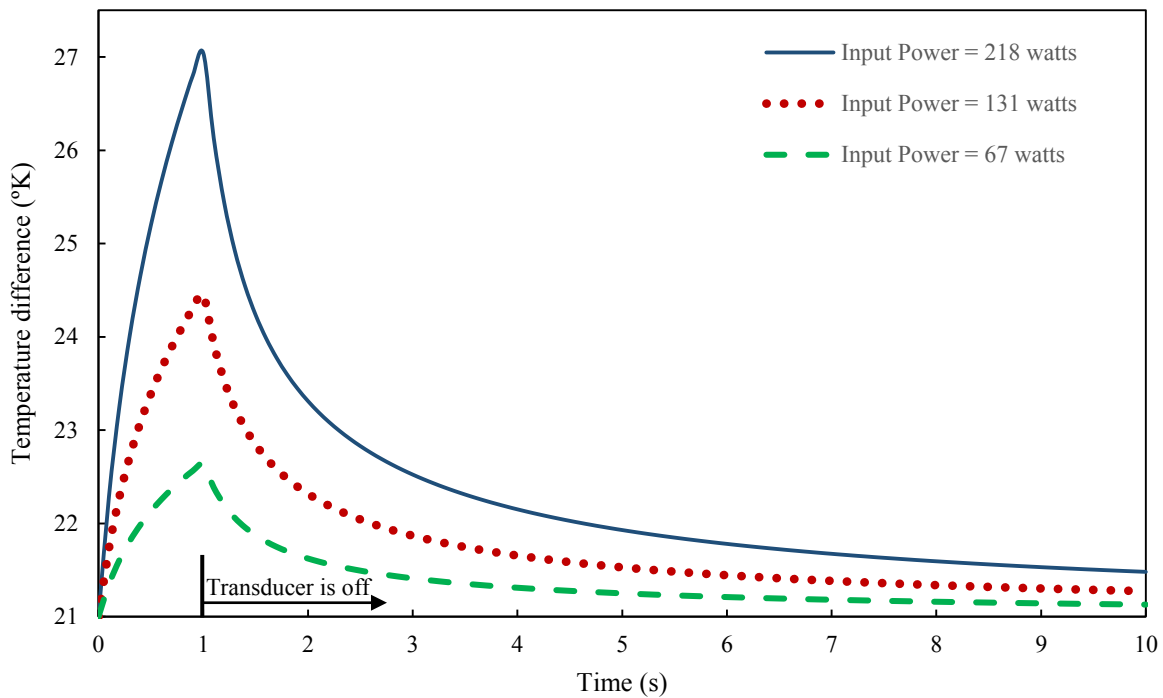


**Figure 3-10** The heat transfer over a period of 10 seconds inside the water

In another study, sensitivity of results with respect to time steps and mesh size at focal region have been investigated. It was found, by decreasing the time step, changes occurred in temperature at focal point were less than 2.9%. By modifying the focal region mesh size to  $\lambda/8$  and  $\lambda/10$  the changes in pressure and temperature at this region happened less than 3.6% and 3.8% respectively. As a result, this configuration of meshes has been maintained for continuing studies.

So far, results showed by applying the 218 W input power, maximum pressure, temperature, and intensity achieved. Therefore, the following studies are performed for this input power at frequency of 2.15 MHz.

Generally, transmission of acoustic wave through two adjacent different liquid media associates with diffraction and reflection at the interface of two liquids. The diffraction angle can be determined by Snell’s Law which was introduced by Equation “3-2”. To study this phenomenon, different materials with different properties have been placed in front of transducer

at distance 50 mm. Properties of chosen materials were introduced in **Table 3-2**. Transducer has been operated in 1 second at frequency of 2.15 MHz for the input power of 218 W.

As a matter of fact, a part of acoustic energy during passing through the divider is absorbed by the material. The other part of the wave beam reflects into the water behind the divider and changes the pressure and intensity in this region. Integration of these events causes to deduction of intensity at focal. In **Figure 3-11** the pressure fields in presence of 2 different materials have been presented. **Figure 3-12** illustrates the effect of using multiple dividers on intensity field as well as movement of focal point with respect to the case without inserting the divider, presented in **Figure 3-5**, which is in agreement with the Snell's Law. In fact, **Figure 3-12** indicates by using a divider with lower sound speed, the focal is getting away from the surface of the transducer. In addition, these figures present, by placing the divider in the system the intensity and pressure at focal will decrease. Also, the reflected beams at the interface of divider and water are recognizable in both figures.

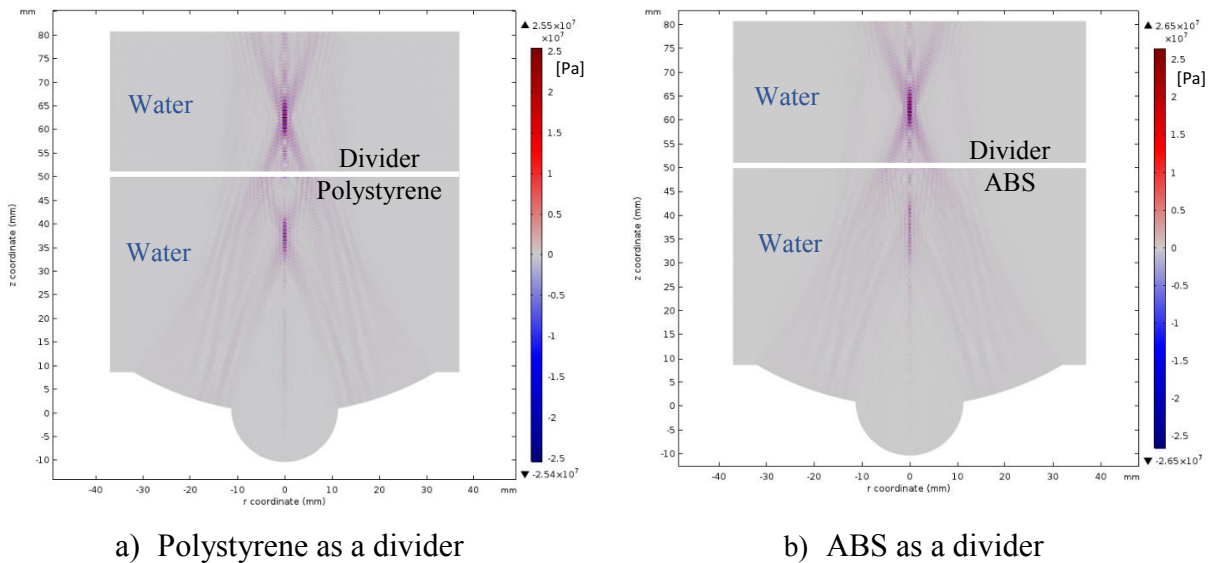
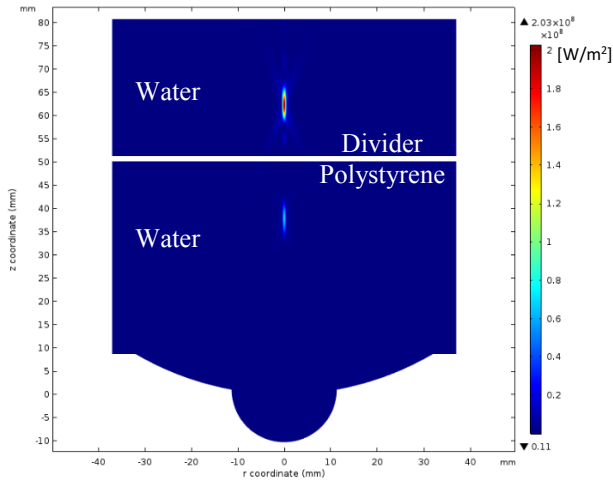
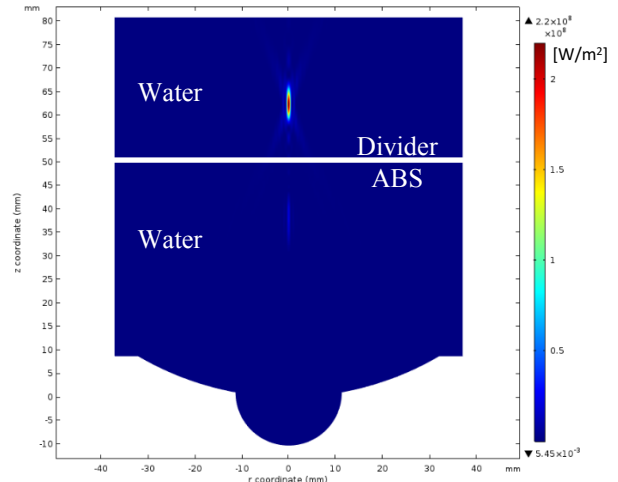


**Figure 3-11** Pressure field in the water at frequency of 2.15 MHz and input power of 218 W in presence of 2 different dividers



a) Polystyrene Divider

focal point movement with respect to case without existing divider = 1.55 mm



b) ABS Divider

focal point movement with respect to case without existing divider = 0.98 mm

**Figure 3-12** Intensity field in the water at frequency of 2.15 MHz and Input power of 218 W in presence of 2 different dividers

Because of the lower acoustic impedance of ABS the more wave energy can pass through this material, therefore, the pressure and intensity at the focal in presence of ABS will be greater than the case with Polystyrene as a divider.

**Figure 3-13** shows the heating up and heat dissipation at focal region due to 1 (s) insonation over a period of 10 seconds in presence of different dividers at the frequency of 2.15 MHz and input power of 218 W. As it has been expected the temperature rise in a model with divider is less than the previous case study. On the other hand, because of the less transmission of acoustic through Polystyrene the temperature rise at the other side will be less than the case with ABS.

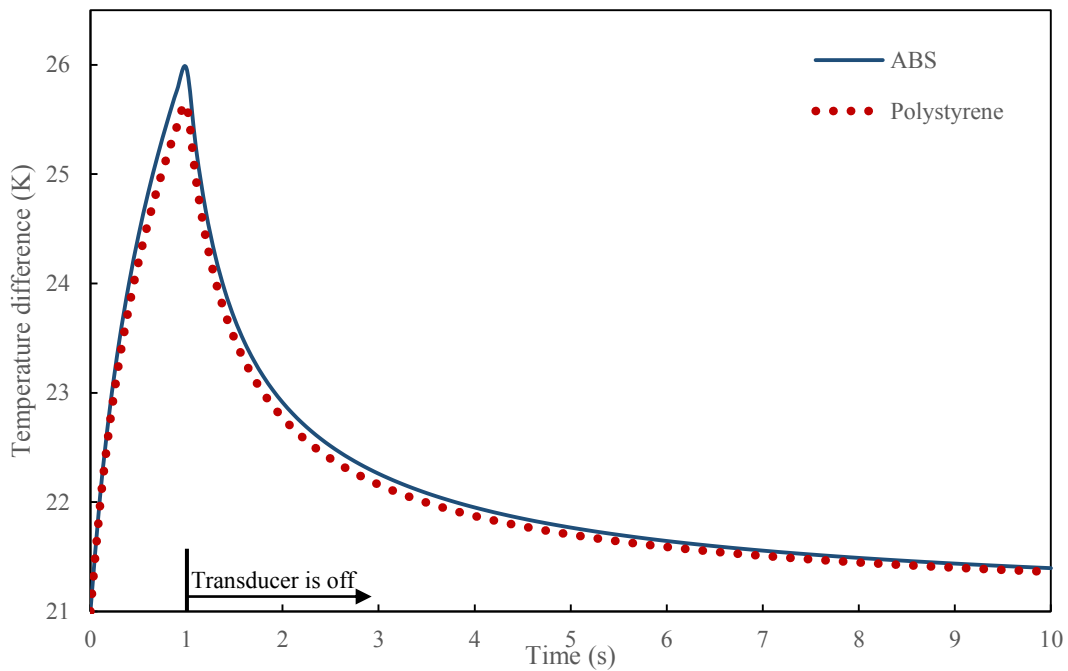
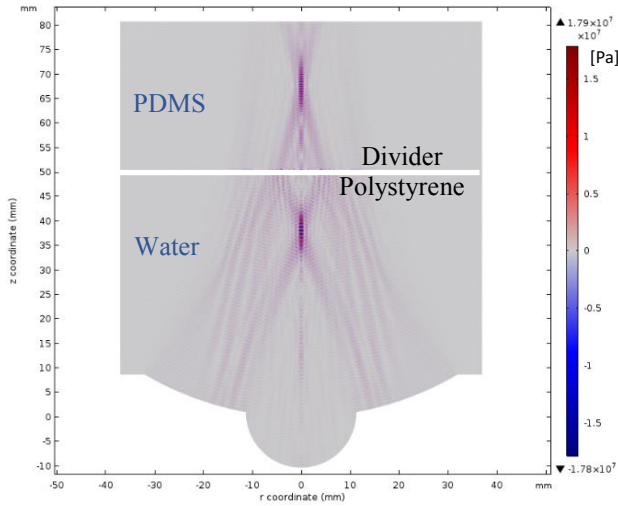


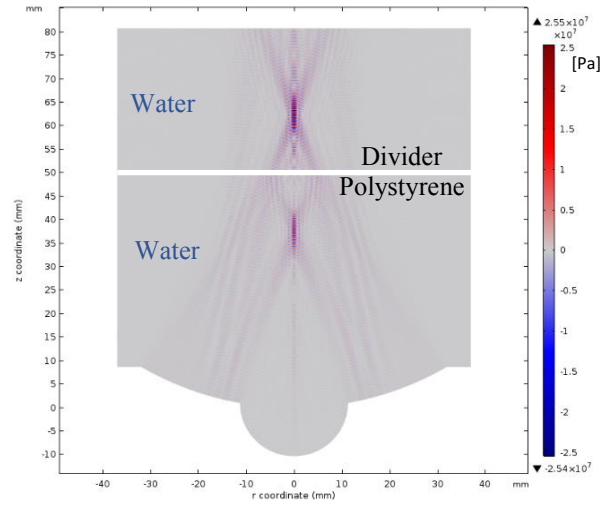
**Figure 3-13** Heat transfer in a period of 10 seconds inside the water in presence of 2 different dividers at frequency of 2.15 MHz and input power 218 W

In the last case study, the liquid cavity is filled by PDMS and Polystyrene has been selected as a divider. The transducer was run for 1 second at a frequency of 2.15 MHz and the input power of 218 W. Material properties of PDMS have been indicated in the **Table 3-3**. PDMS in comparison with water has the higher attenuation and lower acoustic impedance. In fact, the acoustic impedance of water is 1.4 times greater than the PDMS. In contrast, the attenuation of PDMS is 240 times greater than the water.

**Figure 3-14** and **Figure 3-15** illustrate the acoustic pressure and intensity fields in PDMS and water, respectively. Results show that the pressure and intensity magnitude in PDMS is less than water. This happens because of the greater acoustic impedance of PDMS which stands against the transmission of waves through the liquid. So, at the interface of divider and PDMS, the reflection of beams happens more in comparison with water. In the water, the reflection happens due to the existence of divider. The reflected beams can be observed in both cases.

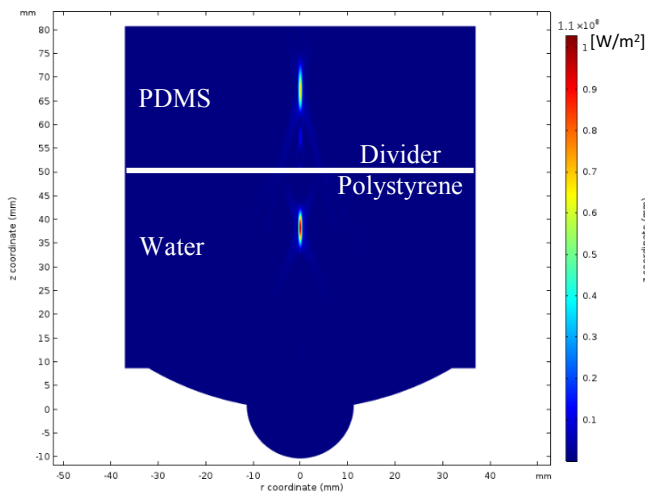


a) Liquid Cavity filled by PDMS

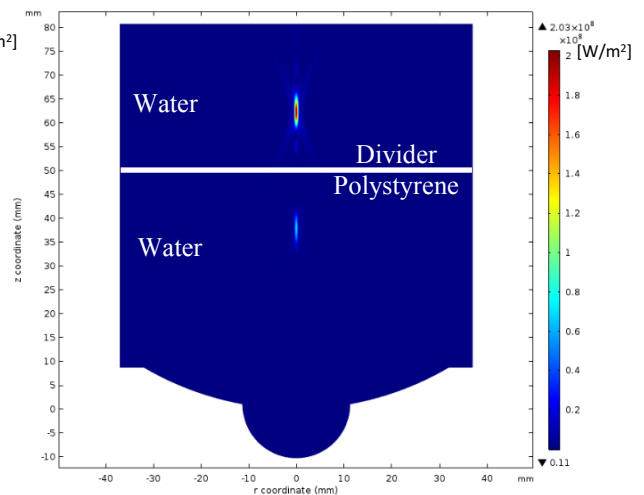


b) Liquid Cavity filled by Water

**Figure 3-14** Pressure field in the liquid cavity at frequency of 2.15 MHz and input power of 218 W in presence of Polystyrene divider



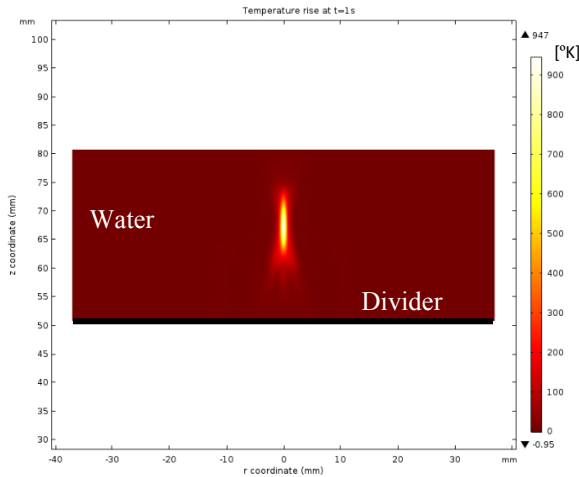
a) Liquid Cavity filled by PDMS



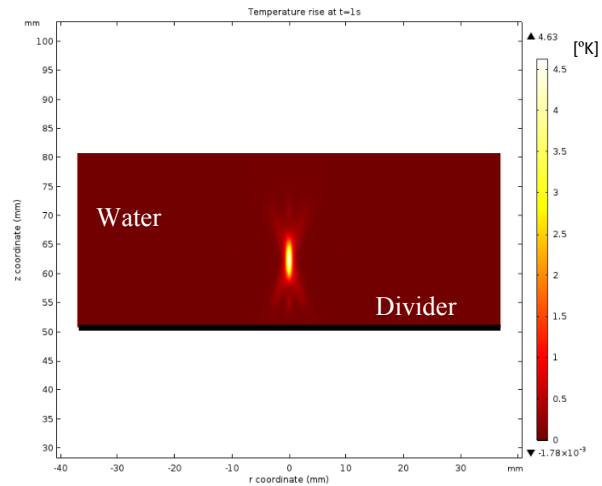
b) Liquid Cavity filled by Water

**Figure 3-15** Intensity field in the liquid cavity at frequency of 2.15 MHz and input power of 218 W in presence of Polystyrene divider

In final study, the heat transfers inside water and PDMS was investigated. Results showed the temperature rise at the focal region in PDMS is much more than the water. This happens because of the higher attenuation and lower heat conductivity of PDMS compare to the water. The temperature distributions inside the PDMS and water at  $t=1s$  are illustrated in **Figure 3-16**. The high magnitude of the temperature inside PDMS is noticeable. In addition, movement of focal point due to different acoustic impedance of water and PDMS is recognizable.



a) Liquid Cavity filled by PDMS  
focal point at  $z = 67.5$  mm



b) Liquid Cavity filled by Water  
focal point at  $z = 62.3$  mm

**Figure 3-16** Temperature field in the liquid cavity at frequency of 2.15 MHz and input power of 218 W in presence of polystyrene divider

### 3.5. CONCLUSIONS

In this chapter numerical simulation of high intensity focused ultrasound (HIFU) wave propagation in multiple materials has been performed. Acoustic waves were generated by HIFU transducer. In order to investigate the effect of altering input parameters such as power and material properties on wave pressure and temperature different case studies were investigated. In addition, to cut down the computation time and computer expenses, 2D axisymmetric simulation has been performed. Results showed wave frequency and fluid properties have the major influence on acoustic and thermal effects in a liquid medium. The present research illustrated the acoustic wave pressure field varied by liquid's acoustic impedance. On the other hand, during traveling acoustic wave among different materials the wave power was changing as a result of acoustic impedance alteration. Furthermore, the magnitude of temperature rise in liquid, directly depends on the absorption coefficient of fluid. So, a small variation in attenuation causes the high order change in heat energy. It should be mentioned the accuracy of computed results depended on alteration of fluids characterization during the process, simulation's time step and model's mesh size. In this study, it was considered that the properties of liquids during the process remained constant.

# CHAPTER 4

## COMMERCIAL 3D PRINTERS

In order to get familiar with the process of additive manufacturing in standard 3D printers as well as exploring the abilities and precision of the these printing machines, an investigation on 3D printed part fabricated by a commercial 3D printer will be performed in following.

A suitable 3D printer will be selected based on availability, precision in printing, and proper surface finish of the final product. After choosing a machine, a simple free standing structure such as cantilever will be built by 3D printer. The Cantilever is a simple structure which can be used in the study of mechanical properties of materials, structural dynamics simulation, or to make sensors in a microscale. Next, the dimensional resolution of the product in comparison with the designed model and surface properties of fabricated part will be investigated.

### 4.1. 3D PRINTERS WORKING WITH PLASTICS AS PRINTING MATERIALS

As it has been mentioned so far, using 3D printing technology leads to reducing the cost, time saving and resolving the limits of fabrication processes for product development. This technology offers various solutions for different requirements such as concept models, functional prototypes or even final parts to use in industry. Over the past years, 3D printers have become reliable and more accurate [42].

Among the technologies which have been used for 3D printers' development, fused deposition modeling (FDM), selective laser sintering (SLS), and stereolithography (SLA) are three most developed technologies for plastic 3D printing [6].

Final product fabricated by FDM has a rough surface, the process is fast but it happens in high temperature [5]. The machine is not expensive in comparison with other 3D printers. ABS and PLA are the common thermoplastics that are generally used in FDM printers. The products made by these materials are solid. **Figure 4-1** shows a picture of a 3D printer which works based on this technology made by About Aleph Objects, Inc. as well as a 3D printed object that has been printed with this machine.



**Figure 4-1** “LulzBot TAZ” FDM 3D printer and a “Flange” prototype printed with this machine

3D printed products with SLS technology have the best mechanical properties, are less anisotropic, and the same as FDM, have a rough surface. In this process, unsintered powders cannot be used for new operation [5]. Nylon is the most common thermoplastic material for SLS which is strong and flexible. Although SLS 3D printers are ideal for functional prototyping, the machine is more expensive [8]. **Figure 4-2** displays a picture of a SLS 3D printer fabricated by 3D Systems company. A part that has been printed by this technology is presented as well.

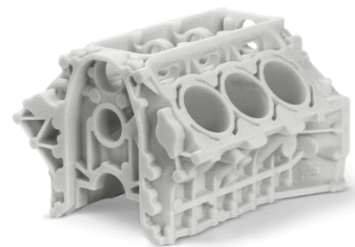


**Figure 4-2** “ProX SLS 6100” SLS 3D printer and a “Engine Body” printed with this technology

Among the other type of 3D printing technologies, SLA provides a highest resolution, smoothest surface finish and more accurate final dimensions of the parts. The parts have excellent surface quality and precision but the mechanical property is poor [5]. Most of the parts need to be post processed. Multiple laser cure resins have been produced for SLA 3D printers. Actually, each 3D printer has its own specific resin. SLA 3D printers are reasonable in price by considering the quality of their final products. They also can be used to fabricate the micro-objects. **Figure 4-3** displays a picture of “Form 2”, 3D printer and printed parts built by this machine.

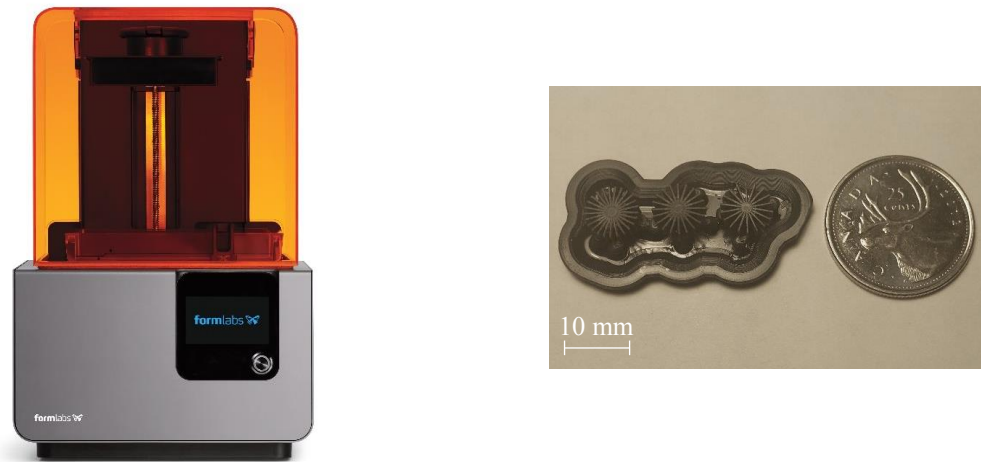


**Figure 4-3** “Form 2” SLA 3D printer and three different small prototypes of “Gears” built by this printer

#### 4.2. 3D PRINTING OF A FREE STANDING STRUCTURE AND SETUP

In this section, 3D printing process of fabricating a simple free standing structure such as cantilever will be explained. Since bending ability of cantilever structures is the main reason for their usage in experiments, using a flexible material to build a component will improve the performance of this structure. The resolution of printing is another main parameter for selection of the 3D printer. Therefore, due to the versatility of material types as well as achieving the high resolution and smooth surfaces in SLA technology “Form 2” SLA printer, was chosen and used to build a flexible cantilever. This 3D printer is manufactured by Formlabs Company.

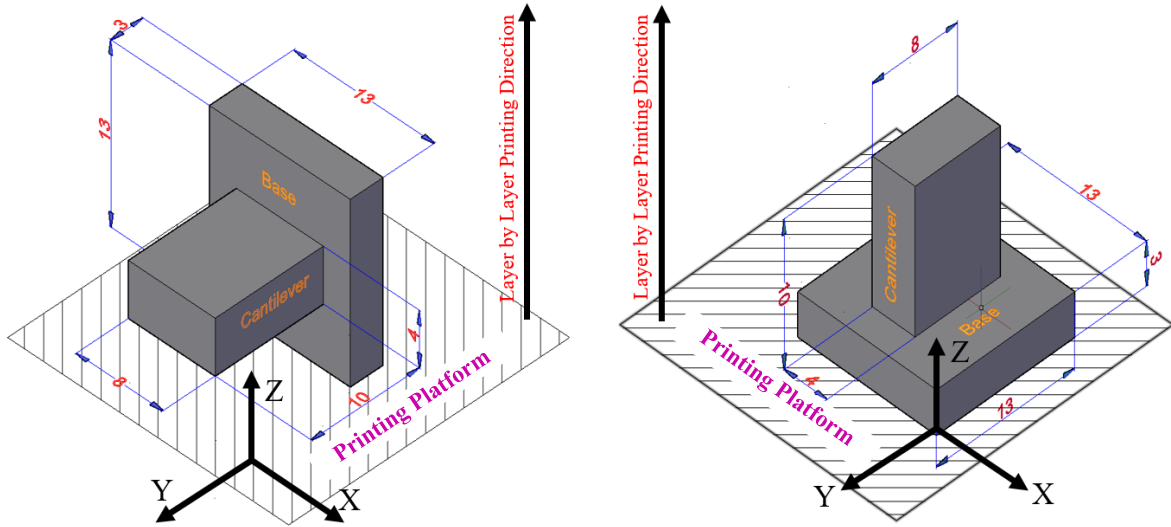
There are multiple types of resins that are presented by Formlabs Company. One of these resins is a flexible resin, which is ideal for functional prototyping and adds enough flexibility to bending structures. **Table 4-1** shows the characteristics of this resin.

**Table 4-1** Characteristics of “Form 2” Flexible Resin

	Green part	Postcured part
<b>Mechanical Properties</b>		
Ultimate Tensile Strength	3.3 – 3.4 (MPa)	7.7 – 8.5 MPa
Elongation at Failure	60%	75 – 85%
Compression Set	0.40%	0.40%
Tear Strength	9.5 – 9.6 kN/m	13.3 – 14.1 kN/m
<b>Thermal Properties</b>		
Vicat Softening Point	231 °C	230 °C

All data have been extracted from flexible resin’s datasheet provided by Formlabs Company. According to Form 2 datasheet, the laser spot size is 140 microns and the highest resolution of device in the XY plane is 150  $\mu\text{m}$  and 25  $\mu\text{m}$  in the Z axis.

In order to verify the effect of printing directions on quality of the final part, 2 identical models of cantilever were fabricated by this printer. A CAD model of cantilever was designed in Autocad (Autodesk). Models were oriented in different directions with respect to the 3D printer’s building platform. In fact, one of the model’s CAD design the long edge of cantilever was oriented parallel to the platform and for another one, it was perpendicular to the platform. Next, all models were exported to the printer as STL file. **Figure 4-4** shows the CAD model of designed cantilevers and orientation of them on printing platform as well as the direction which the part was printed in a layer-by-layer process.



a) Horizontally oriented cantilever

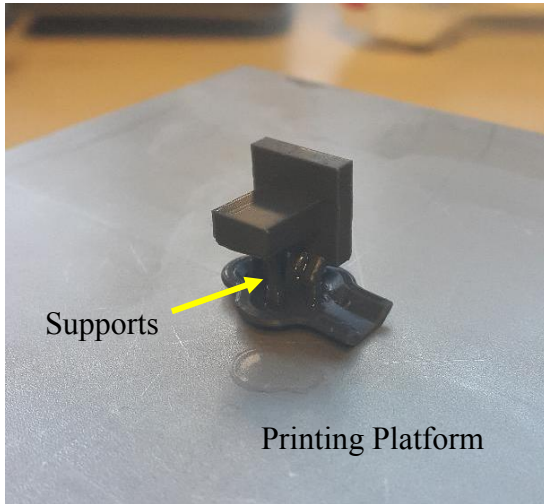
b) Vertically oriented cantilever

**Figure 4-4** CAD models of designed cantilevers (all dimensions are in mm)

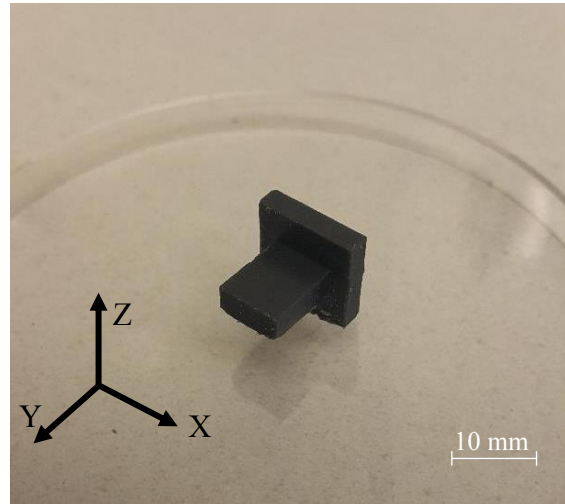
After finishing the printing, green parts were washed with isopropanol for removing the uncured resins. As it has been mentioned so far considering the supports for stabilizing the parts during the 3D printing is part of this process therefore in the next step printed supports were detached from the objects. Supports of these parts are illustrated in **Figure 4-5** (a) and (c). Then, printed parts were exposed to UV light in a Stratalinker® UV Crosslinker 2400 for 3 minutes. Finally, dimensions and line roughness of the printed cantilevers were measured by using a Confocal Laser Scanning Microscope (Olympus Inc.).

### 4.3. RESULTS

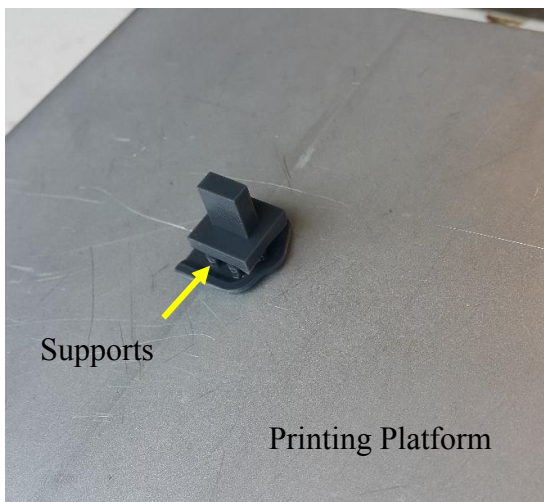
Samples' green parts and Postcured parts are illustrated in **Figure 4-5**. As it was expected, by the visual test, samples have the smooth surfaces. Printing of each the samples took about 4 hours.



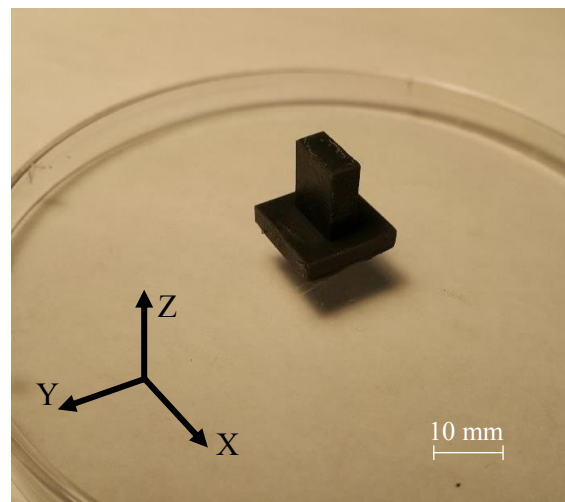
a) Green part on a printing platform – Horizontal Orientation



b) Postcured sample – Printed Horizontally



c) Green part on a printing platform – Vertical Orientation



d) Postcured sample – Printed Vertically

**Figure 4-5** Postcured parts – Printed in different directions with respect to the platform

Samples' dimensions have been measured by using Confocal microscope. Making a comparison between the designed and measured sizes shows a small difference. As a matter of fact, in a standard printing condition, when the printer is fully aligned and the proper resin is

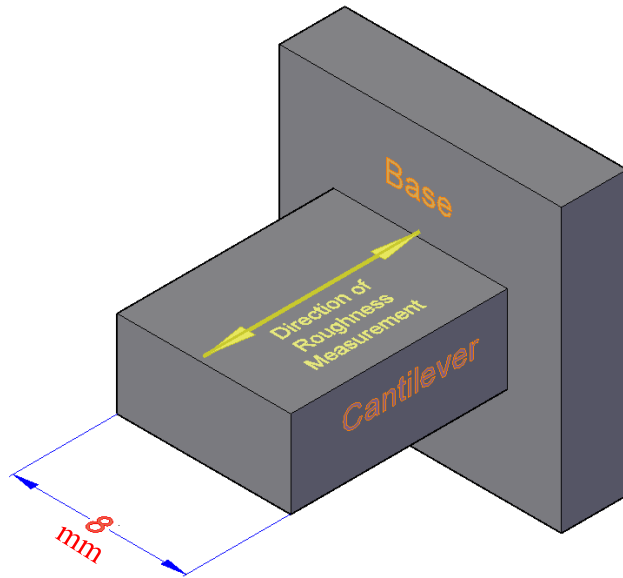
being used, the dimensional resolution of printing part is affected by the radial beam scattering [43]. **Table 4-2** illustrates the quantities.

**Table 4-2** Dimensional comparison between the designed and printed samples

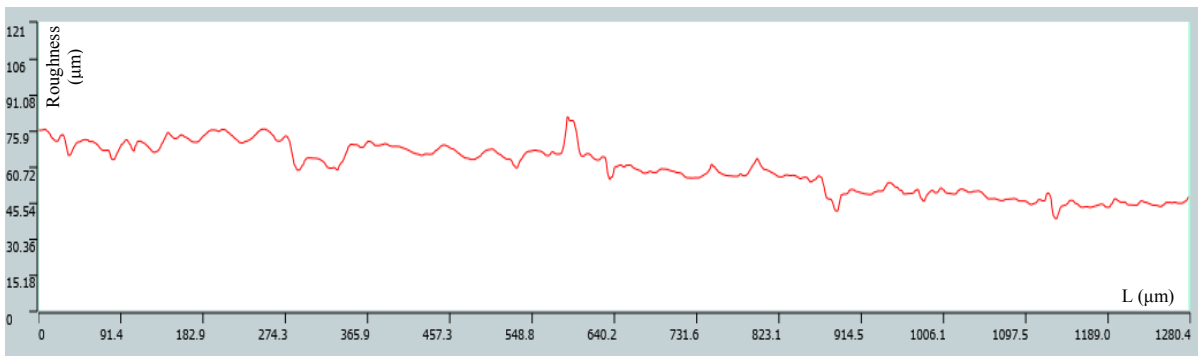
		Base sizes (mm)			Cantilever sizes (mm)		
		Length (along X)	Width (along Z)	Height (along Y)	Length (along X)	Width (along Z)	Height (along Y)
Parts (a) and (b)	Designed Sizes	13	13	3	8	4	10
	Measured	13.04	13.02	3.01	8.07	4.03	10.03
	Difference (mm)	0.04	0.02	0.01	0.07	0.03	0.03
Parts (c) and (d)	Designed Sizes	13	3	13	8	10	4
	Measured	13.03	3.02	13.02	8.04	10.02	4.02
	Difference (mm)	0.03	0.02	0.02	0.04	0.02	0.02

Deviations identify the resolution of the printing process in different directions. Therefore, before starting the process of printing considering the proper orientation of the model in order to obtain a desired dimensional accuracy is the key parameter.

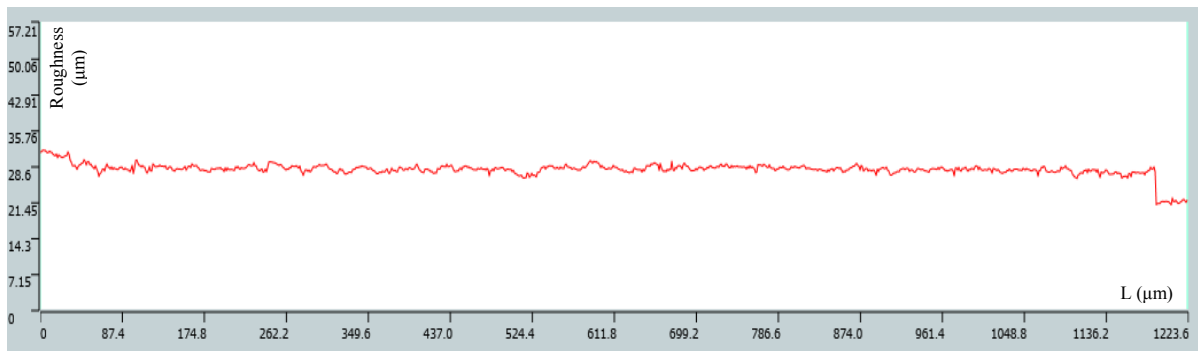
As it has been mentioned so far, in SLA technology, 3D part is completed layer-by-layer which the thickness of each layer determines the roughness along the normal axis of the layer. So, Line roughness was measured by a 10x lens of the Confocal Microscope and the cutoff value was set to 2.5 mm. The average roughness over the length of the object ( $R_a$ ) for horizontally and vertically printed cantilevers was determined 0.692  $\mu\text{m}$  and 3.383  $\mu\text{m}$  respectively. In **Figure 4-6** the edge of cantilevers along which the roughness was measured is identified. Also, this figure presents the measured roughness results.



(a) The direction of roughness measurement



(b) Measured roughness of vertically oriented cantilever



(c) Measured roughness of horizontally oriented cantilever

**Figure 4-6** The direction of roughness measurement, and measured roughness over the length of printed cantilevers

Results show that the higher value of average roughness was measured in vertically oriented cantilever, **Figure 4-5** (d). As a matter of fact, in the layer-by-layer process the horizontal layers are bonded in vertical direction altogether. Therefore, depends on a thickness of each layer as well as its edge sharpness, the roughness of the part's edge could be changed. **Figure 4-7** illustrates this explanation.

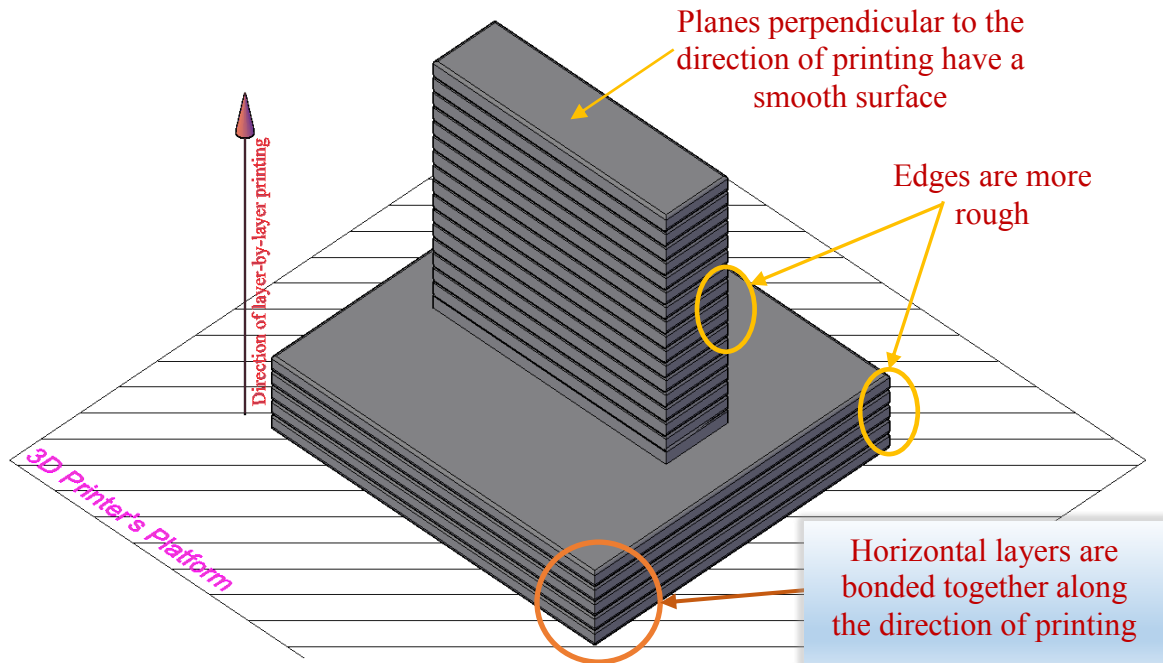


**Figure 4-7** Schematic for layer-by-layer printing of a 3D object

Therefore as it has been illustrated in **Figure 4-6**, the average line roughness of vertically printed cantilever along its length is more than the horizontally printed one. In fact, achieving the desired roughness for a specific surface will be attained by changing the angle of the surface with respect to the printing direction. This action can be performed in a CAD software just by adjusting the orientation of a surface with respect to the horizontal plane with a proper angle.

By the way, the line roughness is not a significant characteristic for a cantilever object, although this parameter can define the microscopic resolution of SLA 3D printer.

#### 4.4. CONCLUSIONS

In this chapter three different types of 3D printers that works with plastics as printing materials were introduced and “Form 2” 3D printer was selected to fabricate a simple 3D object for study the characteristics of printing process and a printer. By investigation of results, it can be verified that the 3D printer is more accurate in XY plane compared to the Z direction. Also, acquiring the highest resolution associates with increasing of printing time. As a matter of fact, before starting the process of printing considering the proper orientation of the model in order to obtain a desired dimensional accuracy is the key parameter. Although the flexible resin adds a proper flexibility to the printed cantilever, this material is not biocompatible and cannot be used in bio-experiments.

By getting familiar with the SLA process performed by one of the commercial 3D printers, in next two chapters the experimental setup and results extracted from HIFU additive manufacturing method’s experiments, as a main objective of this research, will be presented.



## 5.1. HIFU TRANSDUCER AND PULSE GENERATOR

HIFU transducer was selected as a sound source. This device is fabricated from a piezoceramic material. It is a spherically focused transducer which focuses the generated ultrasound waves at a focal point. This transducer has a hole at the center which can be used as a place for mounting the hydrophone. The focal region is in an oval shape. The transducer characteristics are represented in **Table 5-1**.

**Table 5-1** HIFU transducer's characteristics

Frequency (MHz)	Focal Length (mm)	Focal Region Size (mm)		Aperture Diameter (mm)	Hole Diameter (mm)	Maximum Intensity at Focal Region (Watts/cm <sup>2</sup> )	Maximum Pressure at Focal Region (MPa)	Maximum Input Power (Watts)	Power Efficiency (%)
		Length	Girth						
2.15	63.2	5.33	0.7	64	22.6	54695.36	40.24	218	85

This kind of transducers is used in the biomedical applicant and needs to be immersed in water for performing an operation.

Furthermore, in order to supply an input power of the transducer a pulse generator was purchased. Device could provide maximum power 218 (w) for the range of frequencies between 2 to 2.49 (MHz) with the 0.1 (ms) steps as an interval. Also by adjusting the time, the duration of supplying power could be controlled.

## 5.2. CNC MACHINE

In order to move the transducer precisely, it is mounted on a Computer Numerical Control (CNC) machine. **Figure 5-2** shows the picture of the CNC which is used in this research. Transducer is mounted on a holder. This system has three stepper motors that provide movement in 3 directions in Cartesian coordinate system (X, Y, Z).

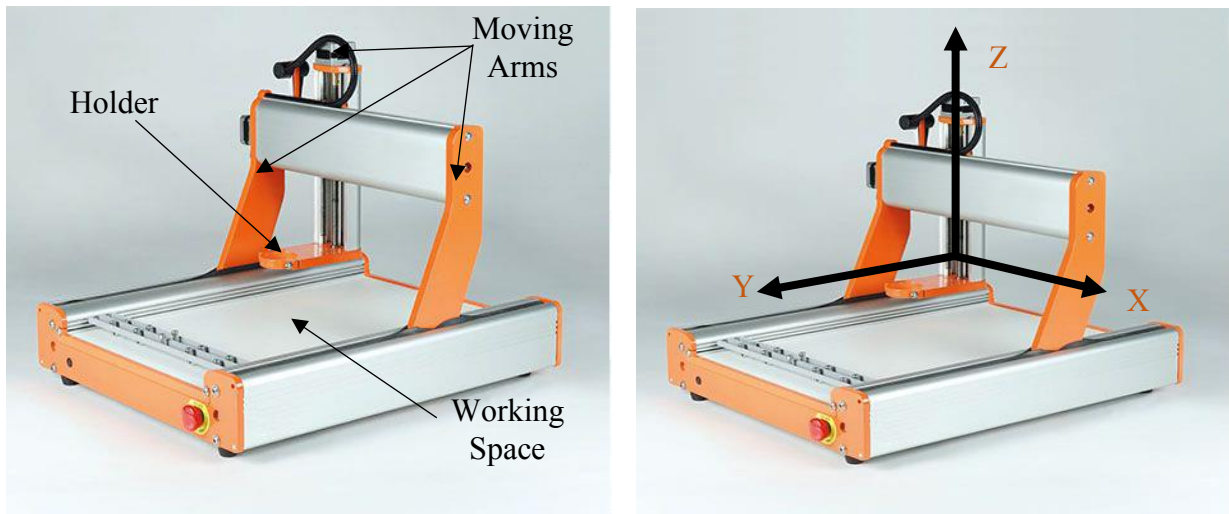


**Figure 5-2** CNC machine used in this research and its axes of movements

The desired movement of a system, which is determined by required speed, location of the focal point, and geometry of the object to be printed, is imported to the interface software by using the G-Code program.

After installation of transducer, according to axes definition shown in **Figure 5-2**, it is expected that by applying movement along the X and Z direction the plane geometry of the final part can be printed, and with moving along Y, the height of 3D part will be adjusted. The characteristics of the CNC machine are illustrated in **Table 5-2**.

**Table 5-2** Characteristics of the CNC machine

Working Space (X,Y,Z) (mm)	Repeatability (mm)	Maximum Speed (mm/sec)	Input AC Voltage (V)	Programmable Resolution (mm)	Interface Software
300 x 420 x 140	0.04	50	100 - 240	0.005	UCCNC

### 5.3. TEMPERATURE MEASUREMENT SYSTEM

Temperature is one of the most common types of physical measurements. For measuring the temperature depending on the desired accuracy and range, several sensor options can be used. In the following, 3 devices which have been utilized to define the temperature magnitude at the focal region are introduced.

- **Data Acquisition System**

National Instruments offers a wide variety of devices to make temperature measurements. Compact Data Acquisition System (DAQ) is a portable, rugged DAQ platform that integrates connectivity and signal conditioning into modular I/O for directly interfacing to any sensor or signal. In this work “NI 9212” has been purchased as a data acquisition system. By using this system combined with the LabVIEW software the needs for measuring the temperature field inside a liquid cavity was reachable. **Table 5-3** presents some information from the specification of this device.

**Table 5-3** Specification of DAQ NI 9212

Voltage Measurement Range (mV)	Conversion Time at High-Speed Mode (ms)	Sample Rate at High-Speed Mode (Samples/s)	Temperature Measurement sensitivity for T-type thermocouples (°C)
±78.125	10.5	95	0.01

- **Thermocouples**

Thermocouples are the most popular temperature measurement transducers available. Because of their low cost and wide temperature acceptance range, they can be used for a wide variety of applications in all industries. In this research two types of “T-type” thermocouples, with the measuring junction at the tip, have been purchased from National Instruments Company and OMEGA Engineering. Specification of the thermocouples is illustrated in **Table 5-4**.

**Table 5-4** Thermocouples’ specification

Supplier	Wire Diameter (mm)	Material	Maximum Permitted Error* (°C)
National Instrument Company	1.7	Copper- Constantan	0.5
OMEGA Engineering	0.125		

\* Maximum permitted error complies with IEC 60 584-2 (1995)

- **Liquid Crystal Sheets**

Generally, liquid crystal sheets are used for a thermal mapping. As a result of low accuracy in determination of temperature as well as limited operation temperature, this type of sensors is not comparable with other instruments, in this work they were used just for identification of focal point's location as well as the approximate size of the focal region. **Table 5-5** shows the specification of this item.

**Table 5-5** Liquid Crystal Specification

Supplier	Operating Temperature (°C)	Thickness (in)	Output Wavelength (nm)
Edmund Optics	40 - 45	0.007	0 - 650

#### 5.4. RESINS

In this project, a 3D printing process is introduced as a method to create 3D object by curing a thermoset resin and converting it to the thermoset solid. The process of curing or cross-linking is the main distinguishing element of a thermosetting material. The word “thermo” indicates that the cross-linking happens by adding a heat energy, although, much cross-linking occurs at room temperature or even below it [44]. Lately, some researchers have described the thermoset, which cures at or below the room temperature, as “chemoset” although this term has not been universally accepted [44]. The second term “setting” implies that the process of cross-linking is an irreversible reaction.

The cross-linking process can be tracked by observing the change of viscosity within a time at a certain temperature. While all commercial thermosetting reactions are exothermic [44], the viscosity of the mixture at the beginning of the process will be decreased due to generated heat from the reaction. Since during the process the molecular weight of the mixture will increase by cross-linking of the molecules, the resultant viscosity of the mixture will increase and quickly overcomes any happened reduction in viscosity by heat. The molecular growth will continue over a time until reaching the gel-like state. The time of sensing this state is called gel time. After passing this point the viscosity goes to infinity. **Figure 5-3** shows the described process and indicates the gel time.

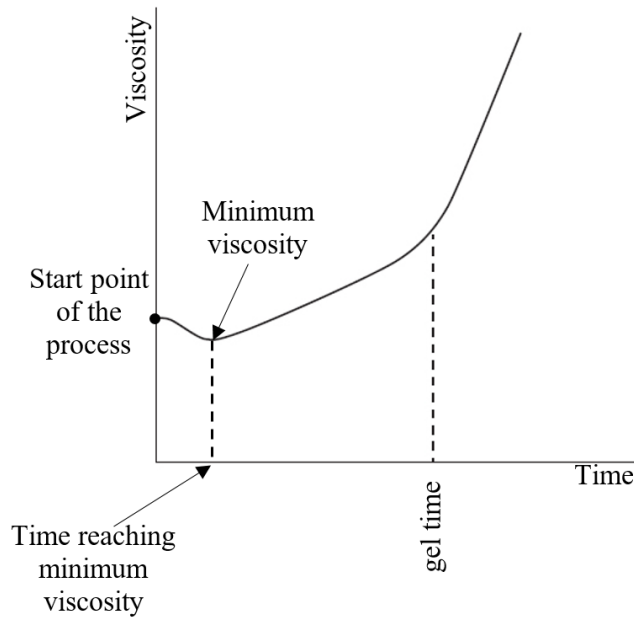


**Figure 5-3** Viscosity vs Time for a thermoset resin material [44]

Most of the curing processes are normally occurred by adding a curing agent or hardener to the resin. Curing agents have a major effect on curing kinetics, gel time, the degree of curing, viscosity and the properties of the cured products [45].

In addition to the curing agent, the resolution and dimensional accuracy of the final cured product also depend on the resin characteristics. In fact, curing time and required an amount of heat energy to become cured are two characteristics of resins [44]. In some thermoset resins, because of the low amount of generated heat in an exothermic reaction, curing process speeds up when a certain amount of heat energy is applied to the specific volume of resin within a period of time [46].

In this work, the required heat energy for the curing process was generated by conversion of acoustic pressure to heat energy inside the resin. As it has been explained, HIFU transducer was the source of acoustic energy.

In this research, three different types of thermoset resins were purchased. **Table 5-6** shows the characteristics of selected resins. Each resin's curing agent was introduced by suppliers.

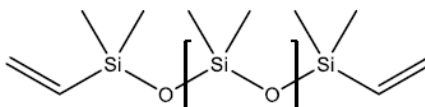
**Table 5-6** Selected resins' characteristics

Resin	Curing Agent	Mixing Ratio	Viscosity (CP)	Density (Kg/m <sup>3</sup> )
EPON™ 828	EPIKURE™ 3270	6:4	110-150 @ 25 °C	1160 @ 25 °C
EPON™ 8021	EPIKURE™ 3271	6:4	85-115 @ 25 °C	120 @ 25 °C
Sylgard 184 (PDMS)	Catalyst 87- RC	10:1	3500 @ 25 °C	1030 @ 25 °C

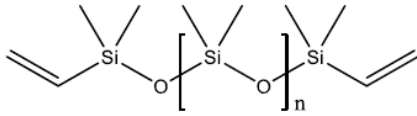
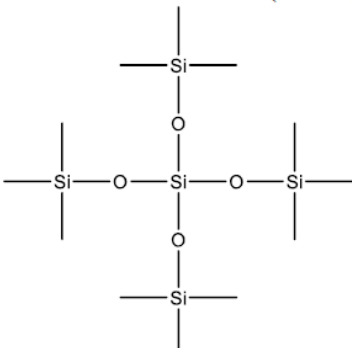
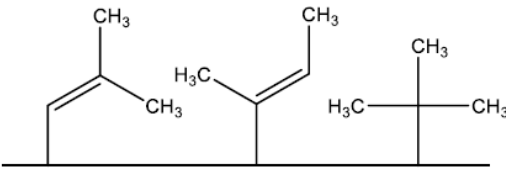
Before starting to use the thermoset resins, a small volume of each resin was mixed with the curing agent to understand their curing process in a normal condition. For epoxy resins with the mixing ratio of 6:4, it was seen that the curing reaction started during mixing. Then, after passing a short time, less than six minutes, epoxies became fully cured. As it has been mentioned so far, due to the exothermic reaction of this curing process, significant amount of heat was generated during the process which decreased the duration of curing process. Actually, generated heat deformed the plastic container of the resin. In contrast, curing process of Sylgard 184 with mixing ratio of 10:1 produces negligible heat energy. In fact, for preparation of fully cured Sylgard in one hour, it should be baked at 80°C. As a matter of fact, longer duration of Sylgard curing process provided proper time to perform the printing. Therefore, this resin was selected as a printing liquid.

Sylgard 184 is a two-part, liquid silicone-based polymer: base resin and resin accelerator [47]. The composition of the resin accelerator, Sylgard resin, and the curing agent are presented in **Table 5-7**, **Table 5-8** and **Table 5-9**.

**Table 5-7** Resin accelerator component [47]

CAS #	Wt%	Component
68083-19-2	>60	Dimethylsiloxane, dimethylvinyl-terminated 

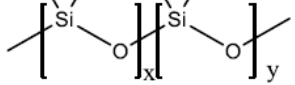
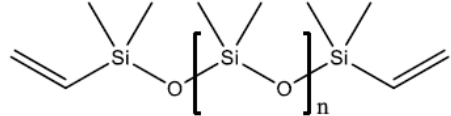
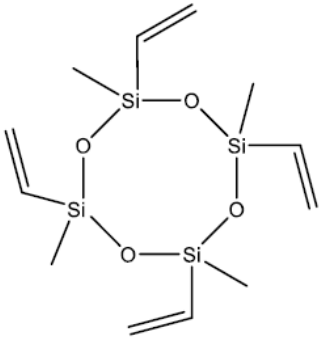
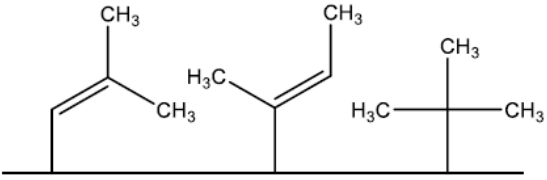
**Table 5-8** Sylgard resin component [47]

CAS #	Wt. %	Component
68083-19-2	>60.0	Dimethylsiloxane, dimethylvinyl-terminated 
3555-47-3	1.0-5.0	Tetra(trimethylsiloxy)silane  Branched volatile siloxane (VMS)
68988-89-6	30.0-60.0	Dimethylvinylated and trimethylated Silica  SiO <sub>2</sub>

Surface modifier  
Silica filler

Resin accelerator is used to modify the Sylgard base resin [47].

**Table 5-9** Curing agent component [47]

CAS#	Wt. %	Component
68037-59-2	40.0-70.0	Dimethyl, methylhydrogen siloxane 
68083-19-2	15.0-40.0	Dimethylsiloxane, dimethylvinyl-terminated 
2554-06-5	1.0-5.0	Tetramethyl tetra vinyl cyclotetrasiloxane  Network formation
68988-89-6	10.0-30.0	Dimethylvinylated and trimethylated silica  SiO <sub>2</sub>

Surface modifier  
Silica filler

### 5.5. TANK AND LIQUID CAVITY

The tank was employed as a water container for operation of transducer. It was fabricated from Acrylic plastic sheet with an internal size 46.5 x 27.5 x 14.5 (cm). In addition, polystyrene petri dish was used as a PDMS cavity. Uniform thickness of plastic was 1.1 mm. The petri-dish's cap is considered as a divider which has been introduced in simulation of problem in Chapter 3. Specification of polystyrene has been shown in **Table 3-2**.

By considering the introduced experimental setup's equipment, the performed experiments based on HIFU additive manufacturing method will be presented in next chapter.

# CHAPTER 6

## EXPERIMENTAL RESULTS AND DISCUSSION

In order to reach the acceptable 3D printed objects, different experiments have been designed and executed to be ensured about the integrity of the setup devices to achieve the precise results as well as fabrication of a 3D printed object as a final product.

It was expected, manipulation of significant parameters such as input power of transducer, transducer's frequency as well as material property were playing the major role in achieving the desired results. As it was explained so far since the working frequency of transducer was 2.15 MHz, this frequency has been considered as a constant parameter in all experiments.

By the way, temperature variation at the specified points in the cavity has been measured by employing thermocouple probe as well as data acquisition system DAQ NI 9212 during a certain period of time. Both devices have been introduced in the previous chapter.

By considering the introduced experimental setup in Chapter 5, in following sections designed experiments and their corresponding results are explained.

### 6.1. EXPERIMENTAL CONDITIONS

All experiments have been performed at room temperature (21°C). The water tank was filled by degassed Distilled Water. The water temperature during the experiments was also at 21°C.

### 6.2. DETERMINATION OF FOCAL REGION'S LOCATION AND SIZE

Three different experiments were performed to find the location of the focal region inside water. In addition to location and size of focal, the focal region's size change in response of altering the input power was investigated. In this section, each experiment will be explained in detail.

#### 6.2.1. FINDING THE LOCATION AND SIZE OF FOCAL FROM CHANGING THE LEVEL OF WATER'S FREE SURFACE

Firs, the central axis of the transducer was aligned with the static water's free surface which was at the level 12 (mm). Then device was run with input power 218 W and frequency 2.15 MHz. **Figure 6-1** shows the schematic of this setup.

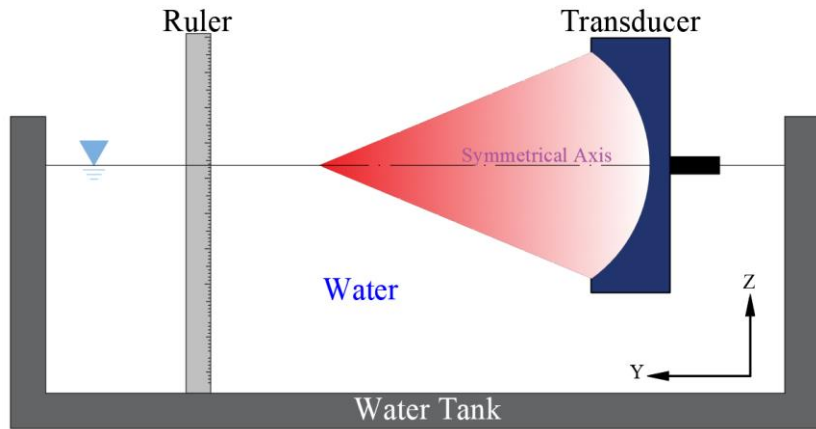


**Figure 6-1** Schematic of the setup used for determination of focal location and effect of power on its size

By performing the experiment, it was observed that at the distance 62 (mm) ahead of transducer's face the water surface raised up to 12.3 (mm) and became in a form of a spindle. The level change of free surface was identified by using the ruler which was put inside the water tank. **Figure 6-2** displays this result. Although part of the transducer was placed out of the water, this location was a good approximation for specifying the location of the focal region.

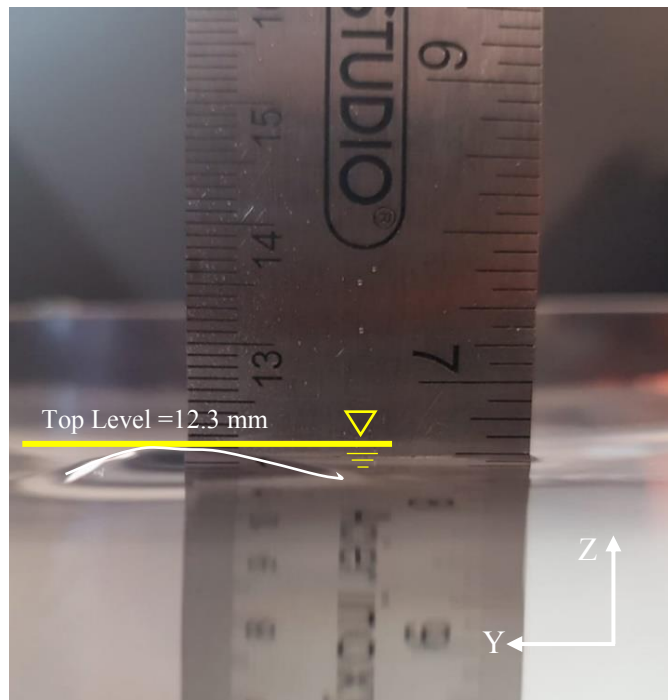
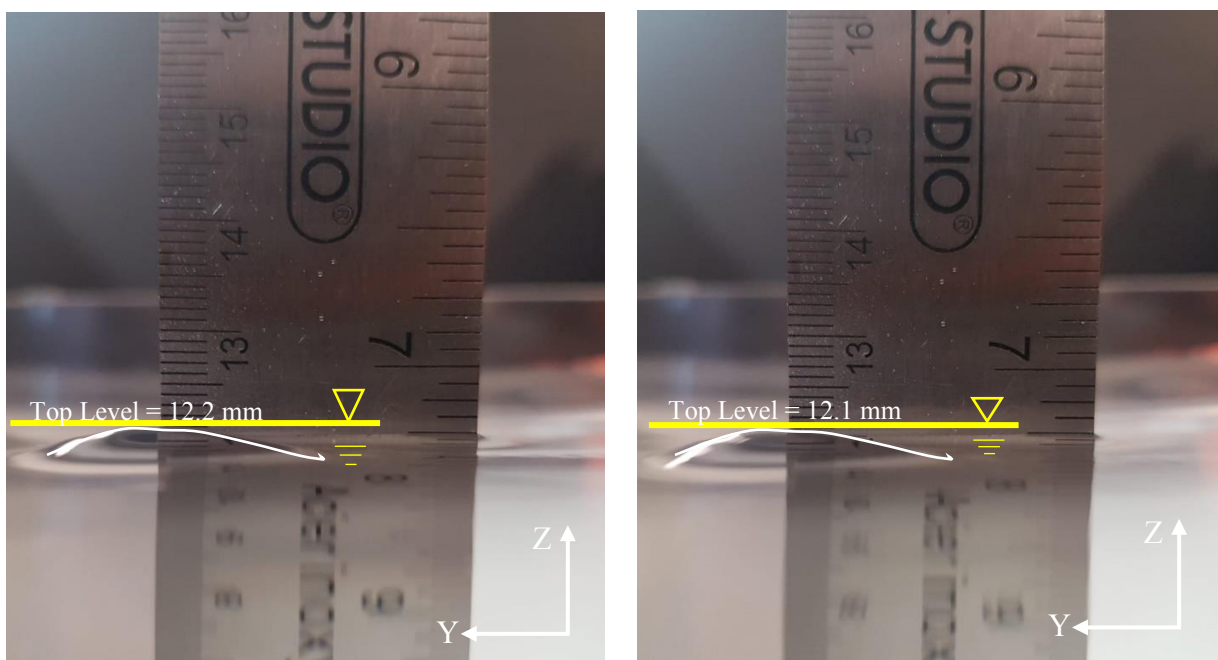


**Figure 6-2** Rising up the surface of the water while running the transducer with input power 218 W

Changing the form of water's free surface is due to the applied acoustic pressure at that location. Formation of spindle shape at the surface of water showed that the generated streams inside the water were following the oval shape of the focal region.

By decreasing the magnitude of input power from 218 W to 131 W and 67 W it was observed that the girth of the spindle was getting flatten simultaneously and the level of rising water decreased. These results are illustrated in **Figure 6-3**. This shows the direct relation between the magnitude of the acoustic pressure wave and input power of transducer and is completely in agreement with the results shown in **Figure 3-7** and **Figure 3-8**.



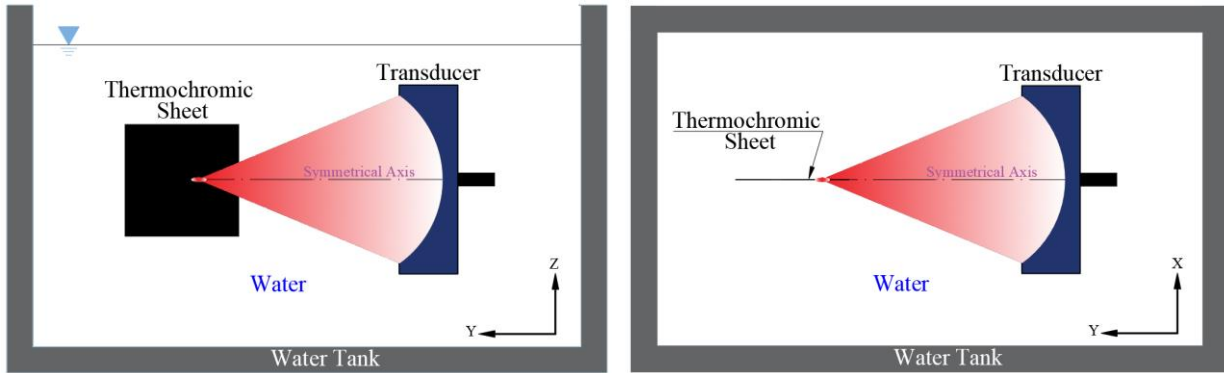
a) Input power equal to 131 W

b) Input power equal to 67 W

**Figure 6-3** Change in the size of the spindle's girth due to decreasing the applied input power

### 6.2.2. USING THERMOCHROMIC SHEET FOR FINDING THE LOCATION AND SIZE OF FOCAL

In addition to finding the position of focal point with previous experiment, by using the thermochromic sheet, recognition of focal region's shape as well as its location will be possible. By placing the thermochromic sheet along the symmetrical plane of the transducer inside water and running the acoustic source, image of the focal region appeared on the surface of the sheet. **Figure 6-4** represents the schematic of the setup.

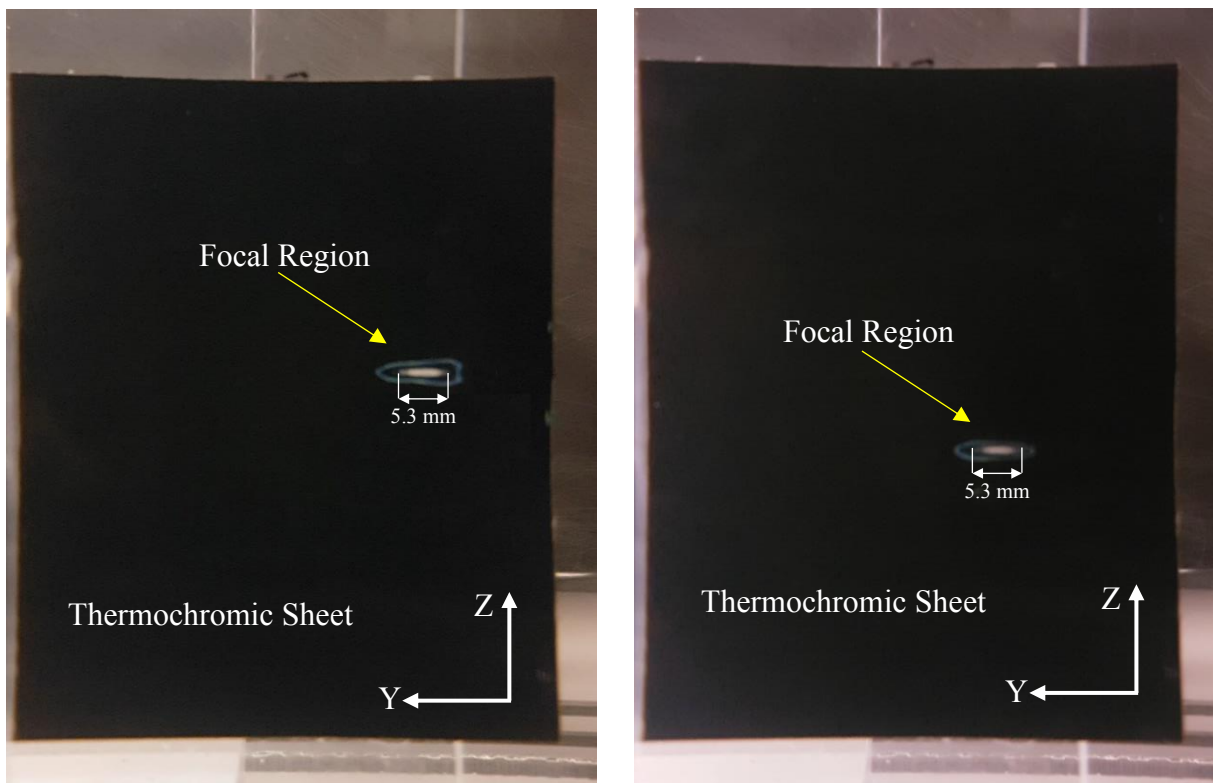


a) Side view of setup

b) Top view of setup

**Figure 6-4** Schematic of setup for using thermochromic sheet

In this experiment transducer's frequency and input powers were 2.15MHz and 218 and 131 watts respectively. Obtained results are illustrated in **Figure 6-5**.



a) Input power = 218 W

b) Input power = 131 W

**Figure 6-5** Focal region appearance on the thermochromic sheet that has been positioned along the vertical symmetrical plane of transducer

By looking at the images it can be realized that the focal region does not have a regular shape which is completely in agreement with the transducer's datasheet but its shape is close to the oval. Furthermore, by altering the magnitude of input power, the length of focal region remained constant but the shape of heat region was changed. According to thermochromic sheet's specification, in **Table 5-5**, the developed color spectrum on a surface of plate represents temperature gradient inside the focal region. However, due to low precision of thermochromic sheet in showing temperature magnitude, the exact determination of temperature variation inside the region is not possible. But this setup is reliable for finding the location of focal region.

### 6.2.3. USING ACRYLIC PLASTIC SHEET FOR DETERMINATION OF FOCAL SIZE

As it has been discussed so far, absorption of acoustic wave in solids and liquids generates a heat inside the media and the amount of generated heat depends on the attenuation of material. Applying the heat to solids makes the different effects such as rising temperature, deformation, size change, etc. The temperature rise in plastics mostly associates with the shape deformation. By using this effect, identification of focal region size along different sections of its shape will be possible.

Therefore, a thin plastic plate made of acrylic was placed inside the water medium in front of the transducer but far from the focal region. The focal region's primary location could be obtained by using each of two previous methods. **Figure 6-6** and **Table 6-1** display schematic of setup and the material property of acrylic sheet respectively.

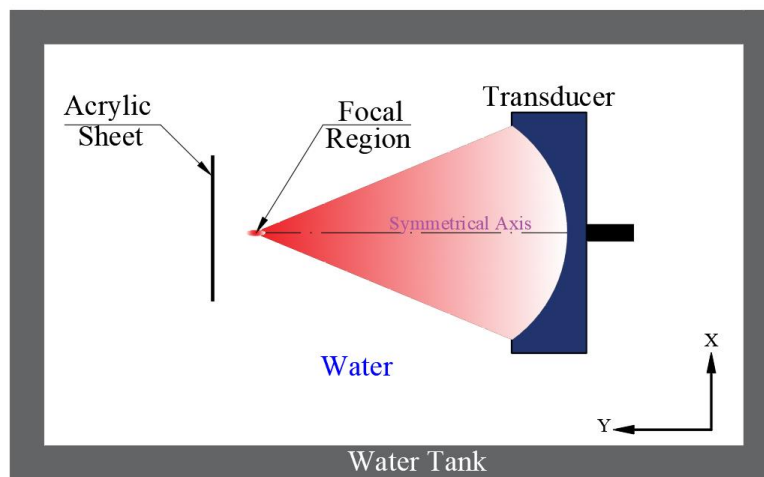


**Figure 6-6** Schematic of setup (Top View) in presence of Acrylic sheet in order to define the focal region's size

**Table 6-1** Material Properties of Acrylic Plastic [36]

Material	Density (kg/m <sup>3</sup> )	Sound Speed (m/s)	Acoustic Impedance (kg/m <sup>2</sup> .s)	Attenuation (Np/m) @ 2.15 (MHz)	Thickness (mm)
Acrylic, Clear	1190	2750	$3.272 \times 10^6$	13.63	2.5

By moving the transducer towards the acrylic sheet along Y direction, focal point became close to the surface of the plate. Once the tip of the focal region touched the sheet, the sign of burning with a circle section appeared on the surface. By continuing the forward movement, in Y direction, and placing the transducer at certain distances from plastic sheet, different burned signs appeared at plate. In this experiment, transducer was run for 1 second at each station. Due to the semi oval shape of the focal region which was observed in the last experiment it was expected by approaching the transducer towards the sheet, the size of sections kept growing up until reaching the maximum size at girth then by continuing the motion the sizes started to reduce while reaching the tail of oval. **Figure 6-7** illustrates size of sections with respect to distance of transducer with the acrylic sheet. The experiment has been done at frequency 2.15 MHz and input power 218 W and the total movement of transducer along Y axis was 6.5 mm.

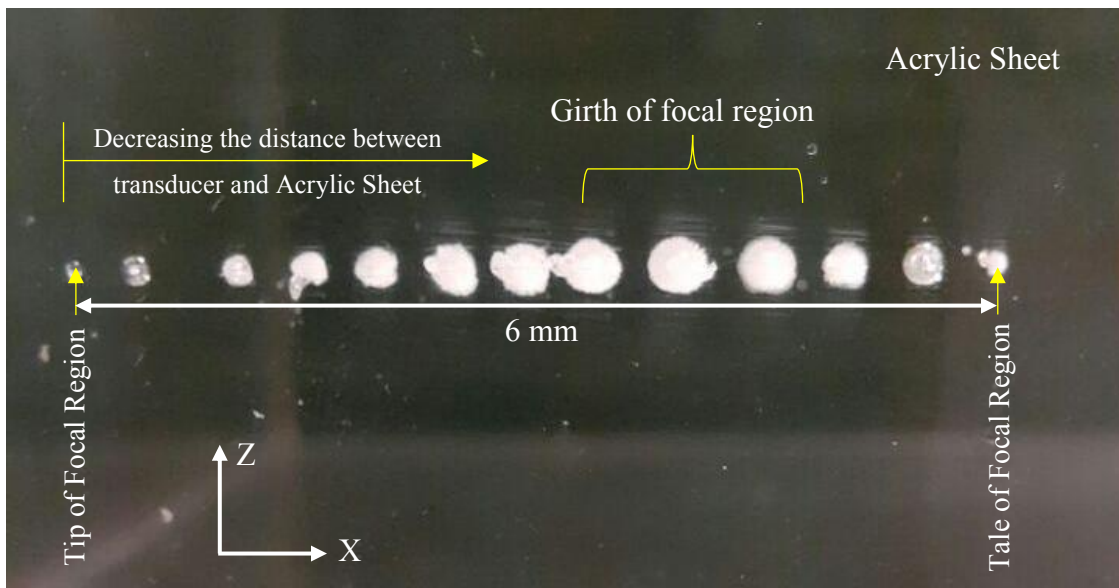
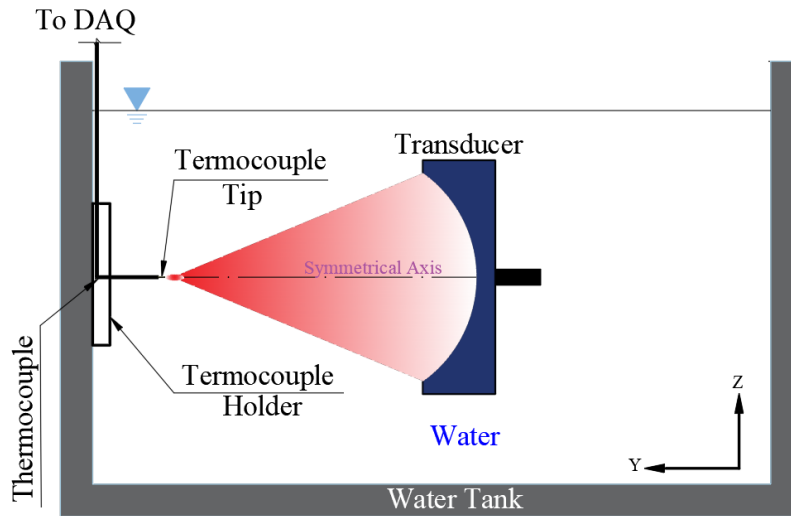


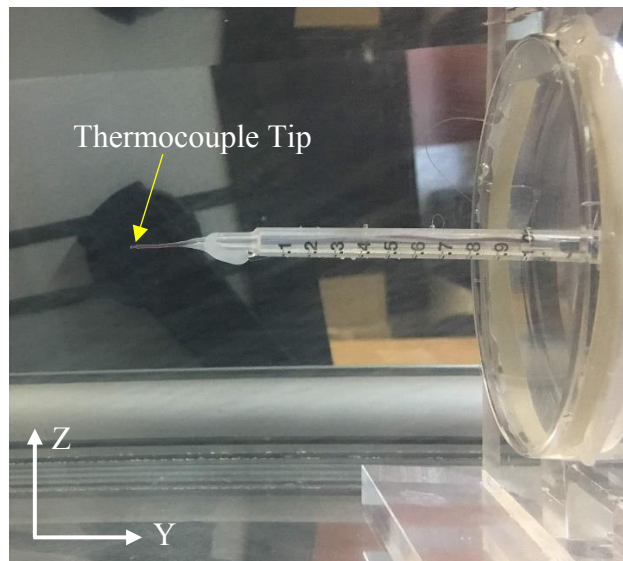
**Figure 6-7** Focal region sections appeared by burning the acrylic sheet

### 6.3. TEMPERATURE MEASUREMENT INSIDE WATER

To measure the temperature inside the focal region a T-type thermocouple, which was introduced in section 5.3, has been used. The schematic of the setup is illustrated in **Figure 6-8** (a). The probe was located horizontally inside the water tank that has been illustrated in **Figure 6-8** (b). The syringe shown in this figure was used to hold the thermocouple in a straight line.



a) Schematic of setup for positioning the thermocouple inside the tank



b) Close view of thermocouple setup

**Figure 6-8** Setup for positioning the thermocouple inside water tank

Next, by knowing the location of the focal point from previous experiments, the transducer was moved toward the probe's tip in order to place the focal point on it. Then, by running the transducer for 1 second in a frequency 2.15 MHz with input power 218 W, the temperature profile was obtained. This profile illustrates the heating up and cooling down process in the centre of focal region inside water for a period of 3.5 seconds. **Figure 6-9** displays these results.

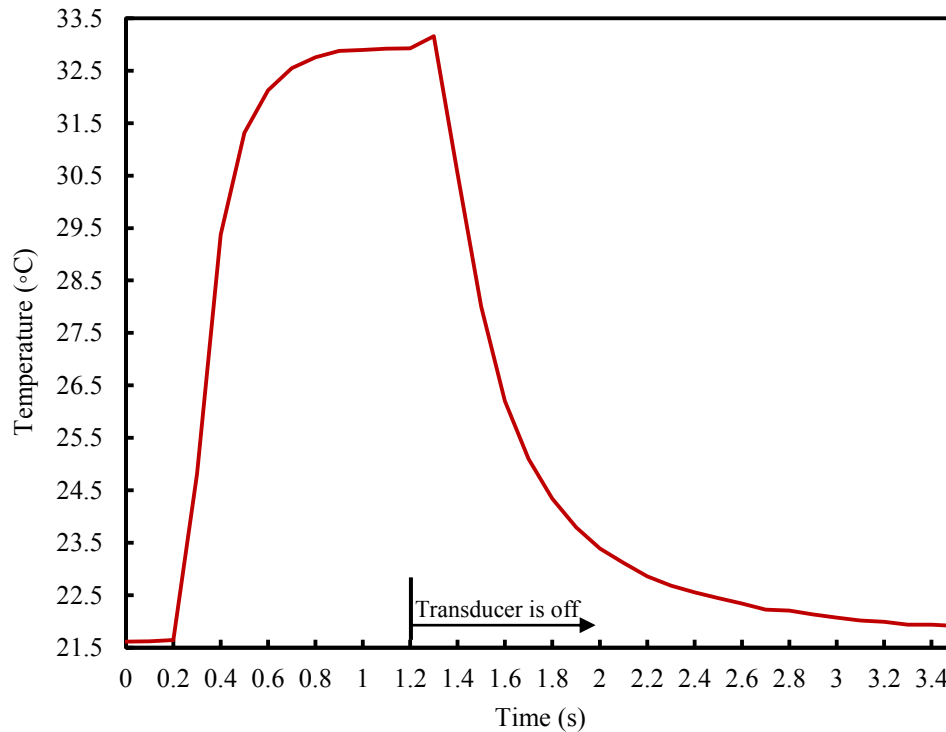


**Figure 6-9** Temperature profile at focal point inside water for 1 (s) sonication with input power of 218 W

This graph shows that the water was heated up gradually during the sonication and slightly after finishing it. Then, the water started to cool down sharply. In contrast, simulation's results illustrated in **Figure 3-10**, showed the peak at time 1 (s) in which water was heated up sharply and cool down process started quickly after finishing the sonication, then water gradually went back to its initial temperature within 9 seconds. This difference between simulation and experiment results could happen due to applied linear acoustic equation as well as the assumption regard to ignoring the variation in material properties of water during the sonication in simulation. Another effect is well known as "Thermocouple Artifact" which is caused by increasing the

temperature of the thin layer of water around the thermocouple due to heating up the probe in acoustic field [34].

#### 6.4. CURING OF PDMS INSIDE LIQUID CAVITY

According to information explained in section 5.4, PDMS was selected as a printing liquid. Therefore, discussion about PDMS 3D printing as well as parameters that influence the process are performed in this chapter.

A polystyrene petri dish was selected as a cavity for PDMS. This container had the unified wall thickness equal to 1.1 mm in all sides. Petri dish was fixed inside the water tank and parallel to the transducer's surface. As it has been mentioned so far the cap of petri-dish has been considered as a divider. **Figure 6-10** shows the schematic configuration of setup.

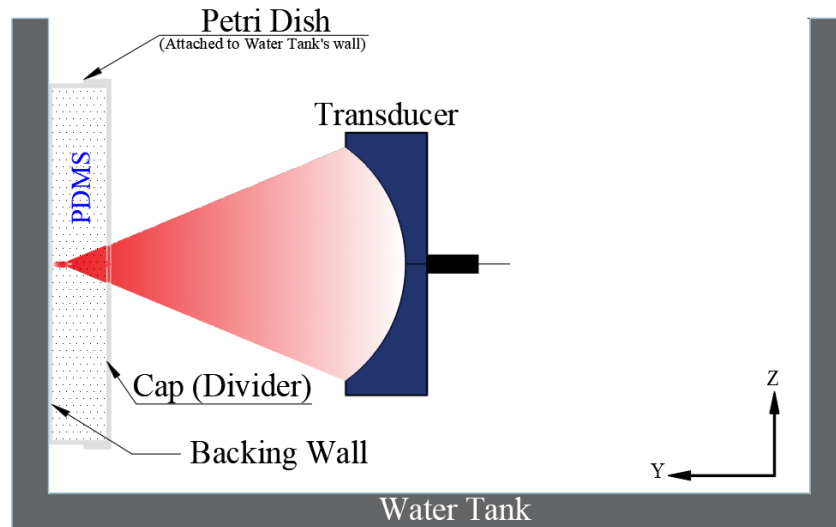


**Figure 6-10** Schematic configuration of setup for printing the PDMS

As it has been explained in Section 3.1.1 by passing the acoustic wave through the petri dish's cap and entering into the PDMS medium, the angle of transmission would change due to different sound speed property of each medium. Therefore, for determination of focal region's location inside the cavity, a calculation based on a Snell's law was performed. The Result showed by 0.5 mm movement of the transducer toward or away from the petri dish front wall, the location of focal point inside PDMS cavity will change equal to 0.75 mm. In the printing process, this quantity has been used to adjust the location of a new layer with respect to the last printed one.

After calculating the approximate location of the focal point, the printing process started by focusing the focal point on a spot in PDMS adjacent to the backing wall of petri dish. Therefore, the PDMS at this spot became cured and adhered to the surface. Therefore, by maintaining this process the first layer of the desired 3D object was printed. By repeating the process other layers were printed over the previous ones. **Figure 6-11** illustrates this explanation. Finally, after finishing this operation full shape of the desired object were printed completely.

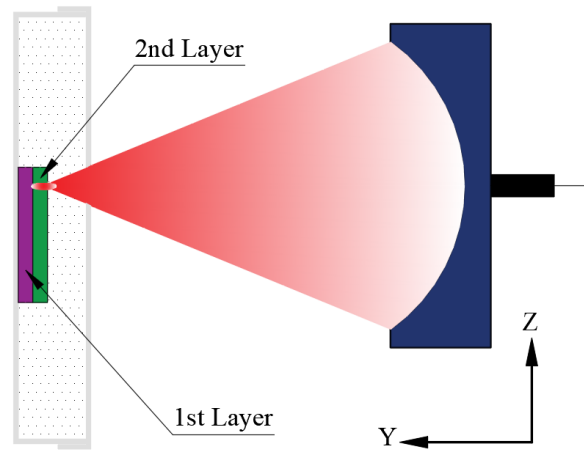


**Figure 6-11** Sequence of building the layers

## 6.5. TEMPERATURE MEASUREMENT AT FOCAL REGION INSIDE PDMS

In order to understand the temperature change at a focal region inside the PDMS cavity during sonication, a thermocouple probe was embedded inside petri dish. The probe was aligned along the symmetrical line of transducer and its tip was located close to the backing plate of the cavity. Next, the location of transducer with respect to petri dish was set so that the focal region placed at the tip of the embedded thermocouple. **Figure 6-12** shows the schematic configuration of the setup.

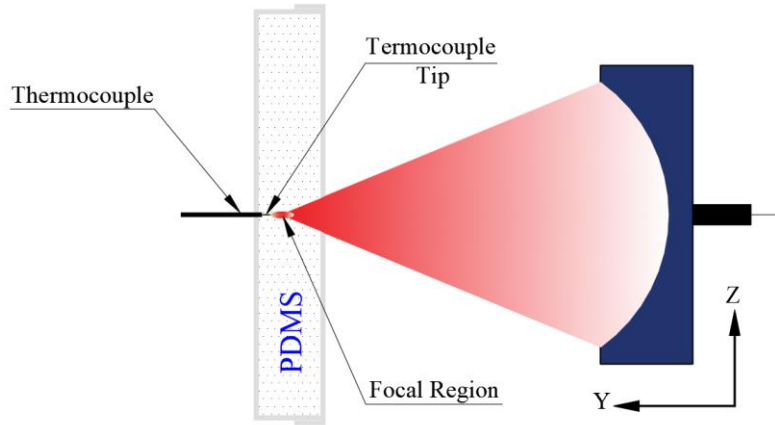


**Figure 6-12** Embedded thermocouple inside PDMS cavity to measure the temperature during sonication

Next, the transducer was run for a period of 15 seconds with input power 218 W at frequency 2.15 MHz. To investigate the heating up and cooling down processes at focal, temperature data were acquired for 30 seconds.

Results showed that the temperature rise continued for a second after finishing the sonication due to exothermic curing process and after that the temperature declines because of the natural conduction. The maximum recorded temperature was 40.858 (°C) which happened at  $t = 16.2$  (s). **Figure 6-13** illustrates the experiment result.

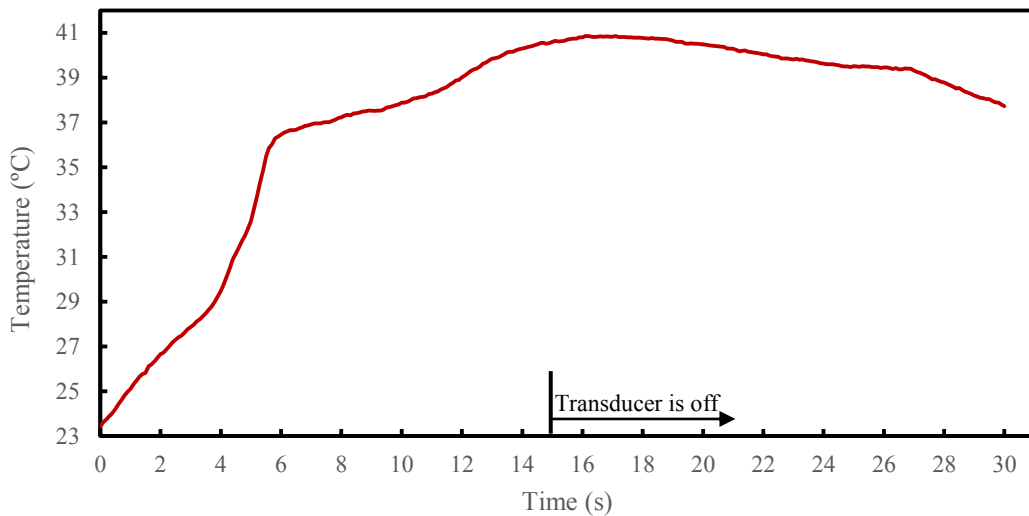


**Figure 6-13** The heat transfer over a period of 10 seconds inside the PDMS resulted from experiment

It should be mentioned, the maximum temperature rise recorded in this experiment is much less than the temperature rise resulted from the simulation. This result happened because of streaming occurrence inside the cavity which helps in heat dissipation. The streaming phenomenon was not considered in simulation and it is beyond the scope of this research. In fact, in presence of streaming accurate measurement of temperature is not possible, although the generated heat at the focal is enough for curing the PDMS at this region though.

## 6.6. FINAL PRINTED PRODUCT

After examining the effect of parameters such as applying different input powers, changing CNC’s feed rate and movement along Y as well as altering the PDMS ratio, the proper results were achieved with employing optimized operating conditions that are shown in **Table 6-2**. Therefore, in this section by applying these optimized parameters, 2 copies of a cantilever beam have been printed in one PDMS cavity. The geometry of cantilever was the same as a model presented in **Figure 4-4**. Purposes of this experiment were to determine the operability of setup for printing a simple 3D objects as well as repeatability of the printing process.

**Table 6-2** Optimized operation conditions of the printing

Input Power (W)	Frequency (MHz)	PDMS Ratio	CNC Feed Rate along Z and X axes (mm/min)	CNC total movement along Y axis (mm)	
				Step Movement	Total movement
218	2.15	10:1	300	0.5	9

The generated G-code of samples’ CAD model was imported to CNC. Then printing was started. This process took about 10 minutes for printing each of cantilevers. Actually, the printing time was drastically less than the “Form 2” printing operation that was introduced in Section 4.3. Printed samples are presented in **Figure 6-14**.

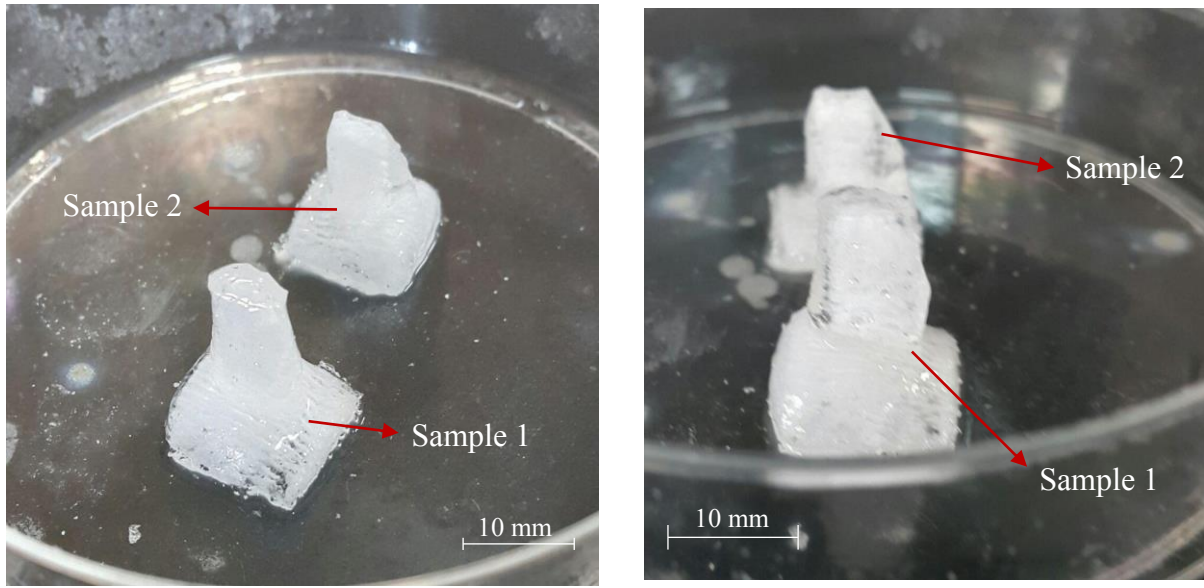


**Figure 6-14** Directly 3D printed cantilever beams

**Table 6-3** presents the dimension of CAD designed cantilever and average measured dimensions of two directly 3D printed samples.

**Table 6-3** Dimensions of cantilevers (CAD designed and 3D printed)

	Dimensions (mm)		
	Length (L)	Width (W)	Thickness (th)
CAD Designed Cantilever	10	8	4
Directly 3D Printed Sample 1	9.8	8.8	4.5
Directly 3D Printed Sample 2	10.2	8.4	4.3

Illustrated information in **Table 6-3** identifies the resolution of printing setup which is influenced by the size of the focal region, accuracy in determination of its location during the process, and controlling streaming inside the cavity.

Furthermore, **Figure 6-14** illustrates the existence of bulgy appendages on samples which deformed the expected shape of the sample. This happened because after finishing the printing operation, the curing process was being continued until fully dissipation of heat inside the liquid and decreasing the magnitude of temperature below the PDMS gel temperature. This unfinished process caused to steak an unexpected cured PDMS to printed sample after finishing the

operation. In fact, in addition to the size of focal region that has the major effect on the resolution of printing, avoid adding extra PDMS to model is another factor which has to be taken into account. Therefore, to improve the quality of printing after finishing the printing process, liquid cavity should be discharged from residual Liquid or semi-liquid PDMS quickly.

## 6.7. ELASTIC BEHAVIOR OF 3D PRINTED CANTILEVER BEAM

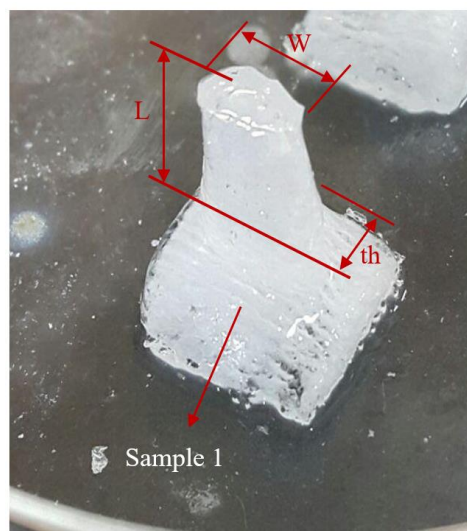
Material's stiffness is one of the characteristics which shows the elastic behavior of material. So, in this research in order to study the elastic behavior of 3D printed cantilever, a comparison between the stiffness of the 3D printed part and the object produced by the conventional fabrication of PDMS, was performed. For this purpose, the PDMS model of one of the two 3D printed cantilevers presented in **Figure 6-14** was fabricated. In following the applied approach is explained.

### 6.7.1. FABRICATION OF IDENTICAL CANTILEVER BY USING MOLD

In order to fabricate an identical PDMS model of 3D printed cantilever following procedure was followed:

- 1- Selection of 3D printed cantilever
- 2- Fabrication of mold from the selected cantilever
- 3- Fabrication of identical PDMS cantilever by using a mold

**Figure 6-15** shows the image of the selected cantilever with its average dimensions.



L (average length) = 10.2 mm

W (average width) = 8.4 mm

th (average thickness) = 4.3 mm

**Figure 6-15** Selected cantilever with its average dimensions

To fabricate a mold, the selected cantilever was washed with isopropanol for 2 minutes, and it was dried by using nitrogen gas. In order to decrease the adherence between the cantilever with new PDMS mold, the cantilever was coated with fluorinated silane (Trichlorosilane, Sigma-Aldrich, Inc.) for 4 hours at 65 °C. As a result, the cured PDMS mold and cantilever could be separated easily after curing the mold. Next, a small box was made from thin aluminum sheet for making a mold then the coated cantilever was put inside a box. **Figure 6-16** shows this setup.

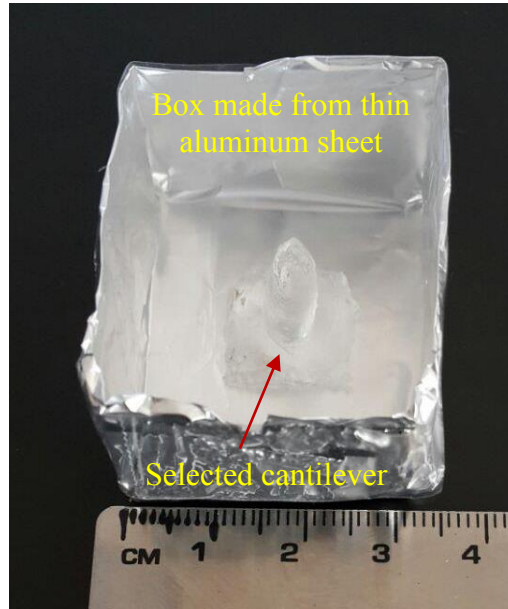


**Figure 6-16** Preparation of box for fabrication of PDMS mold

Sylgard 184 (PDMS resin) was prepared by mixing 30 ml base resin and 3 ml curing agent (in a ratio of 10:1) and then degassing the mixture by using vacuum until complete removal of the trapped bubble inside mixture. Then the mixture was poured into a prepared box shown in **Figure 6-16**.

Then, the setup was put inside the oven and baked for 90 minutes at 70°C. After curing process, cured PDMS was removed from the aluminum box and then the 3D printed cantilever was pulled out of the cured part. **Figure 6-17** shows the fabricated PDMS mold.

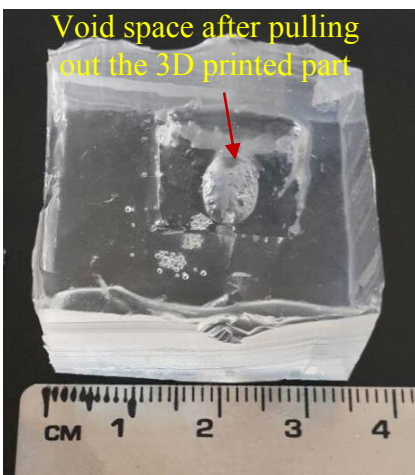


**Figure 6-17** Fabricated PDMS mold

For the fabrication of PDMS cantilever, in next step, the previous approach was repeated again. PDMS mold was coated with fluorinated silane for 4 hours at 65 °C. Then, 10 ml PDMS with the mixture of base resin and curing agent in a ratio of 10:1 was prepared. Next, the fabricated mold was filled by PDMS and resin was baked for 90 minutes at 70°C. After finishing the process, the new PDMS cantilever was removed from the mold. **Figure 6-18** shows a fabricated part.

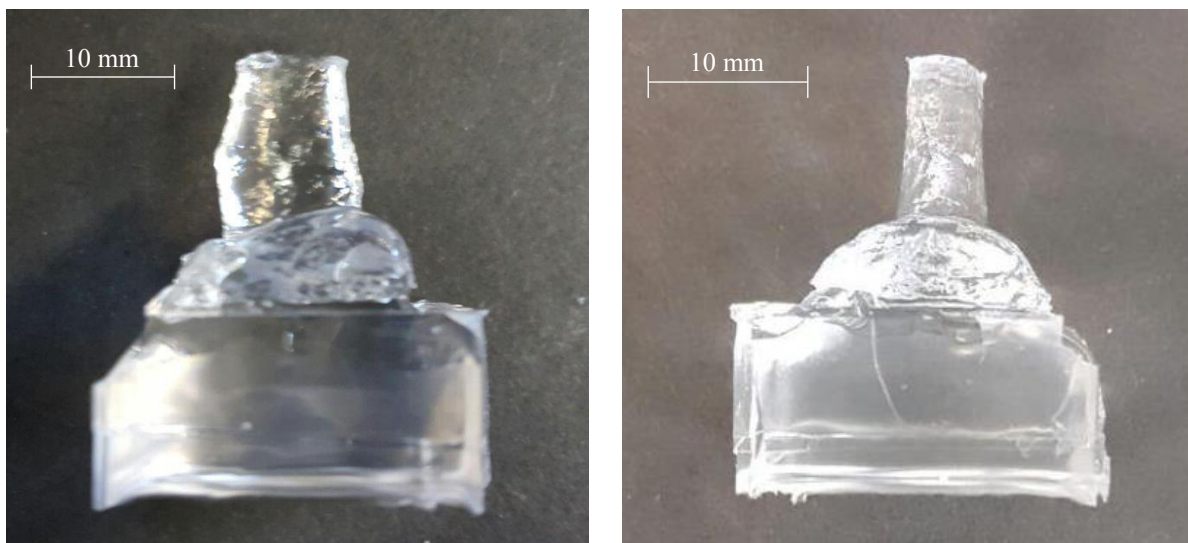


**Figure 6-18** Two side views of fabricated PDMS cantilever with an appendage to help for pulling out the part from the mold

The dimension of the fabricated PDMS cantilever was measured and the results were the same as the dimensions of printed cantilever that has been shown in **Figure 6-15**.

## 6.7.2. STIFFNESS DETERMINATION OF CANTILEVERS

A precision balance method was employed to measure the force on the tip of the cantilevers and hence the stiffness of them. **Figure 6-19** shows the schematic of this experimental setup.

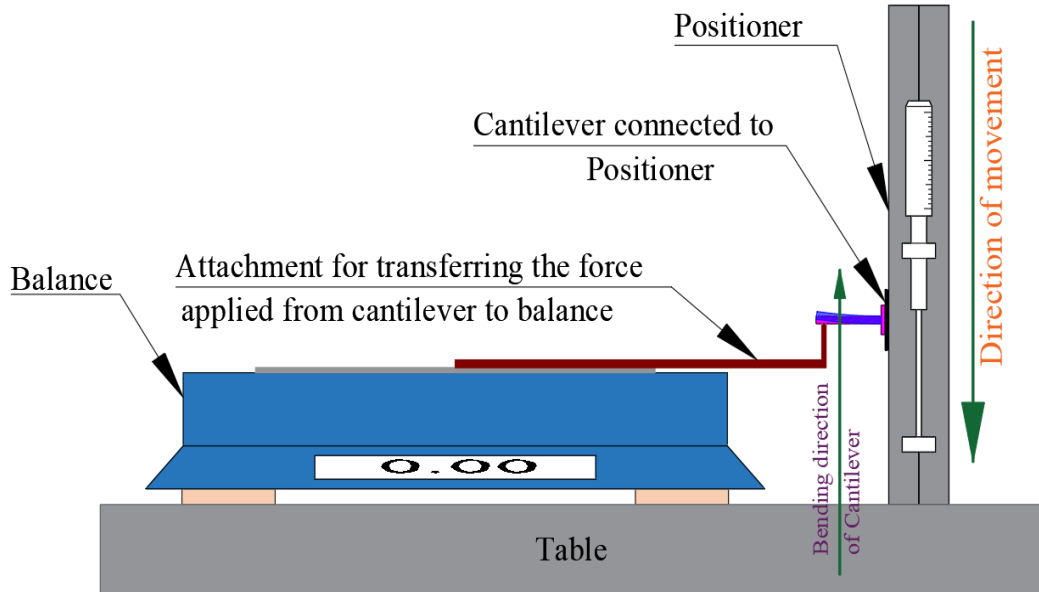
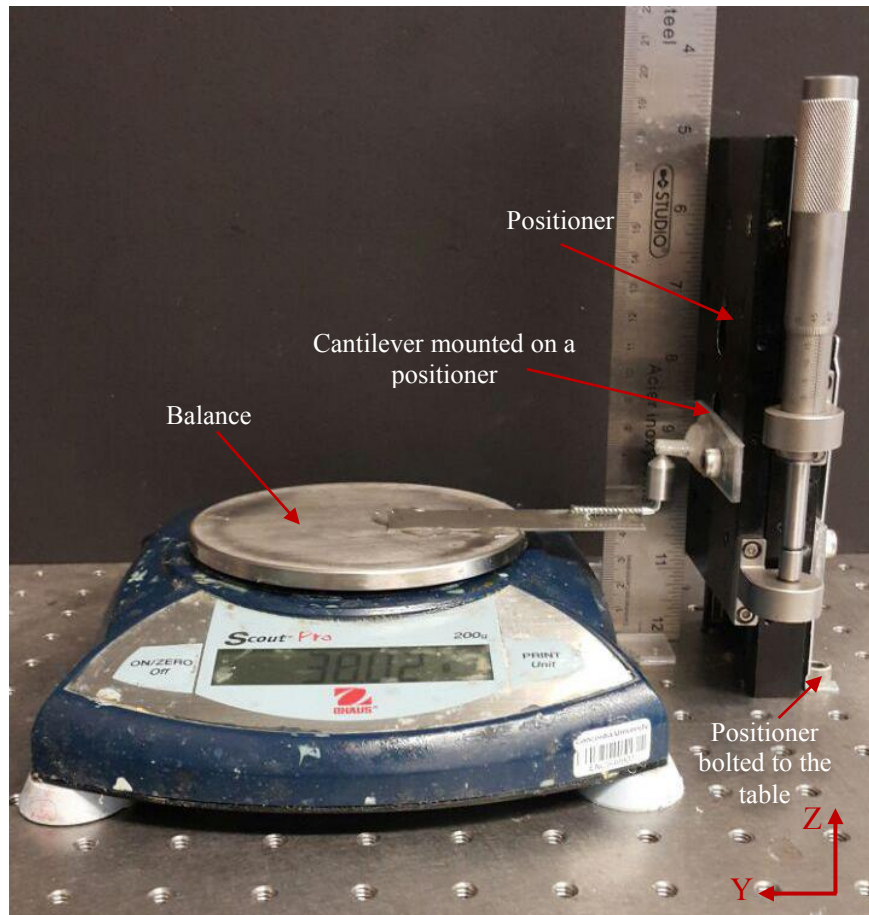


**Figure 6-19** Schematic of employed balance method to obtain the stiffness of cantilevers

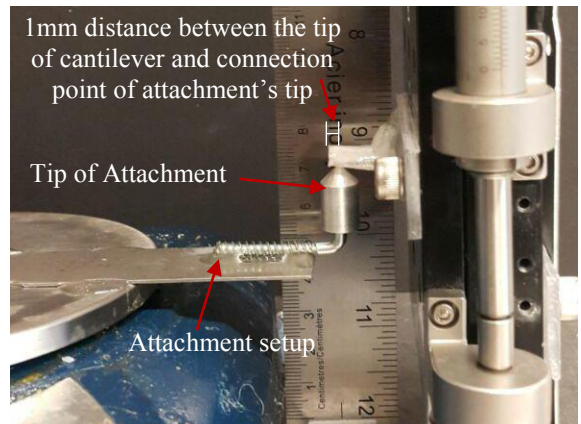
Each of cantilevers was bonded on a small 3 mm thick rectangular plexiglass sheet. After sticking the part, the contact surface of cantilever with plastic sheet became fully solid and hence there was no relative movement between the cantilever and the sheet. After that, the new component was mounted on a positioner. On the other hand, a type of solid attachment was made and bonded to the surface of the balance (Ohaus Scout Pro Portable Electronic Balance, 200g Capacity, 0.01g accuracy) to serve a rigid body and in order to transfer the applied load from cantilever to the balance. For aligning the setups, positioner was moved toward the balance and bolted to the table in a manner that the tip of attachment placed at 1 mm behind the tip of the mounted cantilever which considered as the location of applying force to the cantilever. **Figure 6-20** shows all the experimental setups.



a) Location of positioner with respect to the balance



b) Cantilever bonded on a small plexiglass sheets

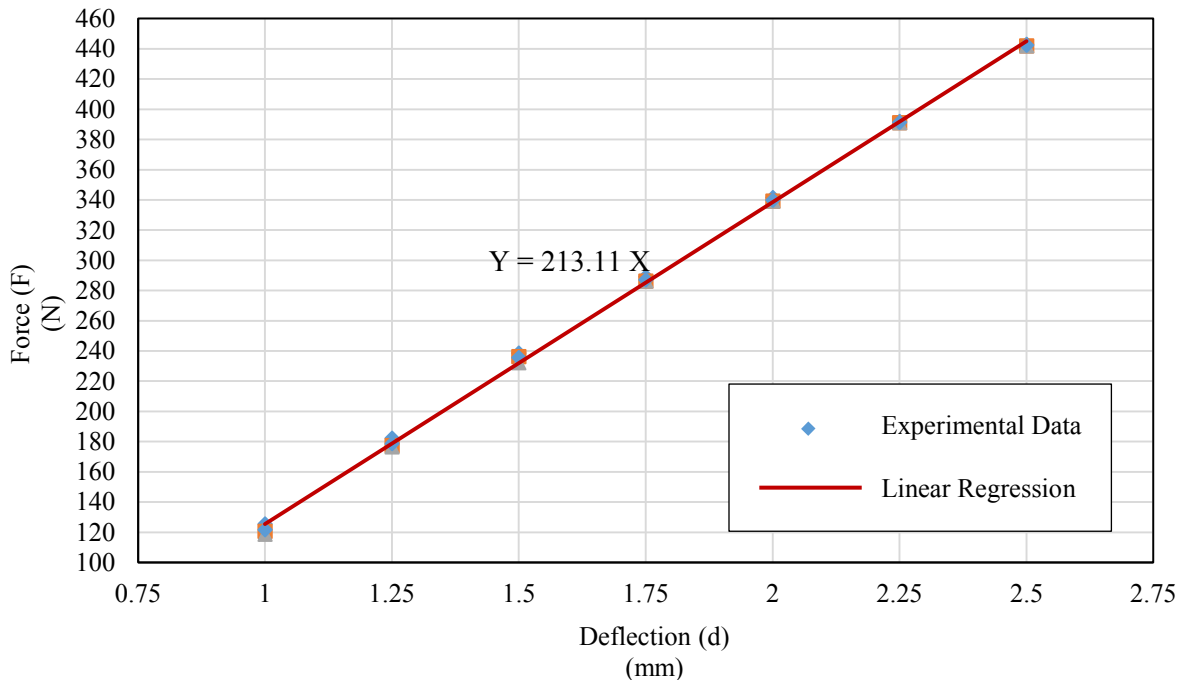


c) Attachment for transferring the load from cantilever to the balance, bonded to the surface of the balance

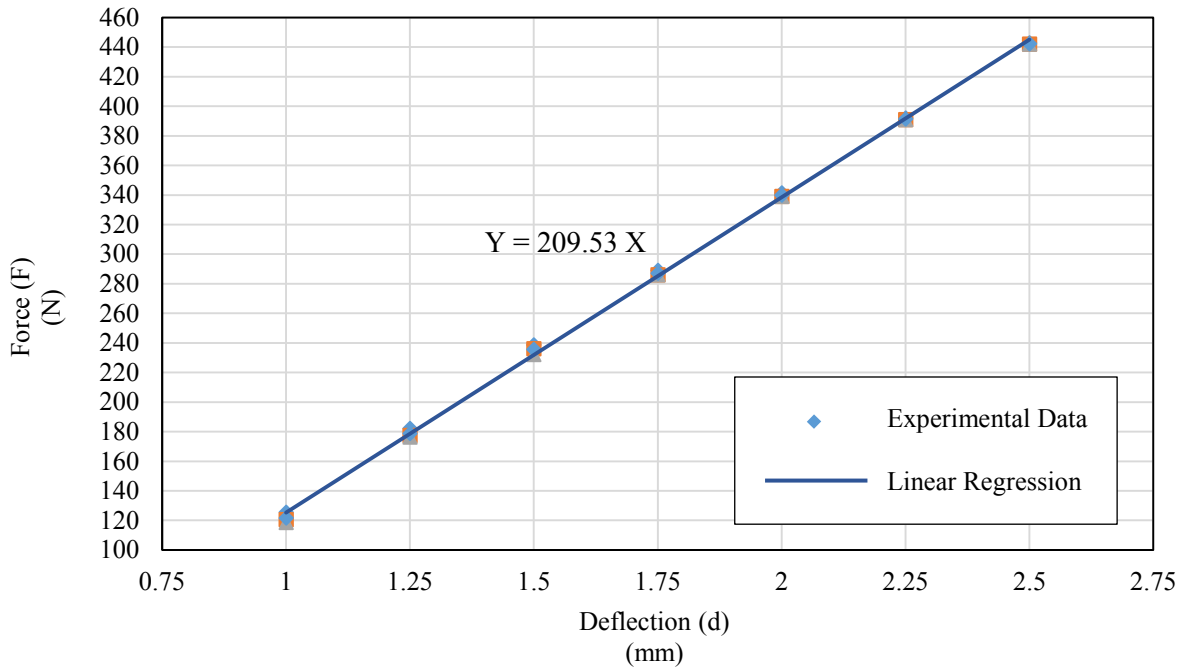
**Figure 6-20** Balance method setup for measuring the force on the tip of the cantilevers

### 6.7.3. MEASURING THE STIFFNESS

At first, the 3D printed cantilever was mounted on a positioner. When the setup was completed and positioned at the certain location that was explained in the previous section, the positioner was gradually moved down until touching the tip of the attachment without exerting a force. This location was considered as a start point of measurement. Then by continuing movement of the cantilever, the variation of force (F) against deflection (d) was obtained based on the displacement of positioner (d) and the force that was recorded from the balance. In order to investigate the effect of out of centre error in this method, a sample mass was positioned on the centre and out of centre on the tip of attachment [48]. The measured deviation due to the out of centre was 0 g, which could be happened due to the sensitivity of balance, therefore the out of centre error for this system was neglected. In continuation of process, the force (F) was measured for the deflections (d) of {1.0, 1.25, 1.5, 1.75, 2.0, 2.25 and 2.5} mm. This procedure was also repeated for the PDMS cantilever. **Figure 6-21** shows the recorded data. The slight non-linearity in results was due to the large deflections compare to the size of the cantilevers. Also, these data were extracted from repeating the experiments 3 times.



a) Directly 3D printed cantilever



b) Indirectly molded PDMS cantilever

**Figure 6-21** Force-Deflection graph for directly 3D printed cantilever and indirectly molded PDMS cantilever

As it has shown in this figure, the linear regression was employed to estimate the stiffness of cantilevers based on linear equation of  $F = kd$  [48]. According to graphs, calculated stiffness for directly 3D printed and indirectly molded PDMS cantilevers is 213.11 N/mm and 209.53 N/mm respectively. For making a visual comparison between two stiffness both of fitted lines are shown in the same graph as displayed in **Figure 6-22**.

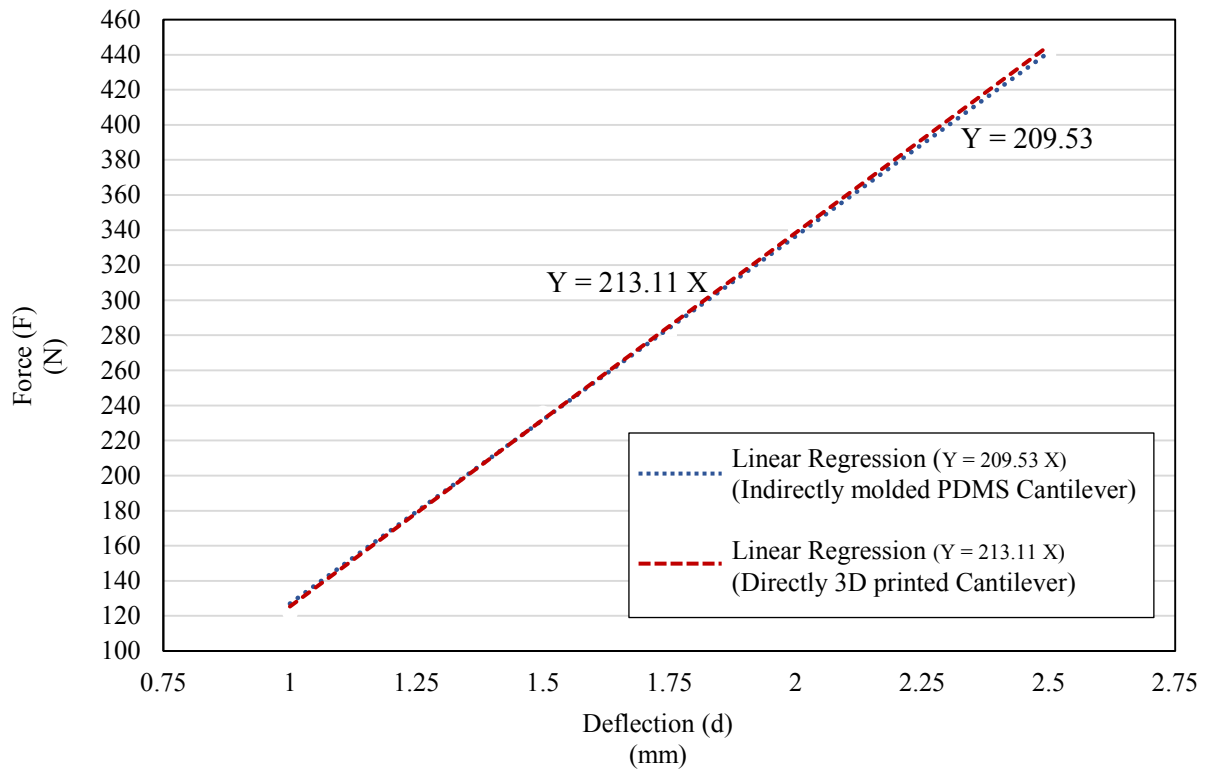


**Figure 6-22** Linear graphs of force-deflection for 3D printed cantilever and PDMS cantilever

As it has been mentioned the graph shows that both of cantilevers have almost the same stiffness. Having close look at the graph, linear elastic behavior of 3D printed cantilever can be distinguished.

## 6.8. CONCLUSIONS

In this chapter different experiments have been performed in order to examine the ability of HIFU additive manufacturing method and integrity of the setup devices for fabrication of a 3D printed object as a final product as well as achieving the precise results. The PDMS was selected as a printing resin. Results showed accuracy and resolution of final object depends on the size of the focal region, accuracy in determination of its location during the process, and controlling streaming inside the cavity. In continue, two identical cantilevers were printed as a final directly 3D printed objects. Printing process took about 10 minutes for printing of each samples. By measuring the dimensions, the existence of 2 to 12.5% dimensional deviation between the CAD designed model and printed objects was investigated. In addition, in order to study the elastic

behavior of the 3D printed object, another cantilever by using the molding method was fabricated. Then, by employing a balance method comparison between the stiffness of two built objects was performed. Results showed the directly 3D printed object has almost the same stiffness as the indirectly molded PDMS cantilever. Also, linear elastic behavior of 3D printed cantilever was confirmed.

# CHAPTER 7

## CONCLUSIONS AND FUTURE WORKS

A novel additive manufacturing technology using high intensity ultrasound as the energy source was introduced in this work. In order to achieve the inclusive overview of the expected experimental results, numerical simulation of the problem was performed in order to validate the accuracy of approaches. Simulation results showed input power and fluid properties have the major influence on acoustic and thermal effects in a liquid medium. It was shown that the acoustic wave pressure field varied by liquid's acoustic impedance. Also, during traveling acoustic wave among different materials the wave power decreased as a result of acoustic impedance alteration. In addition, the magnitude of temperature rise in liquid directly depends on the absorption coefficient of fluid so that a small variation in attenuation causes the high order change in heat energy.

Next, in order to get familiar with the process of additive manufacturing in standard 3D printers as well as exploring the abilities and precision of these printing machines further investigation on 3D printed cantilever, fabricated by a Form 2 SLA 3D printer, was performed. Results showed that the dimensional resolution of 3D printed part is more accurate in horizontal, XY, plane in comparison with the vertical, Z, direction. In fact, increasing the resolution of printing will associate with increasing the printing time. While Form 2 printer operates based on layer-by-layer process, the surface finish of the printed objects strongly depends on the direction of printing.

Finally, in order to examine the integrity of the setup devices in achieving the precise results for fabrication of a 3D printed object as a final product, different experiments were designed and executed. Results showed that the magnitude of input power for transducer and properties of the fluid medium in which acoustic wave propagates, had a major effect on intensity and generated acoustic field pressure. This result was completely in agreement with the simulation results. In contrast, the size of the focal region was independent of input power and medium properties.

Investigation of heat transfer inside the water showed the difference between the simulation and experiment results. This could happen due to the applied linear acoustic equation and the assumption of ignoring the variation in material properties of water during the sonication in the

simulation. Another effect that influenced the results was the “Thermocouple Artifact” which happened because of increasing the temperature of the thin layer of water around the thermocouple due to heating up the probe in the acoustic field.

In the next step, the temperature rise during the curing of the PDMS was measured. The maximum temperature recorded at this experiment was much less than the temperature rise resulted from the simulation. This result happened because of streaming inside the cavity which helped in heat dissipation.

After examining the effect of parameters such as applying different input powers, changing CNC’s feed rate and movement along Y as well as altering the PDMS ratio, the optimized operation conditions for performing the 3D printing of an object were achieved. Based on these parameters 3D printing process was performed in order to fabricate a simple cantilever beam. Printing operation took about 10 minutes that was drastically less than the normal printing time with “Form 2”. By measuring the dimensions of 3D printed cantilever, 2 to 12.5% difference with the dimensions of design model was found.

The linear elastic behavior of 3D printed cantilever was confirmed by obtaining the relation between force and deflection. Furthermore, results showed the 3D printed object had almost the same stiffness as the PDMS cantilever that was fabricated by employing the conventional molding method.

As a future work, by employing the nonlinearity of acoustic phenomenon in simulation the accuracy of results can be improved. Furthermore, in this work the streaming phenomenon was not considered in simulation and was beyond the scope of this research but the implementation of the streaming in simulation would help obtaining more accurate results from the numerical analysis.

As it has been mentioned, the resolution of printing setup is influenced by the size of the focal region, accuracy in determination of its location during the process, and streaming inside the cavity. Therefore, by employing a HIFU transducer with the smaller focal region and controlling the streaming inside cavity more accurate results will be obtained.

By improving the dimensional resolution of printing, accurate determination of other characteristics of printed object such as moment of inertia and elastic modulus is possible.

## REFERENCES

- [1] A. Pandian, and C. Belavek. "A review of recent trends and challenges in 3D printing." Proceedings of the ASEE North Central Section Conference, 2016.
- [2] E.M. Sachs, J.S. Haggerty, M.J. Cima, and P.A. Williams. "Three-dimensional printing techniques." US patent 5,204,055, 1989.
- [3] D.A. Roberson, D. Espalin, and R.B. Wicker. "3D printer selection: A decision-making evaluation and ranking model", *Virtual and Physical Prototyping*, 2013, vol. 8(3), pp. 201-212.
- [4] P. F. D. M. Dudek. "FDM 3D printing technology in manufacturing composite elements." *Archives of Metallurgy and Materials*, 2013, vol. 58(4), pp. 1415-1418.
- [5] S.C. Ligon, R. Liska, J. Stampfl, M. Gurr, and R. aupt. "Polymers for 3D printing and customized additive manufacturing." *Chemical reviews*, 2017, vol. 117(15), pp. 10212-10290.
- [6] "Additive manufacturing - General principles – Terminology", ISO/ASTM 52900, 2015, Retrieved 2017-06-15.
- [7] M. Vaezi, S. Hermann, and Y. Shoufeng. "A review on 3D micro-additive manufacturing technologies." *The International Journal of Advanced Manufacturing Technology*, 2013, vol. 67.5(8), pp. 1721-1754.
- [8] S. Kumar, A. K. S. Choudhary, A. K. Singh, A. K. Gupta. "A Comparison of Additive Manufacturing Technologies." *IJIRST-International Journal for Innovative Research in Science & Technology*, 2016, vol. 3(01), p. 06.
- [9] D. Bourell, J.P. Kruth, M. Leu, G. Levy, D. Rosen, A. M. Beese, and A. Clare. "Materials for additive manufacturing." *CIRP Annals*, 2017, vol. 66(2), pp. 659-681.
- [10] A.V. Wijk, and I.V. Wijk. *3D Printing with Biomaterials: Towards a Sustainable and Circular Economy*. Amsterdam, The Netherlands: IOS Press, 2015, pp. 10-15.
- [11] V. Ozbolat, D. Madhuri, A. Bugra, P. Adomas, C.D. Melik, and I.T. Ozbolat. "3D printing of PDMS improves its mechanical and cell adhesion properties." *ACS Biomaterials Science & Engineering*, 2018, vol. 4(2), pp. 682-693.
- [12] H. Nguye, H. Nguyen, J. Uan and D. Wang. "A nonrational B-spline profiled horn with high displacement amplification for ultrasonic welding." *Journal of Ultrasonics*, 2014, vol. 54(8), pp. 2063-2071.

- [13] W. Han, J. Liu, D. Chong and J. Yan. "Analysis of Temperature Field in a High-Intensity Ultrasonic Chamber." *Journal of Thermophysics and Heat Transfer*, 2015, vol. 30(4), pp. 745-753.
- [14] M. Solovchuk, T.W.H. Sheu, and M. Thiriet. "Simulation of nonlinear Westervelt equation for the investigation of acoustic streaming and nonlinear propagation effects." *Acoustical Society of America*, 2013, vol. 134(5), pp. 3931-3942.
- [15] G.T. Haar, and C. Coussios. "High intensity focused ultrasound: physical principles and devices," *International Journal of Hyperthermia*, 2007, vol. 23(2), pp. 89-104.
- [16] G.N. Levy, R. Schindel, and J.P. Kruth, "Rapid manufacturing and rapid tooling with layer manufacturing (LM), state of the art and future perspectives." *CIRP Annals - Manufacturing Technology*, 2003, vol. 52(2), pp. 589-609.
- [17] J. Bakkelund, R. Karlsen, and Ø. Bjørke. "Fabricating metal objects using laser manufacturing technologies and powder metallurgy science." *Annals of CIRP*, 1997, vol. 46(1), pp. 135-138.
- [18] T. Duda, and L.V. Raghavan. "3D metal printing technology." *IFAC-Papers On Line*, 2016, vol. 49(29), pp. 103-110.
- [19] H. Tan, W. Shang, F. Zhang, A.T. Clare, X. Lin, J. Chen, and W. Huang. "Process mechanisms based on powder flow spatial distribution in direct metal deposition." *Journal of Materials Processing Technology*, 2018, vol. 254, pp. 361-372.
- [20] D. King, and T. Tansey. "Rapid tooling: selective laser sintering injection tooling." *Journal of Materials Processing Technology*, 2003. Vol. 132(1-3), pp. 42-48.
- [21] A.T. Sidambe. "Biocompatibility of advanced manufactured titanium implants-A review." *Materials*, 2014, vol. 7(12), pp. 8168-8188.
- [22] W.J. Sames, F.A. List, S. Pannala, R.R. Dehoff, and S.S. Babu, "The metallurgy and processing science of metal additive manufacturing." *International Materials Reviews*, 2016, vol. 61(5), pp. 315-360.
- [23] P. Parandoush, and L. Dong. "A review on additive manufacturing of polymer-fiber composites." *Composite Structures*, 2017, vol. 182, pp. 36-53.
- [24] C.K. Chua, K.F. Leong, and C.S. Lim. *Rapid prototyping: principles and applications*. 2<sup>nd</sup> ed. Singapore: World Scientific Publishing Co., 2003.

- [25] S. Telfer, J. Pallari, J. Munguia, K. Dalgarno, M. McGeough, and J. Woodburn. “Embracing additive manufacture: implications for foot and ankle orthosis design.” *BMC musculoskeletal disorders*, 2012, vol. 13(1), p. 84.
- [26] D.W. Cho, J.S. Lee, J. Jang, J.W. Jung, J.H. Park, and F. Pati. “Organ Printing”, Morgan & Claypool Publishers, Chapter 4, 2015, pp.4-1-4-4.
- [27] H. Ahasan, V. Sathish, S. Mallik, and B. Khoda. “3D printability of alginate-carboxymethyl cellulose hydrogel.” *Materials*, 2018, vol. 11(3), p. 454.
- [28] COMSOL Multiphysics 5.2a, application ID: 12659, Focused Ultrasound Induced Heating in Tissue Phantom, [Online]. Available: <https://www.comsol.com/model/focused-ultrasound-induced-heating-in-tissue-phantom-12659>.
- [29] H. Kuttruff, *Acoustics: an introduction*. New York: CRC Press, 2006.
- [30] N. Zinoviy, V. Skalskyi, and O. Serhiyenko. “Propagation of elastic waves in solids.” Springer, Cham, 2017, Chapter 2: In *Acoustic Emission*, pp. 29-73.
- [31] L.W. Schmerr. *Fundamentals of Ultrasonic Nondestructive Evaluation-A Modeling Approach*, Springer Series in Measurement Science and Technology, 1998, 2<sup>nd</sup> ed.
- [32] Panametrics-NDT, *Ultrasonic Transducers Technical Notes*, OLYMPUS, 2006.
- [33] F.B. Jensen, W.A. Kuperman, M.B. Porter, and H. Schmidt. *Computational Ocean Acoustics*. Series: *Modern Acoustics and Signal Processing*, 2<sup>nd</sup> ed., New York: Springer, 2011, Chapter 2, pp. 65-71.
- [34] J. Huang, R.G. Holt, R.O. Cleveland, and R.A. Roy. “Experimental validation of a tractable numerical model for focused ultrasound heating in flow-through tissue phantoms,” *The Journal of the Acoustical Society of America*, 2004, vol.116(4), pp.2451-2458.
- [35] R.B. Bird, W.E. Stewart, and E.N. Lightfoot, *Transport Phenomena*, 2nd ed., New York: John Wiley & Sons, 2007, pp. 333-361.
- [36] A.R. Selfridge. “Approximate Material Properties in Isotropic Materials.” *IEEE Transactions on Sonics and Ultrasonics*, 1985, vol. su-32(3), pp. 381-394.
- [37] 26th ITTC Specialist Committee on Uncertainty Analysis, ITTC recommended procedures, “Fresh Water and Seawater Procedure,” *International Towing Tank Conference*, Rev. 02, 2011, vol. 7.5(02), pp. 01-03.

- [38] J.J. Markham, R.T. Beyer, and R.B. Lindsay, "Absorption of Sounds in Fluids," *Reviews of Modern Physics*, 1951, vol. 23(4).
- [39] J.P. Abulencia, and L. Theodore, "Fluid Flow for the Practicing Chemical Engineer," New York: John Wiley & Sons Inc., 2009, pp. 555-556.
- [40] J.M.M. Pinkerton, "A pulse method for the Measurement of Ultrasonic Absorption in Liquids-Results for Water", Nature Publishing Group, 1947, vol. 160(4056), pp. 128-129.
- [41] B. Zeqiri. "Reference liquid for ultrasonic attenuation." *Ultrasonics*, 1989, vol. 27(5), pp. 314-315.
- [42] C.K. Chua, M.V. Matham, and Y.J. Kim. "Lasers in 3D printing and manufacturing." World Scientific, 2017, pp. 1-13.
- [43] B. C. Gross, J. L. Erkal, S. Y. Lockwood, C. Chen, and D. M. Spence, "Evaluation of 3D printing and its potential impact on biotechnology and the chemical sciences," *Anal. Chem.*, 2014, vol. 86(7), pp. 3240-3253.
- [44] H. Dodiuk, and S.H. Goodman. "Handbook of Thermoset Plastics." 3<sup>rd</sup> ed., Springer, 2014, pp. 1-12.
- [45] N. Karak. *Vegetable oil-based polymers: properties, processing and applications*. Elsevier, 2012.
- [46] D. Ratna. *Handbook of thermoset resins*. Shawbury: UK, ISmithers, 2009, pp. 1-53.
- [47] D. Ortiz-Acosta, and C. Densmore. "Sylgard® Cure Inhibition Characterization-Report." Los Alamos National Laboratory, Chemical Diagnostics and Engineering Group, 2012.
- [48] A.S. Nezhad, M. Ghanbari, C.G. Agudelo, M. Packirisamy, R. Bhat, and A. Geitmann. "PDMS microcantilever-based flow sensor integration for lab-on-a-chip." *IEEE Sensors journal*, 2013, vol.13(2), pp. 601-609.